U N I V E R S I T A' D E G L I S T U D I D I N A P O L I

"F E D E R I C O I I"

FACOLTA' DI INGEGNERIA

DOTTORATO DI RICERCA IN

INGEGNERIA CHIMICA

XXI ciclo

AUTOIGNITION AND PARTICLES FORMATION IN DIESEL ENGINES: MODELING AND EXPERIMENTS

COMITATO SCIENTIFICO: Candidato:
Relatore: Valentina Fraioli
Prof. Andrea D'Anna

Correlatori:
Dott. Ing. Paola Belardini
Dott. Ing. Claudio Bertoli

Abstract

The present work of thesis is focused on multidimensional simulations of combustion in diesel engines, performed through a modified, parallel version of the KIVA3V numerical code, coupled with ChemKin for detailed reaction kinetics implementation.

The modeling activity has been constantly validated through experimental data collected on a single cylinder diesel engine. Such engine has been developed in Istituto Motori in order to set all the operative conditions in a fully controlled and independent manner: its peculiar flexibility in the control of all the parameters permits to obtain a precious validation tool.

In a first part of the work, detailed kinetics reaction schemes have been introduced in the parallelized version of KIVA3V and a reaction mechanism for n-dodecane combustion was adopted to simulate combustion taking place in the mentioned single cylinder engine (fuelled with commercial diesel fuel).

Then numerical tests have been carried out, in order to study the computational issues arising from the introduction detailed kinetics. In particular, two different general-purpose libraries of solvers have been tested, in order to optimize the calculations in terms of accuracy and computational times. The possibility to locally select, during the computations, the most appropriate solver has been implemented, applying a kinetics-based switching criterion.

Subsequently, a wide set of experimental data have been collected fuelling the engine with a single-component fuel, n-heptane, in order to perform a proper comparison with simulations carried out using heptane kinetics.

These measures aimed at carrying out a validation campaign for the modified version of the code, therefore many engine operative conditions have been varied , thus building a reliable experimental database for subsequent numerical comparisons. All the different conditions have been tested at two values of the engine compression ratio, 16.5 and 14.5 respectively.

The correspondent simulations were performed adopting a skeletal reaction scheme for n-heptane autoignition without pollutants formation mechanisms.

The modified version of the code has proven to be a very reliable tool and more detailed reaction mechanisms can easily be adopted for specific simulation purposes.

Afterwards the n-heptane reaction scheme has been extended, to include PAH kinetics, and a sectional model to account for carbonaceous particles formation has been implemented, thus allowing the calculation of the particles size distribution. The qualitative analysis of the results has given a reasonable picture of the general development of the particles formation phenomenon and a tentative comparison with the size distribution function measured by a DMA at the exhaust has been conducted. Both the model and the experiments provided similar values of the size distribution function for particle sizes between 10 and 100nm, while calculations also predict a nucleation mode that is not experimentally detected.

In order to make up a judgment on the model performance and reliability, further tests need to be conducted to verify the model sensitivity with respect to different operating conditions, still the preliminary results achieved represent a good starting point for particles formation modeling in diesel engine combustion.

Contents

Chapter 4 – **Autoignition modelling and experimental validation**

Chapter 5 – **Particles formation modelling**

Chapter 6 – **Conclusions**

Abbreviations

ATDC	After Top Dead Centre.
BTDC	Before Top Dead Centre.
CAD	Crank Angle Degree.
CR	Compression Ratio.
DPF	Diesel Particulate Filter.
ECU	Engine Control Unit.
EGR	Exhaust Gas Recirculation.
FC	Fuel consumption.
HCCI	Homogenous Combustion Compression Ignition.
LD	Light Duty Engine.
LTC	Low Temperature Combustion.
NEDC	New European Driving Cycle.
ODE	Ordinary Differential Equation.
PCCI	Premixed Compression Combustion Ignition.
PM	Particulate Matter.
P_{rail}	Pressure in the common rail.
RANS	Reynolds Averaged Navier Stokes
RoHR	Rate of Heat Release.
RSD	Relative Standard Deviation.
SIMPLE	Semi-Implicit Method for Pressure-Linked Equations.
SOEC	Start of Energizing Current.
SOI	Start Of Injection timing.
SR	Swirl Ratio.
TDC	Top Dead Centre.

Chapter one

Background and motivations

1.1   Introduction

The next European legislation on passenger cars emission standards (EURO6) represents for diesel engine manufacturers a real challenge.

As well known, a further simultaneous reduction of nitrogen oxides (NOx) and particulate matter (PM) emissions from diesel combustion, has to be guaranteed, keeping low unburned gaseous emissions (HC and CO).

In Fig.1.1 the emission standards evolution in terms of NOx and PM is displayed.
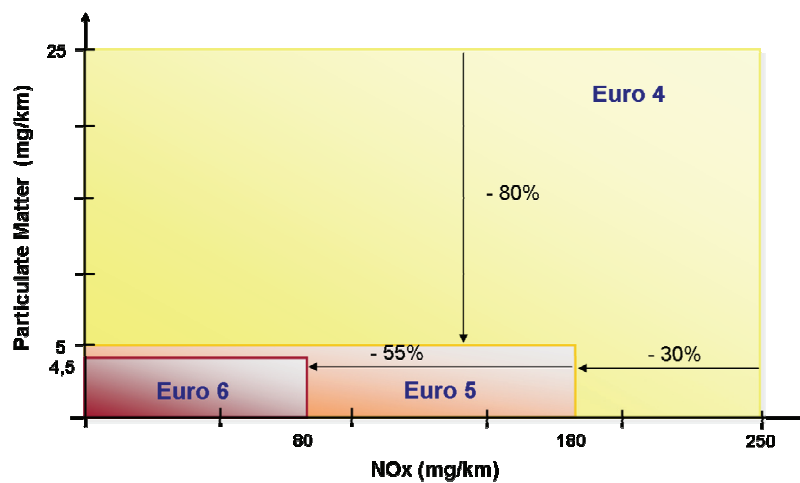
Figure 1.1 – Emission standards development[1]

Current and proposed standards employ a mass based quantification criterion, while alternative metrics related to number, size and surface area of emitted PM are screened, since these criteria seem to be better correlated to the adverse health effects of particles emissions.

[1] Source: Imarisio R., Combustion Technology to Meet EURO 6 Diesel Emission Standards, XXXI Comb Meeting

As a result, research activities are devoted, on one hand, to support the practical need of manufacturers to fulfill the fixed limits and, on the other hand, to qualify the particles emissions as long-term investigation on their formation mechanisms.

At the moment, the attention of public and manufacturers research centres is focused on two conceptually different approaches. The first one attains to the further refinement of the classic diesel combustion coupled to the development of complex after-treatment systems (affording a possible detrimental effect on fuel consumption). The second option is linked to the development of new combustion systems, in order to directly cut the raw emissions. This second approach is very attractive, as it will probably present less costs with respect to the former and will probably match with the EUROV passenger car limits.

These combustion modes are commonly referred to as HCCI (Homogeneous Charge Compression Ignition), PCCI (Premixed Charge Compression Ignition), LTC (Low Temperature Combustion) in dependence on the specific realization.

The understanding of the potentialities of such combustion modes and of the correspondent pollutants formation mechanisms has not only an academic but also very practical motivations, as alternative combustion modes are likely to have an impact on the characteristics of the particulate matter emitted by future engines and legislations will require a deeper characterization of the particulate matter emitted from production engines.

In this framework, multidimensional simulations of combustion can be a helpful tool to deepen the understanding of combustion features and pollutants formation and to enrich experimental investigations with an additional point of view.

In particular, an interesting application of the calculations could be modeling particles formation for engines operating in LTC mode: numerical calculations could provide useful insights in the soot formation mechanism applied to the under-development engine-technology.

At the moment multidimensional simulations of in-cylinder particles formation cannot yet be considered fully predictive: here a modeling attempt has been developed.

In the following some background information is given, concerning the alternative combustion modes and the particulate matter formation in diesel engines. Then in Par.1.1.3 a very brief outline on general mechanisms of carbonaceous particles formation in combustion is reported.

1.1.1 Alternative combustion modes

Alternative burning conditions are so called as they are alternative to the traditional spark ignition (SI) and compression ignition (CI) engines: the basic "rule" is to ignite a diluted and (more or less) premixed air-fuel mixture by means of compression (Eng, 2003). Therefore the charge does not exhibit the great inhomogeneity typical of the diesel functioning: thanks to the premixing, combustion would occur simultaneously throughout the combustion chamber and the absence of very rich zones can reduce particulate matter formation.

The ignition does not require any spark: the compression ignition can be achieved with high compression ratios, so in theory the efficiency can be kept similar to the diesel engine. Moreover, the dilution of the mixture permits to keep the temperature sufficiently low to strongly reduce NOx formation.

In Fig.1.2 a map representing equivalence ratio versus temperature is reported: the violet path is followed during alternative combustion development, whereas the orange arrows identify conventional combustion evolution.
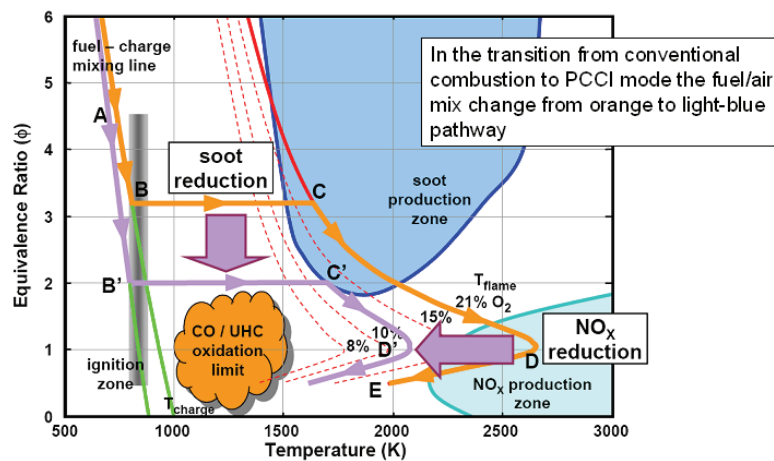
Figure 1.2 – Equivalence ratio – temperature routes followed during conventional and PCCI combustion. (Source M. Potter, GM, DEER2006)

It is possible to see that, thanks to the reduction in the maximum temperature, the NOx production zone can be avoided and the lower range of equivalence ratios values present during combustion (i.e. after the ignition zone) move the whole route out of the soot production area.

The major drawback of such combustion modes is the increased emission of unburned hydrocarbons and CO, due to the lower temperatures.

Despite the interesting advantages offered by PCCI condition in terms of very low NOx and soot emissions, several problems still remain for its large application to the modern diesel engines.

At the moment, one of the main issues, is the limitation of its use in the low and medium load/speed range of the whole engine operating map, due to the difficulties in controlling contemporary both the premixed air-fuel charge and the ignition timing. The extension to higher speed and load ranges, in fact, is coupled with problems of combustion noise control and excessive fuel consumption increment (Beatrice, 2008). At the same time, of course, it is essential to enlarge the PCCI applicability in the whole NEDC[2] cycle, to take advantage of its well known potentiality in reaching the very low NOx emissions in view of the future EURO 6 regulation.

Multi-dimensional simulation can provide some insight into the phenomenon and detailed kinetics can be a particularly suitable way to represent the typical pressure development and the heat release rates in these combustion modes. Many fuels, such as n-butane and n-heptane, under some operating conditions, exhibit a two stage ignition, determining the presence of a cool flame before the main heat release. This feature can easily be explained through the autoignition kinetics development (as outlined in Par.4.1). As an example, in Figure 1.3, a comparison of pressure cycles and ROHR between a conventional and a PCCI combustion condition is reported.
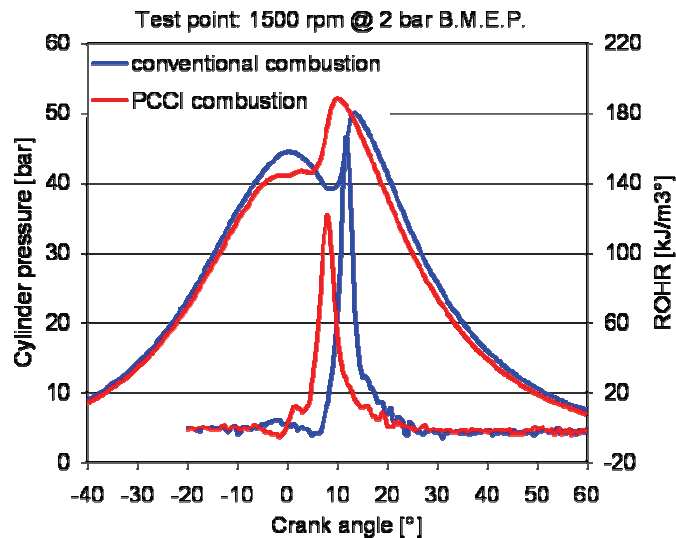
Figure 1.3 - Comparison between PCCI and conventional combustion

The measures have been performed at Istituto Motori-CNR on a direct injection diesel Engine -FIAT 1.9 JTD Multijet. The working points have identical speed and mean effective pressure: the PCCI condition has been obtained through an earlier injection and higher EGR rate.

At the end of the compression phase, temperatures are lower, because of air dilution and the thermal effect of fuel vaporization: therefore a typical flat shape of pressure

---

[2] The acronym New European Driving Cycle is referred to the driving cycle chosen as representative of a typical usage of a car during which the regulated emissions have to be sampled.

appears between the injection start and TDC. Then the first small peak in the ROHR can be noted before the main release, correspondent to the slight pressure increase a little after TDC. Finally, the "hot" combustion starts: owing to the better premixing achieved, the maximum pressure value is higher than the one reached in the conventional case.

1.1.2 Particulate from diesel engines

Diesel Particulate matter is a complex mixture of solid material produced during combustion and volatile organic and inorganic material added as the exhaust gases cool down. It is commonly accepted that diesel PM is responsible for adverse health effects, including carcinogenic ones.

Current legislation defines diesel PM according to a sampling method in which the emitted material is collected on a filter after exhaust sampling and dilution at temperatures below 52°C. Such material consists of agglomerated carbonaceous particles (soot) but also ash and adsorbed organic and inorganic material. It is commonly accepted that soot is produced during combustion, while volatile species are adsorbed as exhaust gas cool down during transfer and dilution.

The amount of adsorbed matter strongly depends on sampling conditions.

Ash come from lube oil and fuel (additives, impurities), normal engine wear and corrosion of the exhaust system.

The schematic commonly used for the composition of diesel particulate matter distinguishes the total emitted matter into three categories:

- ➢ Soot – solid carbon particles
- ➢ SOF – soluble organic fraction, made up of heavy hydrocarbons condensed on the particles surfaces (it refers to the organic material that can be extracted using a Soxhlet apparatus).
- ➢ IF – inorganic fraction contains volatile and semivolatile compounds like sulfates and nitrates.

SOF, together with sulfates and nitrates, form a volatile fraction that can be determined by heating particles in an inert atmosphere.

PM in atmosphere is usually distinguished in three different modes: the ultrafine mode ($Dp<0.1\mu m$), the fine mode ($0.1<Dp<2.5\mu m$) and the coarse mode ($2.5\mu<Dp<10 \mu m$).

However in the case of the aerosol at the exhaust of diesel engines, a slightly different classification is usually adopted (Kittelson, 1998) which distinguishes a nuclei size range ($Dp<0.05 \mu m$) and an accumulation mode ($0.05 \mu m<Dp<1\mu m$), as illustrated in Fig.1.4.

PM emitted in conventional diesel combustion exhibits therefore an essentially bimodal number size distribution function with the larger size mode made up of combustion generated soot particles with adsorbed volatile material.

The origin of the nuclei-mode is commonly ascribed to hydrocarbon and sulfate nucleation: these nuclei only account for 1-20% of the particles mass, but contain more than 90% of the total number of particles.

However the actual size distribution function of the emitted particles varies according to the engine operation, fuel composition, lube oil, after treatment technology, and exhaust sampling procedure.
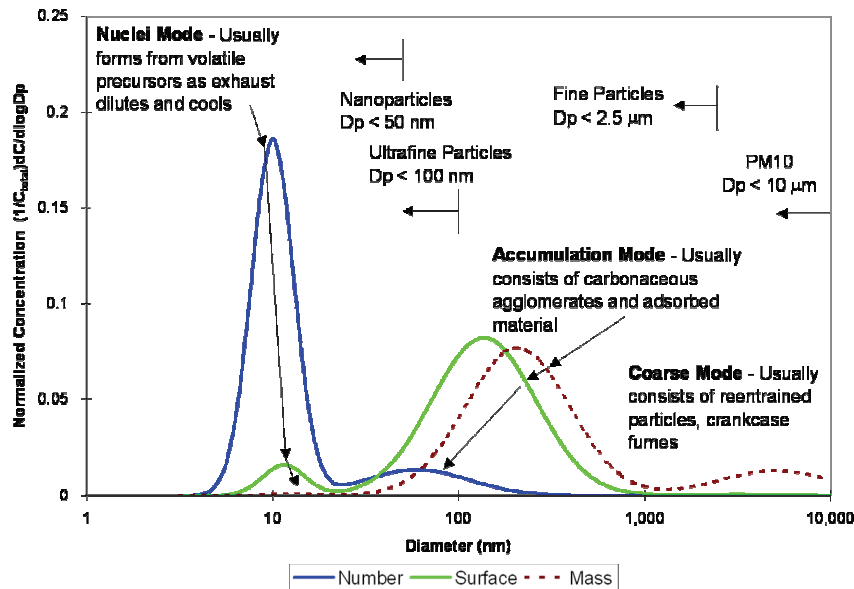
Figure 1.4 – Particles size distribution function adapted from (Kittelson, 2003)

The formation of nuclei is commonly explained as resulting from of condensation of semivolatile material after exhaust exits tailpipe that exceeds saturation pressure (Kittelson, 1998). On the other hand, recent observations suggest that the nucleation mode may contain nonvolatile cores (Kittelson, 2002), that could be combustion-generated during high-temperature in-cylinder reactions.

To sum up, the source of the smallest particles is still a contentious topic and, in this respect, simulations of particles formation in diesel combustion, coupled with proper experimental investigations, could be helpful in the understanding of this complex phenomenon.

1.1.3 Carbonaceous particles formation in combustion

Carbonaceous material formed in combustion exhibits various microstructure, morphology and composition, dependent on the specific combustion device, fuel and conditions, therefore a different nomenclature has been developed that classifies such particles according to their dimensions and sources.

Particulates formed from residual matter of solid fuels after the volatile contents of the fuels have been released are called char, appearing as highly porous, black particles.

The term soot usually refers to the carbonaceous particulates formed in gas-phase combustion at high temperature.

The chemical composition of the emitted particulate is not uniquely fixed: even though more than 90% of the atoms is represented by carbon atoms, a variable content of hydrogen, oxygen and sulphur can be present, according to the age of the particles, the temperature, the formation history. An empiric formula typically assigned to mature particles is C_8H, while younger particles may contain considerable more hydrogen.

Soot particles are clusters of smaller particles that agglomerate in chain-like structures.

These roughly spherical components, also referred to as primary particles, can vary in size from 10 to 50 nm and consist of large number of crystalline sheets.

The graphitic adjacent layers, randomly oriented, give rise to a so called turbostratic structure, as illustrated in Fig.1.5.
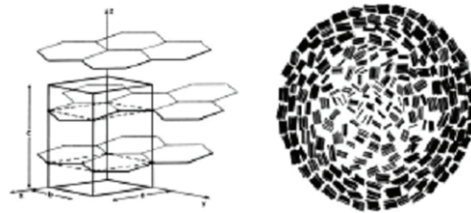
Figure 1.5 – Schematic of soot microstructure

It has to be stressed that, although a general agreement has been reached on the main formation pathways, this complex phenomenon, especially when applied to real fuels and to industrial combustion devices, is not completely understood.

A huge amount of literature is focused on carbonaceous particles formation in combustion, in the following only a rough outline of the soot formation mechanism is recalled, whereas for further details on chemical pathways the reader is referred to (Richter, 2000), (D'Anna, 2007).

The formation process includes many chemical and physical steps: as depicted in the sketch in Fig.1.6, the phenomenon starts with the formation of gaseous precursors of increasing molecular weight.

The first step involves benzene formation: the main pathway leading to the ring closure occurs through the recombination of two resonantly stabilized radicals of propargyl (C_3H_3) or through the addition of acetylene to i-C_4H_3 and i-C_4H_5.
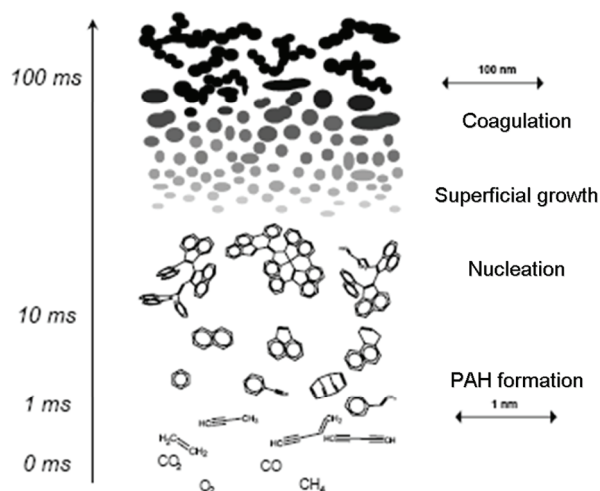
Figure 1.6 – Particles formation mechanism adapted from (Bockhorn, 1994)

The subsequent build up from benzene to naphthalene can take place through the HACA mechanism -Hydrogen Abstraction Acetylene Addition – that is a two-step process involving hydrogen abstraction, thus activating the aromatics, followed by acetylene addition. The HACA mechanism also involves multi-ring species, eventually leading to structures like phenantrene and coronene.

The alternative way for polycyclic species formation is the combination of two cyclopentadienil radicals or of benzyl and propargyl radicals.

Large PAHs can undergo further acetylene additions thanks to the high number of available sites, thus peri-condensed aromatic hydrocarbons (PCAH) are formed.

Moreover, the addition of aromatic molecules to aromatic radicals can give rise to biphenyl-like structures, also referred to as aromatic aliphatic-linked hydrocarbons (AALH).

PCAHs and AALHs grow up forming agglomerates of a few nanometers in diameter: such structures are held together by van der Waals interactions, whose intensity increases as the molecular mass of the compounds grows. Once stable clusters are formed, completely coalescent collisions among molecular particles yield to the smallest nanoparticles.

Recent works also address the importance of the PAH stacking (Happold, 2008) in the mechanism of particles inception.

These first solid particles are roughly spherical in shape and can undergo to several different growth processes: surface growth, further coagulation and agglomeration.

Acetylene and PAH are considered the most likely candidates for superficial growth.

As their size increases, rather than coalesce, the particles agglomerate into the mentioned chain-like structures.

In parallel, oxidation phenomena by hydroxyl radical and O_2 take place, causing a depletion of the particulate mass. As a result, the soot actually emitted in a combustion process may represent only a fraction of the soot formed in the combustion zone.

1.2   Organization of the thesis

In Chapter 2 the single cylinder diesel engine used to collect experimental data is described, together with the auxiliary systems and the engine instrumentation.

The modified version of the KIVA3V numerical code is addressed in Chapter 3, including the integration with the ChemKin code, the subsequent parallelization and the motivations for detailed kinetics adoption.

Chapter 4 reports the numerical tests carried out to study the computational issues arising from the introduction detailed kinetics, comprising a stiffness analysis and the study of the performances of two libraries of solvers for the solution of chemistry.

Chapter 4 also includes the description and the results of the activities of validation of the modified code, carried out comparing the measures collected fuelling the engine with pure heptane and the correspondent simulations.

Finally, in Chapter 5 the carbonaceous particles formation modeling is described, together with the first results achieved and a tentative comparison of the simulated particles size distribution functions with experimental data.

Bibliography

BOCKHORN H., *Soot Formation in Combustion*, Springer Verlag Berlin Heidelberg 1994.

BEATRICE, C., GUIDO, C., DEL GIACOMO, N., BERTOLI C., *Study of the compression ratio influence on the performance of an advanced automotive diesel engine operating in conventional and PCCI combustion model*, THIESEL 2008 Conf. on Thermo and Fluid Dynamic Processes in Diesel Engines, 2008.

D'ANNA, A., *Particle inception and growth: experimental evidences and a modelling attempt*, Proc. Intern. Workshop Anacapri, 2007.

ENG J.A., *Homogeneous Charge Compression Ignition (HCCI) Engines: Key Research and Development Issues,* PT-94, chapter 5, SAE, 2003.

HAPPOLD, J., GROTHEER, H.-H., AIGNER, M., *Soot precursors consisting of stacked pericondensed PAHs*, Proc. Intern. Workshop Anacapri, 2007.

KITTELSON, D.B., *Engines and nanoparticles: a review*, J.Aerosol Sci., 29, 1998.

KITTELSON D.B., WATTS W.F., JOHNSON J.P., *Ultrafine and Nanoparticle Emissions: A New Challenge for Internal Combustion Engine Designers*, Intern. Conf. "Engines of Sustainable Development", Naples 2003.

KITTELSON D.B., *Particle Measurement Methodology: Comparison of On-road and Lab Diesel Particle Size Distributions*, CRC Workshop on Vehicle Exhaust Particulate Emission Measurement Methodology, 2002.

SGRO, L.A., DE FILIPPO, A., LANZUOLO, G., D'ALESSIO, A., *Characterization of nanoparticles of organic carbon (NOC) produced in rich premixed flames by differential mobility analysis*, Proc. of the Comb 31, 631-638, 2007.

Chapter two

Experimental apparatus: single cylinder engine

2.1   Introduction

In this chapter the experimental layout and the engine configuration are presented. Only a brief description is included, as the present work mostly focuses on the modeling activities and the comparison between the measurements and the calculations results, while further details on the single-cylinder engine are presented in (Avolio, 2005).

The single-cylinder engine is characterised by the fact that all its components are very easily interchangeable and an independent control of each operating parameter is achieved. In fact, in four cylinder engine experiments, the engine-turbocharger interaction and the presence of all the auxiliary systems (injection pump, alternator etc.), impose the interdependence among the operating parameters. Moreover the exploration of different combustion system architectures, compression ratios and so on, are difficult to realise in a production engine. This is the reason why a single cylinder DI diesel engine prototype was developed at Istituto Motori.

In addition, it is worth recalling that the knowledge of the engine set-up and of the full intake-exhaust layout is very important also from a modeling point of view, because the uncertainty in the measurements, the variability in the engine behaviour are essential information for a sensible comparison between calculated and measured values. As an example, the positions of temperature and pressure sensors along the layout have to be taken into account when boundary and initial values are fixed or estimated.

2.1.1   Main characteristics

As already introduced, the advantage in developing a single cylinder diesel engine is due to the possibility to isolate the effects of individual operating parameters, that can be modified without any reciprocal coupling. As a consequence, the engine obtained is an investigation tool particularly suitable both for numerical simulations and for parameterization studies.

The whole engine system has been designed to achieve the maximum flexibility in the setting of the engine-operating mode. Therefore the engine has been equipped with auxiliary systems for boost, cooling, lubrication, etc. Moreover, for the same reason, it has

been characterised by a modular structure: the crankshaft, the cylinder and cylinder head can be changed keeping the same crankcase. Figure 2.1 shows a general view of the engine.
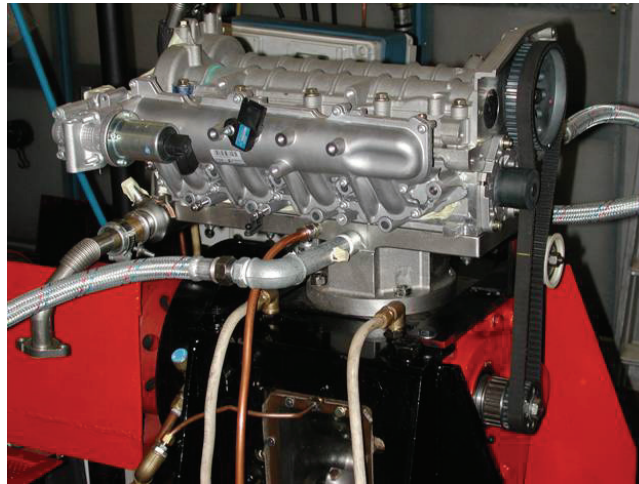

Figure 2.1 – View of the engine system.

Cylinder and crankshaft have been designed in Istituto Motori. Crankcase is a zero-vibration type characterised by two couples of clockwise and counter-clockwise shafts, in order to balance first and second order inertia forces. Cylinder head is derived from production series and is a 4-cylinder Fiat 1.9JTDM 16V; it has been modified to work in single-cylinder mode. Connecting rod and piston are derived from production series.

The engine configuration is reported in Table 1, and, as previously mentioned, refers to the 4-cylinder diesel DI Common Rail Fiat 1.9 JTD 16V Multijet in the Euro IV version.

Table 2.1 – Single Cylinder DI Diesel Engine Main features

Bore [mm]	82.0
Stroke [mm]	90.0
Compression Ratio	16.5 -14.5
Displacement [cm^3]	475
Valve number	4
IVO/IVC [CAD ATDC]	-9/200
EVO/EVC [CAD ATDC]	138.5/6.5
Injection system	Fiat Multijet Common Rail III gen
Injector	Ks 1.3/86 Microsac 7 holes 440mm^3/30 s/ 100bar

Two values of the compression ratio have been adopted, 16.5 and 14.5, whereas the lower one is used to investigate low temperature premixed combustion conditions.

In the next the main characteristics of each module and the auxiliary components are described.

2.2   Crankcase, crankshaft and cylinder

As previously introduced, the crankcase is a zero-vibration crankcase and was developed and supplied by CRF[3]. Two photos are reported in Figure 2.2.
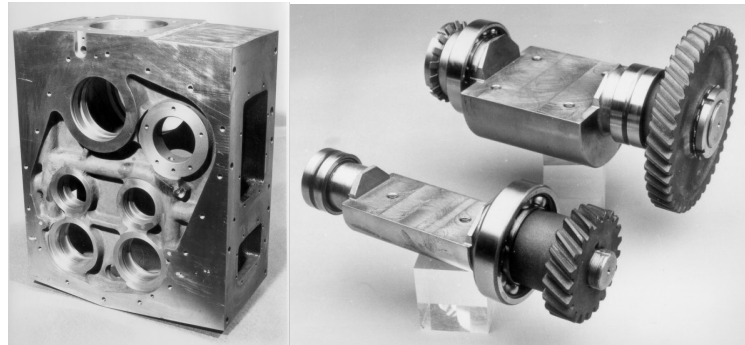
Figure 2.2 - A view of the zero vibration crankcase and balancing shafts.

It is realized by cast iron fusion and presents ducts for lubricating crankshaft mean bearings, balancing shafts bearings and gears. It is characterized by two couples of reciprocating shafts, gear-driven by crankshaft, to balance first and second order inertia forces. Balancing masses can be replaced in order to balance different crank assembly configurations. The crankcase is laterally open to look over crankshaft assembly and cylinder wall status without disassembly the whole engine.

The crankshaft, illustrated in Figure 2.3, has been sized to resist to a max combustion pressure of 180 bar at full load and at 5000 rpm. Besides, to improve the fatigue strength, a particular chemical and thermal process has been implemented. Further details on its design and on the lubrication can be found in (Avolio, 2005).
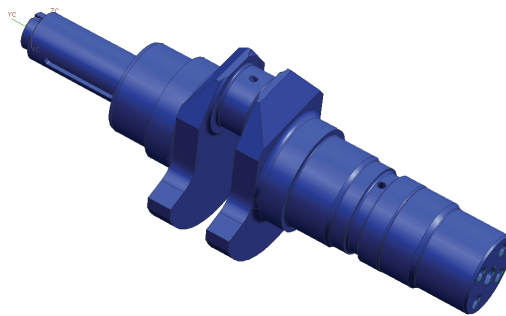
Figure 2.3 – 3D CAD view of engine crankshaft.

---

[3] Centro Ricerche Fiat

The cylinder has been designed in order to couple with the crankcase in the lower part and with the production cylinder head in the upper one.

It has been realized in two machined parts: the external block and the internal cylinder, both of cast iron. The water chamber has been obtained gaining a volume between the two parts. A 3D picture of the cylinder is reported in Figure 2.4.
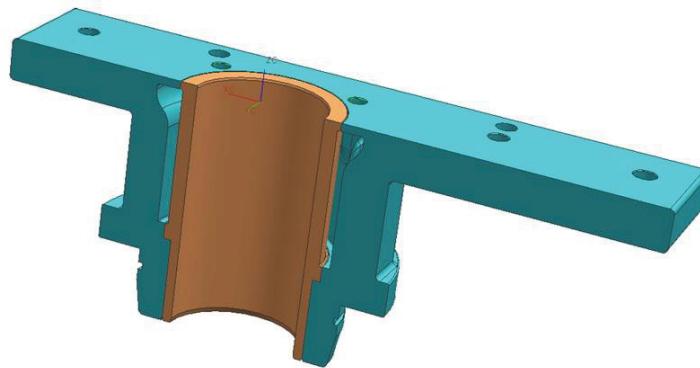
Figure 2.4 – 3D CAD view of the external block and internal cylinder.

It can be noted that the internal gap is thicker in the upper part, due to the higher temperatures reached in this area, therefore here a stronger cooling is required.

The external block widens forming a plate, in order to realize a safe coupling with the 4-cylinder head: in this way, an effective support to the head is obtained, together with the possibility to exploit all the check pins for an optimal sealing.

2.3   Cylinder head and piston geometry

The engine head has been delivered by CRF and is the 4-cylinder head of the reference engine. The choice of installing a multi-cylinder head is mainly due to the complication of reproducing the operating characteristics of the production series one.

Rocker-arms relative to unused valves have been removed and correspondent ducts for the hydraulic control have been plugged in order to achieve the right supply oil pressure to operating rocker-arms.

Two separated water-cooling systems have been adopted in order to ensure a better control of the operating temperatures for cylinder and engine head.

The engine head is a flat type with vertical centred injector and four valves driven by two overhead camshaft. The two intake ducts are helical and directed port type, respectively. A swirl regulation throttle is placed in the last one and controlled via the engine ECU[4], as reported in the scheme of Figure 2.5.
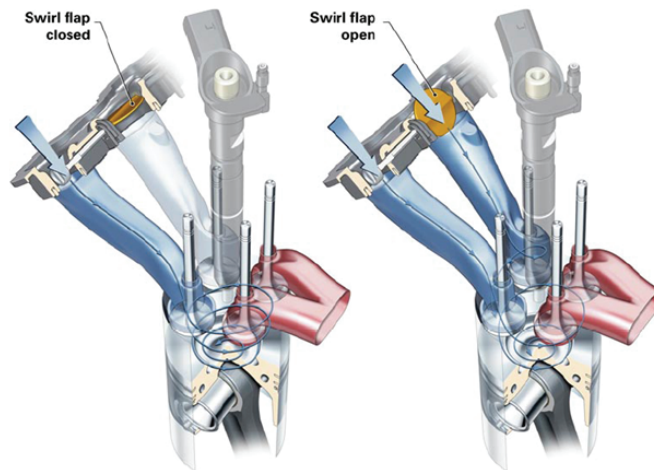
Figure 2.5 Intake and exhaust ducts: swirl index control

The piston, as shown in Figure 2.6, exhibits a hollow in its upper part, usually known as bowl, that constitutes the combustion chamber. Its shape has a crucial role in influencing the air flow during the compression phase: it is usually properly designed in order to enhance the air-fuel mixing (Heywood, 2000) (Della Volpe, 1999) (Bertoli, 1989).

As an example, the central elevation centrifuges the charge and rises the turbulence level, thus improving the mixing process. In addition, several other parameters, such as the squish area (i.e. the piston superior surface excluding the combustion chamber), the ratio between the bowl volume and the dead space (K factor), are capable of modifying the interaction between the fuel jet and the air.

---

[4] Engine Control Unit

Figure 2.6 View of the piston with the internal bowl

A sketch of the bowl section is reported in Figure 2.7, clearly indicating that around the top dead centre the combustion phenomenon takes place inside this volume.
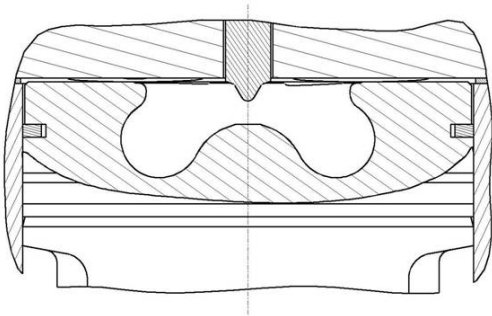
Figure 2.7 Lateral section of the piston bowl

2.4   Auxiliary Systems

2.4.1   Intake and Exhaust Line

Supercharging is realized thanks to an external system, in order to set the inlet air pressure independently from the engine speed: the system is made up of a volumetric compressor and an automatic circuit for the control of the air temperature and pressure. A sketch of the supercharging system is reported in 2.8.
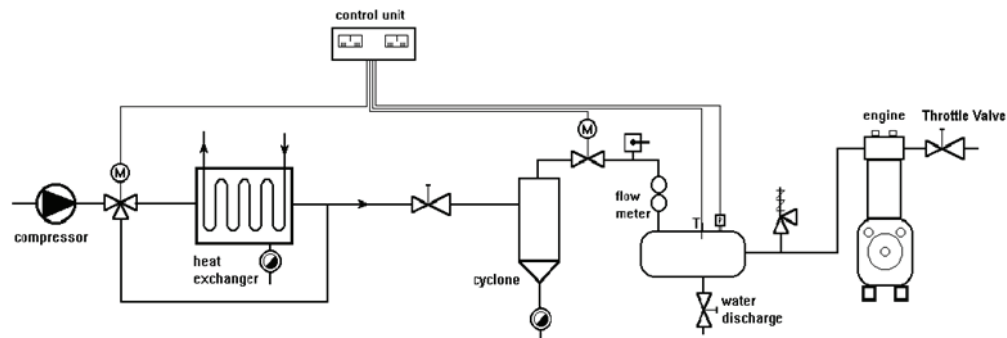
Figure 2.8 – External compressor for supercharging

The compressor is an ATLAS COPCO BE 43, alternative, two-cylinder, cooled by air. Its displacement is 7603 cm3 and the maximum pressure reachable is equal to 3.5 barG.

The compressor is driven by an asynchron electric engine, with a power of 37kW at 2940 rpm: it is possible to vary the electric engine speed thanks to an inverter, thus regulating the air boost pressure at the compressor outlet between 0÷4.5 bar gauge.

Moreover the air temperature can be varied in a wide range of values (20-100°C), thanks to an air-water heat exchanger, while a damping volume for the pressure oscillations ensures a constant air pressure at the internal combustion engine inlet.

The plant also includes a cyclone for the condensed mass separation.

The air flow rate is measured by a lobe flowmeter PRINTSCH BAMAG 66 TYP 150, capable of measuring a maximum flow rate of 180 m3/h.

In the damping volume the air temperature is measured by a thermo-resistance PT100, while pressure is detected through a transductor (H&B AEC 200 0-6 barG), as visible in Figure 2.9: in this way it is possible to calculate the air mass flow rate, once the volumetric flow rate is measured.

In the intake duct temperature and pressure of the total inspired mass, comprising the recycled exhaust gas, are measured, by a thermo resistance PT100 and a transducer (GEMS 220A-G-A25-01-3-U-A 0 – 2.5 barG) respectively.

Finally a fast pressure transducer is installed (Kulite ETL 173-190M 0 – 2 barA) to evaluate the instantaneous pressure in the intake duct and thus to analyse the pressure pulsations.
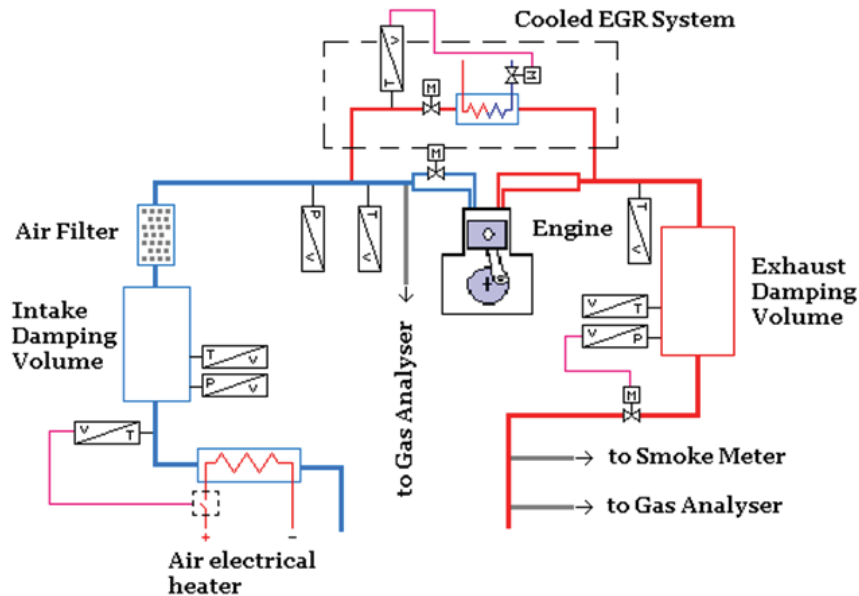
Figure 2.9 - Scheme of intake-exhaust line layout

The exhaust line has been realized simulating the presence of the turbocharger. Therefore a damping volume and, downstream, a throttle valve have been placed. Throttling the valve, in closed loop by the ECU, it is possible to regulate the engine back pressure. By means of an adequate choice of the damping volume and valve diameter it is possible to realize the same back pressure range of the production turbocharger.

The exhaust gas temperature is measured downstream the exhaust valves and in the damping volume through two K thermocouples, while the pressure in the exhaust line is detected by means of a fast pressure transducer (Kulite EWCT 312M 0 - 3.5 barA).

These values are useful to estimate, in the numerical calculations, the internal EGR or the mass still trapped in the cylinder after the exhaust valve closure.

The cooled EGR line has been designed as short as possible in order to reduce pressure losses. Moreover, to ensure a fine regulation of exhaust gas temperature at the inlet manifold, a small-size EGR cooler was chosen. Actually, the production EGR cooler had a too high exchange efficiency for a single-cylinder engine. The cooler is fed by an external water circuit, automatically controlled, in order to regulate EGR temperature independently from the engine water one. Figure 2.9 shows the intake and exhaust line layout.

2.4.2 Fuel supply System

Fuel supply is derived by production series: it is constituted by a low pressure circuit (tank, balance meter, filter, low pressure pump, fuel cooler) and a high pressure one (high pressure injection pump, rail, connection pipe, injector), as reported in Figure 2.10.

In order to regulate the pressure in the rail independently from the engine speed, the injection pump is driven by an electrical motor (Drive AX 3.8 kW at 3000 rpm/min).

The injection system is a third generation one characterized by the control of the quantity of elaborated fuel and maximum pressure up to 1600 bar. The injector is a "microsac" 7 holes.

In the injector back line a one-way valve has been installed to realize a steady constant back-pressure. A water-fuel cooler controls automatically the fuel temperature at the inlet of the low-pressure pump.
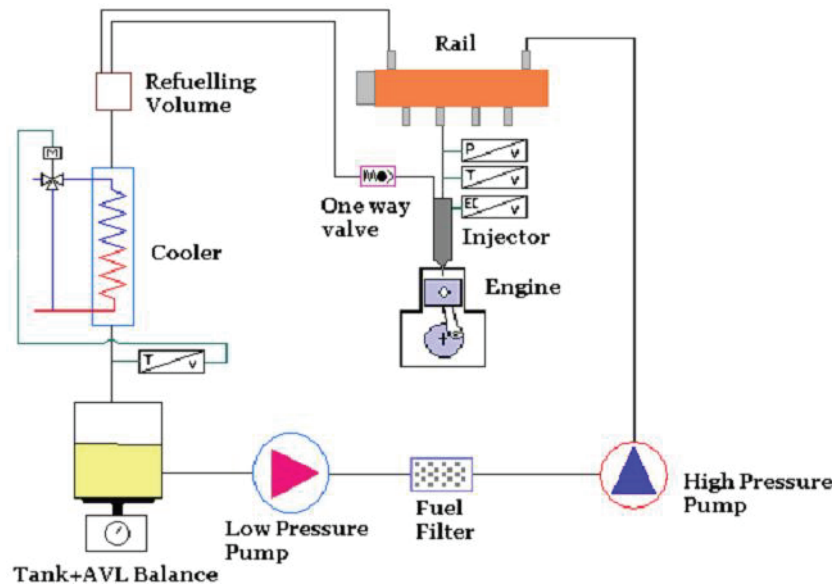
Figure 2.10 - Fuel supply layout

On the connection between the rail and the injector a piezoresistive transducer has been installed (Kistler 4067 A2000), to measure the instantaneous pressure in the duct: such measurements are extremely useful to evaluate the injection rate evolution and to check the engine response to a particular injection strategy. It also permits to verify – for the initial conditions of the numerical calculations – the real injection time, apart from the energizing current signal.

However a measure of the energizing current is available too, in order to check the injection duration and the needle lift timing.

2.5 Engine instrumentation

A list of the sensors necessary for the combustion diagnostics and the numerical simulations validation is briefly resumed in the following.

Inlet air flow measurement and fuel consumption are performed by means of a volumetric air flow meter and a gravimetric balance (AVL 733).

The characterisation of air condition in the intake manifold, in terms of dynamic pressure and temperature values, is performed by a piezo-resistive absolute pressure transducer for instantaneous boost pressure measurement (Kulite ETL193-190M) and by a PT100. A gas sampling probe has also been installed to measure CO_2 and O_2 inlet concentrations.

Cylinder pressure is carried out with a piezo-quartz transducers (Kistler 6121 A1) placed in the glow-plug hole, while temperature and pressure values, immediately downstream the exhaust valves, are preformed by a type-K thermocouple and an instantaneous cooled piezo-resistive absolute pressure transducer (Kulite EWCT-250/312M).

Instantaneous injection pressure and temperature measurements in the connecting pipe between rail and injector are obtained with a piezo-resistive transducer (Kistler A4067 A2000), while the energizing current that drives the injector is acquired by a current sensor (MicroSwitch 9617).

A shaft optical encoder with a maximum angular resolution of 0.1 crank angle degree (AVL 365C) permitted the synchronization of the signals which are acquired by an AVL Indiskop 647.

2.6 Exhaust gas measurement

On the exhaust pipe line, downstream the throttle valve, two gas sampling probes collect the exhaust gas for the measurement of HC, CO, NOx, CO_2 and O_2 concentration.

Moreover it is also possible to measure CO_2 and O_2 concentration in the recycled stream to evaluate the exhaust gas recirculation really realized.

The exhaust gas is collected downstream the damping volume and sent to the analysis test bench through a pipe heated at 180°C, in order to prevent water condensation. Moreover, a particulate filter removes solid particles in order to clean the sampled gas.

The unburned hydrocarbon and nitrogen oxides measures are on a humid basis, while the instruments for the CO, CO_2 and O_2 detection work on a dry basis.

A measure of the mass of the particulate matter emitted can be performed through an AVL smokemeter 415S (AVL): the sampled exhaust gas is filtered and the amount of particulate, in terms of mass concentration, is inferred from the filter blackening, evaluated by a light reflection principle.

Bibliography

AVOLIO, G., BEATRICE, C., BERTOLI, C., *Development of a Single Cylinder Direct Injection Diesel Engine for advanced combustion system studies* – Istituto Motori CNR; HTCES 2005, 26-27 Maggio 2005 Modena Italy.

BERTOLI, C., MIGLIACCIO, M., *Il motore diesel per la trazione stradale*, Rocco Curto Editore, 1989.

DELLA VOLPE, R., MIGLIACCIO, M. *Motori a Combustione Interna*, Cuen Editore, 1999

HEYWOOD, J.B., *Internal Combustion Engine Fundamentals*, McGraw-Hill, 2000.

Chapter three

KIVA3V and detailed kinetics: a parallel version

3.1   Introduction

In this chapter the numerical codes used in the current work are presented, together with the modifications implemented in order to adopt detailed kinetics reaction schemes.

In Par.3.2 the original version of the KIVA3V code is illustrated and in Par.3.3 a quick outline of the ChemKin code is given.

In Par.3.4 the parallel version of the code, coupled with ChemKin, developed at Istituto Motori (Belardini, 2004) is discussed, together with the motivations and some implementation details.

3.2   The KIVA3V code

The numerical simulations performed are obtained by means of a modified version of the KIVA3V rel.2 code (Amsden, 1999).

KIVA is a popular computer program for the calculation of three-dimensional chemically reactive transient flows with sprays, especially suited for engine applications. The code is structured as a collection of Fortran subroutines performing single specific tasks. The program solves the unsteady equations of motion of a turbulent, reactive mixture of ideal gases, coupled to the equations for a vaporizing fuel spray.

3.2.1   Gas phase governing equations

As concerns the gas phase, the problem is represented by the mass, energy and momentum conservation laws: the Navier-Stokes equations for gas flow are used. The presence of the liquid-phase affects the gas-phase equations by additional source terms, representing the mass, momentum and energy exchange.

Given that a reacting flow has to be modelled, a mass balance for each chemical species is written, thus the continuity equation is specified for every species *m* included in the combustion model:

$$\frac{\partial \rho_m}{\partial t} + \nabla \bullet (\rho_m \mathbf{v}) = \nabla \bullet (\rho D \nabla Y_m) + \rho'^c_m + \rho'^s_m \, \delta_{m1} \qquad (1)$$

where ρ_m is the mass density of species m, ρ the total mass density and $\mathbf{v}$ the fluid velocity vector. The first term on the right hand side expresses the Fick's diffusion law: it has to be noted that in KIVA equal Schmidt numbers among all the species are assumed, then the diffusion will have a single diffusion coefficient.

The source term due to chemistry is here synthetically indicated as ρ'^c_m and includes all the reaction rate expressions relative to every reaction in which the species m is involved:

$$\rho'^c_m = W_m \sum_{r=1}^{NRK} (b_{mr} - a_{mr}) \omega'_r (T, \rho_i) \qquad (2)$$

where W_m is the molecular weight of the species, a_{mr} and b_{mr} the stoichiometric coefficients of species m in reaction r, when m appears among products or reactants, respectively. Finally, ω'_r in expression (2) is the net rate of reaction r, depending on the local temperature and on the species concentrations:

$$\omega_r' = k_{fr}(T) \prod_{m=1}^{NSP} (C_m)^{a'_{mr}} - k_{br}(T) \prod_{m=1}^{NSP} (C_m)^{b'_{mr}} \qquad (3)$$

The last term in Eq.(1) ρ'^s_m is the source term due to the spray contribution to the fuel mass. Species 1 is the species correspondent to the fuel, so δ_{m1} is 1 for the fuel and 0 for all the other components.

The momentum equation is then expressed as follows:

$$\frac{\partial (\rho \mathbf{v})}{\partial t} + \nabla \bullet (\rho \mathbf{v} \mathbf{v}) = -\nabla p - A_0 \nabla (\tfrac{2}{3} \rho k) + \nabla \cdot \overline{\overline{\sigma}} + \mathbf{F}^s + \rho \mathbf{g} \qquad (4)$$

where p is the fluid pressure and $\mathbf{F}^s$ is the rate of momentum gain per unit volume due to the spray.
The viscous stress tensor σ in Eq.(4) is modelled as for a Newtonian fluid, according to the following form:

$$\overline{\overline{\sigma}} = \mu \left[\nabla v + (\nabla v)^T \right] + \lambda \nabla \bullet \mathbf{v} \mathbf{I} \qquad (5)$$

where the transport coefficients for turbulent viscosity μ and λ are expressed in dependence on the turbulent kinetic energy and its dissipation rate (Amsden, 1989).

In KIVA3V the turbulence effect on the mean flow is modelled through the classical k-ε model (Launder, 1974), or, alternatively, through its variant Renormalization Group (RNG) model (Han, 1995): in both cases a RANS approach (Versteeg, 2007) to the turbulence modelling is used. As a consequence, only the mean flow field is calculated and turbulence effects are taken into account including some additional terms to the momentum and the energy equations.

So, in Eq.(4) A_0 is zero in laminar cases and unity when one of the turbulence models is active.

The energy conservation law is:

$$\frac{\partial(\rho E)}{\partial t} + \nabla \cdot (\rho \mathbf{v} E) = -p\nabla \cdot \mathbf{v} + (1 - A_0)\overline{\overline{\sigma}} : \nabla \mathbf{v} - \nabla \cdot \mathbf{J} + A_0 \rho \varepsilon + Q'c + Q's \qquad (6)$$

where E is the specific internal energy and the heat flux vector $\mathbf{J}$ is the sum of thermal conduction contribution and enthalpy diffusion due to chemical species diffusion:

$$J = -K\nabla T - \rho D \sum_m h_m \nabla(\rho_m / \rho) \qquad (7)$$

where h_m is the specific enthalpy of species m.

In Eq.(6) the terms Q'_c and Q'_s indicate the energy source terms due to chemical heat release and spray interactions respectively. As in the momentum equation, also in Eq.(6) A_0 is zero for laminar motion, so the turbulent dissipation energy term $A_0\rho\varepsilon$ would be absent in such a case. On the contrary in turbulent flows $A_0=1$ and the energy dissipation term for viscous stresses, $\sigma : \nabla \mathbf{v}$, is excluded.

When the turbulence model is used, the transport equations for the additional unknowns turbulent kinetic energy k and its dissipation rate ε are solved:

$$\frac{\partial(\rho k)}{\partial t} + \nabla \cdot (\rho \mathbf{v} k) = -\tfrac{2}{3}\rho k \nabla \cdot \mathbf{v} + \overline{\overline{\sigma}} : \nabla \mathbf{v} + \nabla \cdot \left[(\tfrac{\mu}{\mathrm{Pr}_k})\nabla k\right] - \rho \varepsilon + W'^s \qquad (8)$$

$$\frac{\partial(\rho \varepsilon)}{\partial t} + \nabla \cdot (\rho \mathbf{v} \varepsilon) = -(\tfrac{2}{3}c_{\varepsilon 1} - c_{\varepsilon 3})\rho \varepsilon \nabla \cdot \mathbf{v} + \nabla \cdot \left[(\tfrac{\mu}{\mathrm{Pr}_\varepsilon})\nabla \varepsilon\right] + \tfrac{\varepsilon}{k}(c_{\varepsilon 1}\overline{\overline{\sigma}} : \nabla \mathbf{v} - c_{\varepsilon 2}\varepsilon \rho + c_s W'^s) \quad (9)$$

where $c_{\varepsilon 1}$, $c_{\varepsilon 2}$, $c_{\varepsilon 3}$, Pr_k and Pr_ε are constants derived from experiments or theoretical considerations. Further details on standard values for engine applications are given in (Amsden, 1989).

The term $W^{'s}$ represents a source term due to interaction with spray and a value of c_s equal to 1.5 in Eq.(9) is usually adopted, based on the postulate of length scale conservation in spray turbulence interactions.

The gas-phase solution procedure is based on a finite volume method called ALE (arbitrary Lagrangian-Eulerian) method. Spatial differences are formed on a finite-difference mesh that subdivides the computational region into a number of hexaedrons. The mesh is block structured and is modified during the simulation to reproduce the cylinder motion.

Each cycle is divided into two phases: a Lagrangian phase and a rezone phase. In the first one the cell vertices move with the fluid velocity, and there is no convection across cell boundaries. In the rezone phase, the flow field is frozen, the vertices are moved to the new user-specified positions and the flow field is remapped onto the new computational mesh.

3.2.2 *Spray models*

The coupling source terms between the gas-phase and the liquid-phase are critical to diesel simulation and they rely on the mathematical description of the spray.

After injection, the jet undergoes a sequence of subprocesses including atomization, droplet breakup and collision, turbulent dispersion, and evaporation.

In the version of the code modified at Istituto Motori, that represented the starting point before parallelization, the atomization process adopted is an hybrid model reported in (Belardini, 1998), based on the break-up models WAVE (Reitz, 1987) and the Taylor Analogy Breakup –TAB- model (O'Rourke, 1989).

The WAVE model, accounting for primary break up, describes the jet break up evaluating the stability of a liquid column under the perturbations due to the interaction with air. The liquid is represented through discrete particles, called blobs, that undergo disintegration. The wavelength of the waves on the blobs surface determines the size of the "son droplets".

The TAB model is developed on the basis of an analogy between an oscillating and distorting droplet and a spring mass system. The droplet equilibrium state corresponds to a sphere, then the displacement of the droplet equator from its equilibrium is determined.

The external force represents the effect of gas aerodynamics forces, the spring elastic reaction corresponds to surface tension and the damping is determined by the liquid viscosity.

The droplet evaporation model is the classical Spalding model, modified in order to include the heating inside the single droplets (Bertoli, 1999).

The instantaneous speed of the injected fuel is measured at the injection test bench: due to the high injection pressure, cavitation at the exit of the injector holes is likely to occur, so the (Kong, 1999) model for the flow through the hole is used.

3.3 The ChemKin code

ChemKin (Kee, 1991) is a software package for the calculation of gaseous reacting flows: it permits to predict the behaviour of a reacting system, once the system kinetics (species considered and correspondent reactions network) is set by the user.

One of the features that made this software very popular is the practical handling of the reaction mechanisms, together with the thermodynamic and transport properties databases: in fact such data are formally separated by those concerning the geometrical and fluid dynamics details, being stored in independent input files.

The data that identify a certain chemical system are therefore represented in an efficient manner, resulting applicable, in a subsequent phase, to different "reaction" environments.

This is the reason why it has been possible to rely on the ChemKin data organization and implement some of its subroutines in a different software like KIVA.

More in detail, it is possible to distinguish two main software components: the Interpreter and the Library. The first one, on the basis of a symbolic description of the reaction scheme (species and reaction rates lists, together with the reaction rate parameters), produces a binary linking file, that contains a complete characterization of the reactive system. In practice, not only the kinetic behaviour, but also all the thermodynamic and transport properties of the species are comprised. This file is then "problem independent" and can be subsequently be applied to whatever flow condition.

The Interpreter also checks whether the input data are correctly edited, coherent and complete: when huge reaction mechanisms are used, such controls turn out to be very useful, as trivial errors are automatically detected before any CFD simulation.

The Library contains all the subroutines necessary for the specific problem calculation, each performing a defined task, like the calculation of the enthalpy of the mixture, or the equilibrium constants etc.

3.4   KIVA3V and detailed reaction kinetics: modified version

The number of chemical species that can be accounted for in the original version of KIVA3V is, in theory, arbitrary, but the code had actually been used with models made up of about ten species. Reaction mechanisms really implemented to simulate combustion kinetics in an unchanged version were therefore small groups of global reactions, while detailed kinetics was not realistically applicable, as even a preliminary check on the thermo-kinetic database was absent.

Furthermore, in the original version of the code, faster reactions were considered at equilibrium: reaction kinetics is taken into account only for the slower steps.

The ignition delay time was calculated on the basis of empirical correlations, instead of deriving from the fuel autoignition kinetics: as a consequence, the resulting combustion model could not be very flexible.

In the following the modifications realized in order to adopt detailed kinetics schemes[5] are presented.

In the next Paragraph 3.4.1 the motivations for such adoption are discussed, while in the subsequent ones some practical implementation details and their numerical consequences are illustrated.

3.4.1   Why detailed kinetics for internal combustion engine simulations?

First of all, when a higher number of reactions and paths make up the whole combustion event, the temporal evolution of the heat release rate and the system thermodynamics derive "naturally" from the gaseous mixture kinetic behaviour. In general the system dynamics is represented in a more realistic way.

Moreover, a network of elementary reaction steps can resemble the sensitivity of the real chemical system to local conditions, thus the model has the intrinsic potentiality to distinguish among spatial variations. The numerical predictions can then provide us with the spatial distributions of significant intermediates, radicals or pollutants and a deeper analysis of the fuel autoignition and of the pollutants formation can be obtained. Consequently, the calculated values could be compared with images from optically accessible engines, having the opportunity to perform a spatial validation too.

In addition, the model sensitivity to different engine operating conditions is another great potential advantage: once boundary and initial conditions are properly updated, a single model can show the capability of covering several points of the engine map, like shown in Chapter 5.

---

[5] Strictly speaking, the expression "detailed kinetics" is usually referred to the most complete reaction mechanisms, typically including up to several thousands steps. Here the term is used to simply refer to reaction schemes made up of elementary steps (thus including different categories, indicated in literature as skeletal, semi-detailed, reduced or detailed mechanisms), independently from the number of reactions. The actual level of detail adopted will then be arbitrarily set by the user (disregarding at the moment the computational issues arising with the adoption of huge mechanisms).

Finally, as already discussed, in the next future the distinction between diesel and spark ignition engine could be more blurred: as a consequence, in LTC-like combustion conditions (see Paragraph 1.1.1), the gaseous kinetics is expected to control autoignition and fully determine the ignition delay. As a result, traditional empirical correlations for the ignition delay are not able to describe the low temperature ignition process and the cool flames preceding the main heat release, thus the combustion models attain a crucial role.

Of course all that glitters is not gold: the implementation of a detailed scheme has a certain cost and several computational issues arise. Therefore, in order to choose a kinetic model and decide which level of detail is worthy, the aim of the simulations and any other sources of uncertainties have to be taken into account.

In fact combustion kinetic models can traditionally comprise very different level of detail of the reaction process: it is possible to found in literature enormous mechanisms made up of hundreds of species and thousands reactions, but also reduced models including very few species (Zheng, 2004), (Ranzi, 1995), (Tsang, 2004). A very high level of kinetic description is not always necessary, or, as an example, the predictions reliability could be vanished by the uncertainties on the boundary conditions, especially in the engine simulation framework.

As an example, if the main scope of the calculation is a qualitative description of the combustion development for a conventional diesel combustion, then the use of a high number of intermediates can be unnecessary: a good prediction of the ignition delay is traditionally already obtained by means of three or four global steps.

To sum up, detailed kinetics adoption in engine multidimensional simulations offers great opportunities, whereas the level of detail best suited for each specific case has to be carefully considered.

3.4.2 A parallel version of KIVA3V with ChemKin format reaction mechanisms

In order to handle the huge thermo-kinetic databases typical of detailed kinetics, in the modified version (Belardini, 2004), the KIVA3V code has been integrated with ChemKin (Kee, 1989).

In this way it is possible to exploit the popular format of the reaction mechanisms and the efficient control of the ChemKin Interpreter over the input data.

The linking ChemKin file containing the reaction rate parameters becomes an additional input file for KIVA. Then the ChemKin Library is incorporated into the original KIVA source code and is devoted to the calculation of all the terms due to the reactivity, like production and consumption rates, the enthalpy of the reacting mixture or the equilibrium constants. In fact KIVA still manages all the other tasks, like the grid evolution, the calculation of the spray and of the gas flow, the boundary conditions etc., except for the computation of the chemical source terms in the mass and the energy conservation equations – Eq.(1) and Eq.(6) in Paragraph 4.2.1.

The subroutines from ChemKin Library are thus called only at the time of the gas-phase reaction modelling.

Bearing in mind the gas-phase equations recalled in Par.3.2.1, it is important to clarify that the KIVA solution procedure employs a so called splitting technique: during a fixed time interval, a sequential solution of the equations is adopted, according to the scheme in Fig.3.1. Once calculated the spray, reaction and diffusion are treated, then the SIMPLE[6] algorithm is used to solve momentum, energy and pressure.

As a result, in a certain phase of the computations, the system arising from the pure solution of reaction kinetics is solved, including only the chemistry source terms and excluding both diffusion and convection terms. This is a system of ordinary differential equations, whose treatment is submitted to independent ODE solvers libraries.

```
set parameters(N_time_steps, N_simple_steps)
for i=1 to N_time_steps do
      define time splitting interval Δt;
      solve spray;
      solve combustion;
      solve mass density;
      for j=1 to N_simple_steps do
              solve momentum;
              solve energy;
              solve pressure;
              if (test_conv) return;
      endfor
      solve turbulence;
endfor
```

Figure 3.1 – General organization of the solution procedure

---

[6] Semi-Implicit Method for Pressure-Linked Equations For a description of this widely used algorithm see, as an example, (Versteeg, 2007).

So the modifications described in the following, like parallelization and the solver choice, essentially involve the ODE system representing the combustion sub-model.

The mass balances calculations, once separated from the "fluid dynamics parts" of the code, do not influence the choice of computing time step: looking again at Fig.3.1, it is possible to see that an overall time step is chosen, as the time-splitting interval in which chemical reaction equations have to be solved. Then, in each grid cell, the ODE solver has to select time sub-step sizes for the ODE system integration.

In this way, chemical reaction time sub-steps are related to the local conditions, rather than to the overall condition of the reactive system: the quality of the computation is locally refined coherently with the complexity of the phenomena.

Due to the introduction of more detailed reaction mechanisms, a much higher number of equations has to be solved - the mass balances of every species taken into account.

Therefore the code has been parallelized: the calculations have been carried out on a Beowulf-class Linux cluster, made of 16 Pentium IV 3.8 GHz processors connected via a Fast Ethernet switch available at Istituto Motori.

In (Belardini, 2004) it was verified that, in a computational domain of about 12000 cells, more than the 95% of the computing time was spent for the chemistry: the time needed for the fluid dynamics and thermodynamic parts of the code was negligible, as shown in Figure 3.2.
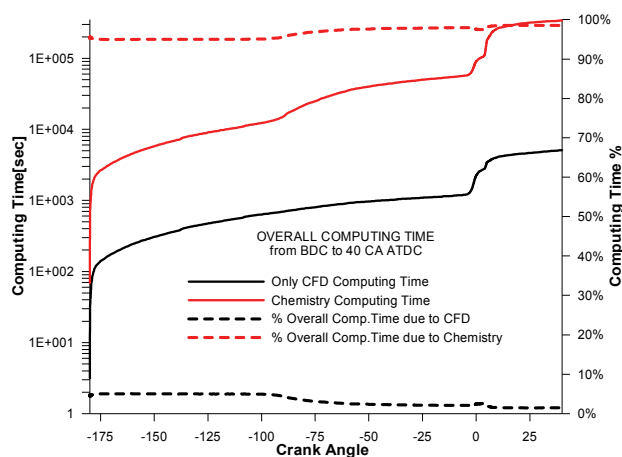

Figure 3.2 – Fractions of computing time devoted to the CFD calculations and to the chemistry solution

So the code modifications were mainly applied to the chemical module. The simulation runs only on the master node until the chemical phase is reached. Then the job is split among all the available nodes. At the end of the chemistry phase, all the data are collected on the master node, where the rest of the computation takes place (Fig. 3.3). Standard message passing software (Lam/MPI) was employed to control the nodes and to synchronize data among the processors.
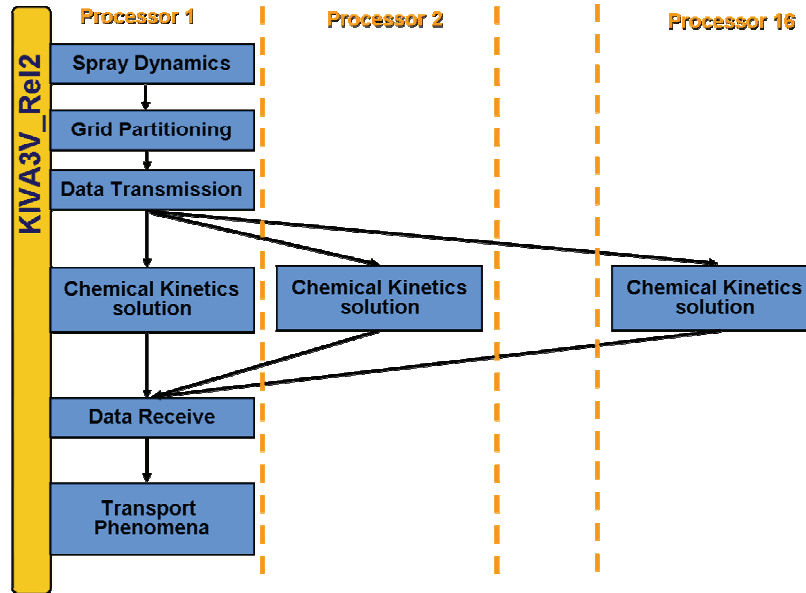
Figure 3.3 – Job splitting among the processors

Due to the great spatial variability typical of diesel combustion, a proper partitioning of the computational domain among the computing nodes is a critical issue in the load balancing. In other words, different groups of cells are characterized by quite different values of temperature and composition, so that, while the fast ignition dynamics occurs in a certain cell, in near positions the reactivity could be substantially idle.

As a result, the integration algorithm chosen for each cell may differ both in terms of method chosen, and of time sub-step, depending the local conditions. In this framework the best balancing of the workload was obtained when cells are split randomly among the processors. In Fig. 3.4, a picture of the random grid partitioning is reported, obtained with a an equally probable distribution of the domain cells, without replications, among all the available processors: the cells are coloured according to the processor they are assigned to.
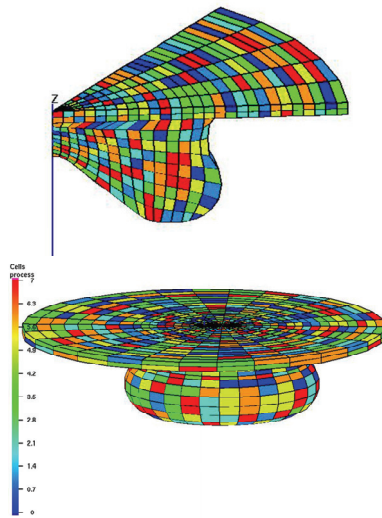
*Figure 3.4* – Random partitioning of the computational domain
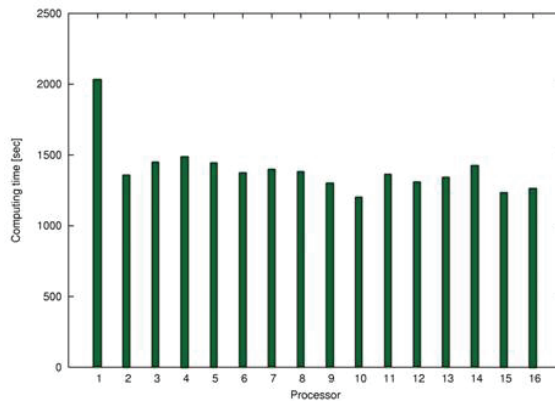
Figure 3.5 – Load balancing among the processors

In Fig. 3.5 the computing time for each process in a run over 16 processors is shown: the diagram indicates a good load balancing. The master node (processor 1) is obviously more engaged due to the CFD computations and to the monitoring operations.

3.5   Turbulence chemistry interactions

As already mentioned, KIVA turbulence calculations essentially rely on the k- ε model, so only the average flow field is computed, according to the RANS approach.

The detail of instantaneous flow patterns is lost and turbulence effects on the flow features are taken into account through the adoption of proper expressions for the transport coefficients.

Moreover, due to the absence of eddies and field fluctuations, it is also necessary to consider the effects of turbulence on the mean reaction rates: since the kinetic rates expressions are highly non linear, average reaction rates greatly differ from rates computed at the average values of temperature and species concentrations in a fixed cell.

In the present version of KIVA a model based on the approach discussed in (Kong, 1995) is adopted. Such approach derives from the eddy-dissipation (ED) model of Magnussen (Magnussen, 1976). The ED model assumed that reaction rate is not controlled by the intrinsic kinetics, but the rate of combustion is comparable to the rate of the dissipation of eddies (i.e., ε/k) which controls the rate of intermixing of fuel and oxidizer.

In this approximation, it was substantially assumed that the fuel and oxidizer are contained in two different eddies and, once mixing is realized, the reaction instantaneously take place.

In (Kong, 1995) a similar approach is combined with the Shell autoignition model, but the turbulent control is active only after autoignition, therefore reaction kinetics controls the combustion rate during the ignition delay time.

This model relies on the assumption that the chemical characteristic time preceding autoignition is comparably larger than the turbulent mixing time.

The model already adopted in KIVA, before the introduction of detailed kinetics, is similar to the mentioned (Kong, 1995) approach: the characteristic time of reaction of each species depends both on a kinetic timescale and a turbulent timescale. The former is defined as the characteristic time needed by a species to reach equilibrium state under perfectly homogeneous conditions, the latter is the eddy break up time. More precisely, the characteristic time of reaction of species m is:

$$\tau_m^c = \tau_k + f \cdot \tau_t \tag{10}$$

where τ_k and τ_t are respectively the kinetic and the turbulent time scales of species m.

The turbulent timescale τ_t, is proportional to the eddy turnover time $\tau_t = C_2 k/\varepsilon$ where $C_2=0.142$ if the standard k-ε model is used, or $C_2=0.1$ if the RNG k-ε model is used. The delay coefficient f in expression (10) was assumed to be given by $f = (1 - e^{-p})/(1-e^{-1})$. The parameter p is the ratio of the combustion products to the total reactants concentrations and indicates the rate of conversion to products in a specific region. Its value varies from 0 (no combustion yet) to 1 (complete consumption of fuel). The delay coefficient f changes accordingly to p, depending on the local conditions.

Then a global kinetic time is calculated as:

$$\tau_k = \max (\tau_{fuel}, \tau_{CO}) \tag{11}$$

Finally, the net production rates due to reaction kinetics are scaled according to expression:

$$\frac{\partial y_m}{\partial t} = \frac{\partial y_m}{\partial t} * \frac{\tau_k}{\tau_k + f\tau_t} \tag{12}$$

It is worth to remark that in this simple model kinetic timescale is the same for all the species and, although turbulence-limited rates can be considered, every computational cell is still characterized by a single value, thereby essentially reproducing a well stirred reactor.

Furthermore, in the described model temperature fluctuations are practically not taken into account: at the moment, their effect on the autoignition predictions and on the particulate matter formation (addressed in Chapter 5) has not been estimated.

Some simulations have been performed to evaluate the effect of this model on the resulting predicted pressure cycle, as shown in Fig.3.6: it is clear that the inclusion of this turbulence effect on the reaction rates only affects the high temperature phase, as the autoignition dynamics in unchanged before the pressure rise.
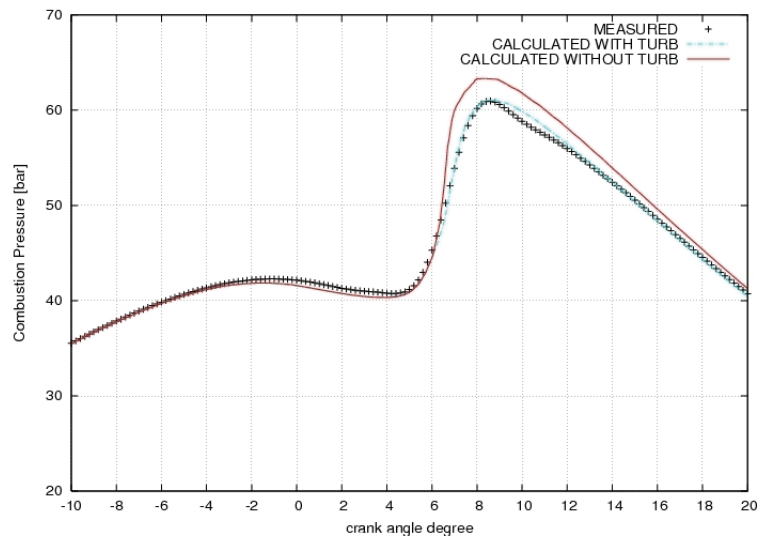

Figure 3.6 – Effect of turbulence-chemistry interaction over the predicted pressure cycle

In addition, it has to be remarked that this approach is a rather dated one: it is likely to be not very well suited to the new version of the code and future developments should of course address this issue.

In fact, although it has been successfully adopted mostly for conventional combustion conditions (and the whole performance of the code has actually given a satisfying agreement with experimental data, as will be illustrated in Par.4.3), in LTC combustion conditions a lack of accuracy in the predicted ignition delay is instead verified.

In the work of (Zhang, 2005) and in (Kung, 2006) a PDF method has been adopted to model a "pure" HCCI engine[7] combustion, thus demonstrating the feasibility of bringing transported PDF methods to bear in modeling a three-dimensional time-dependent turbulent combustion system. In these papers the importance of turbulence-chemistry interactions has been assessed: it is interesting to note that, moving from homogeneous conditions towards higher degrees of mixture in-homogeneity (due to higher swirl ratio) turbulence effects become increasingly important and result in significant changes in predicted values of ignition timing and emissions.

In the present case, simulating a production diesel engine, perfect homogeneity can never be achieved, therefore our engine, when working in LTC conditions, is just generally characterized by a good level of mixing: as a result, the operative condition is ideally near just to the conditions where Zhang identifies the strongest impact of turbulence modeling on combustion features. A possible interpretation is that real LTC is in a delicate intermediate condition between full homogeneity (kinetically controlled) and the complete non-homogeneity typical of classical diesel combustion. The current simplified model can therefore properly behave only in the extreme cases.

It is possible to draw the conclusion that more complex models of interaction with the turbulent flow have to be adopted, especially if the purpose of the simulations is the LTC combustion representation.

---

[7] Fuel injected at the beginning of the compression stroke, i.e. about the bottom dead center. In such a case injection and combustion are fully decoupled.

Bibliography

AMSDEN, A.A., O'ROURKE, P.J., BUTLER T.D., *KIVA-II: A Computer Program for Chemically Reactive Flows with Sprays*, Los Alamos National Laboratory Report No. LA-11560-MS, 1989.

AMSDEN, A.A., O'ROURKE, P.J., BUTLER T.D., *KIVA3V RELEASE II IMPROVEMENTS TO KIVA3V*, Los Alamos National Laboratory Report No. LA-UR-99-915, 1999.

BELARDINI, P., BERTOLI, C., CAMERETTI, M.C., *Numerical analysis of the influence of the jet breakup model formulation on diesel engine combustion computations*, Atomiz. and Sprays Tech., 8, 123-154, 1998.

BELARDINI, P., BERTOLI, C., CORSARO, S., D'AMBRA, P., FRAIOLI, V., *Application of a multi-method ODE software component for simulations of ultra-low emissions diesel engines*, Fisita F2006P027, 10, 2006.

BELARDINI, P., BERTOLI, C., CORSARO, S., D'AMBRA, P*: The impact of different stiff ODE solvers in parallel simulation of Diesel combustion.* In LNCS Vol. 3726 "High Performance Computing and Communications", Springer Berlin, 2005.

BELARDINI, P., BERTOLI, C., DE MARINO, P., AVOLIO, G., *A New Parallel Numerically improved KIVA3V Program for Diesel Combustion Computations*, IMEM, 2004.

BERTOLI, C., MIGLIACCIO, M., *A finite Conductivity Model for Diesel Spray Evaporation,* Intern. Journ. Heat Fluid Flow, 20, 552-561, 1999.

BROWN P.N., BYRNE G.D., AND HINDMARSH A.C, *VODE: A Variable Coefficient ODE Solver*, SIAM J. Sci. Stat. Comput., 1989.

HAIRER, E., WANNER, G., *Solving Ordinary Differential Equations II. Stiff and Differential-Algebraic Problems*, Second Edition, Springer Series in Comput. Mathematics, Vol.14, Springer-Verlag, 1996.

HAN, V Z., REITZ, R. D., *Turbulence Modeling of Internal Combustion Engines Using RNG k-e Models*, Comb. Sci. Tech. 106, 207 , 1995.

KEE, F. M., RUPLEY, MILLER, J. A., *Chemkin-II: A Fortran chemical kinetics package for the analysis of gas-phase chemical kinetics*, SAND89-8009, Sandia National Laboratories, 1991.

KONG, C., HAN, Z., REITZ, R. D, *The Development and Application of a Diesel Ignition and Combustion Model for Multidimensional Engine Simulation*, SAE Paper 950278, 1995.

KONG, S.C., MARRIOT, C.D., REITZ R.D., CHRISTENSEN M., *Modeling and Experiments of HCCI Engine Combustion Using Detailed Chemical Kinetics with Multidimensional CFD,* SAE 2001 01 1026, 2001.

KONG, S.C., SENECAL, P.K., REITZ R.D., *Developments in Spray Modeling in Diesel and Direct Injection Gasoline Engines ,* Oil & Gas Science and Tech 54, 1999.

LAUNDER, B.E., SPALDING, D.B., *The Numerical Computation of Turbulent Flows*, Comput. Methods Appl. Mech. Eng., 1974.

MAGNUSSEN, B. F. HJERTAGER, B. H., *On Mathematical Modeling of Turbulent Combustion with Special Emphasis on Soot Formation and Combustion*, 16th International Symposium on Combustion, Combustion Institute, 719-729, 1976.

O'ROURKE, P.J., AMSDEN, A.A., *The Tab Method for Numerical Calculation of Spray Droplet Break-up*, SAE Paper 872089, 1989.

RANZI, E., GAFFURI, P., FARAVELLI, T., AND DAGAUT, P, *A Wide Range Modeling Study of n-Heptane Oxidation*, Combust.Flame, 103, 1995.

REITZ, R.D., *Modelling Atomization Processes in High Pressure Vaporising Sprays*, Atomisation and Sprays Tech, 3, 1987.

TSANG W. *Progress in the development of combustion kinetics databases for liquid fuels*, Data Science Journal, 3, 2004.

VERSTEEG, H. K., MALALASEKERA, W., *An introduction to Computational Fluid Dynamics*, Prentice Hall, 2007.

ZHANG, Y.Z., KUNG, E.H., HAWORTH, D.C., *A PDF Method for Multidimensional Modeling of HCCI Engine Combustion: Effects of Turbulence/Chemistry Interactions on Ignition Timing and Emissions*, Proc. Comb. Inst. 30, 2763–2771, 2005.

KUNG, E.H., PRIYADARSHI, S., NESE, B.C., HAWORTH, D.C., *A CFD Investigation of Emissions Formation in HCCI Engines, Including Detailed NOx Chemistry*, Multidimensional Engine Modeling Users' Group Meeting, Detroit, MI, 2006.

ZHENG, J., MILLER, D.L., CERNANSKY, P., *A Global Reaction Model for the HCCI Combustion Process,* SAE 2004-01-2950, 2004.

Chapter four

Autoignition modeling and experimental validation

4.1   Introduction

The adoption of kinetic schemes made up of elementary steps typically introduces a very wide range of characteristic reaction times for the considered species, thus the mathematical system representing the model turns out to be very stiff.

A stiffness analysis in the engine simulations performed with the parallel version of KIVA3V is reported in the present chapter, together with the study of two different solvers behaviour in this framework. The numerical tests are relative to the engine and the conditions summarized in Paragraph 4.2.1.

A criterion to select, during the calculations, which solvers library is better suited to the local conditions has been set up and is described in Par. 4.2.2 and 4.2.3.

Afterwards the reliability of the modified version of the code has been tested through an extensive comparison between heptane combustion in the single cylinder diesel engines and correspondent simulations, in a wide range of different operating conditions and with two different values of the engine compression ratio, as described in Par.4.3.

For sake of clarity, some general features of autoignition kinetics in homogeneous systems are recalled here[8].

Looking at the sketch on the right hand side of Fig.4.1, generally speaking, two routes compete for the fuel molecule decomposition: H abstractions with subsequent chain branching through alkyl peroxides and direct decompositions with formation of smaller fragments, including olefins.

As long as the temperature is low, OH radical abstracts hydrogen from the fuel: the resulting heptyl radical undergoes oxygen addition. Then the peroxide isomerization occurs, followed by a further oxygen addition. The resulting species, here indicated as $C_7H_{14}O_2HO_2$, releases one OH radical and produces a ketoheptilperoxide (here C7KET21): up to this point the process is chain-carrying, but C7KET21 further decomposes, making the sequence chain-branching, with a net release of another OH radical.

Therefore C7KET21 is the low temperature chain branching agent: nevertheless such OH production is not responsible for the main heat release, since as soon as the temperature rises (about 900K), the chemical equilibrium for the addition of O_2 to heptyl radicals shifts

---

[8]Although referred to n-heptane, the following development takes place in a similar manner also for larger aliphatic hydrocarbons, whereas a higher number of possible isomers are formed, giving rise to further reaction possibilities and, as a consequence, to huge mechanisms.

strongly toward dissociation back to heptyl and O_2. As a result, due to the lack of $C_7H_{15}O_2$, the low-temperature chain-branching process cannot be supported, while the rates for beta-scission reactions become significant, and the resulting smaller alkyls tend to react with O_2 to form HO_2. The HO_2 reacts with itself to form hydrogen peroxide - H_2O_2, making the sequence essentially chain-terminating until the H_2O_2 dissociates to form a pair of OH.

The hydrogen peroxide dissociation is associated with a slow rate of radical branching, therefore this intermediate-temperature chemistry tends to progress more slowly toward ignition with a rate that increases strongly with increasing temperature.

At higher temperatures the heat release is dominated by the branching reactions between H and O_2 and the chemistry is globally faster than that of either the low- or intermediate-temperature regimes.

Further details on heptane autoignition kinetics can be found in (Ranzi,1995) and (Curran, 1998).

Which path is actually followed during a specific homogeneous ignition process depends on the initial conditions of temperature (and also on the fuel consumption by radicals). Thus n-heptane can exhibit single stage or two-stage ignition[9] according to the initial temperature.

On the left hand side of Fig.4.1 is reported the pressure cycle measured on the engine described in Chapter 2 (see Tab.2.1), with CR=14.5, together with the experimental ROHR (in this test case the engine speed is 1500 rpm , EGR rate is zero and injection starts at about 10 CAD BTDC).

In the same charts the concentration development of some species, calculated during the simulation of this test case, are also displayed: they are the fuel vapour in-cylinder content, the heptyl radical with its peroxide and the correspondent isomer, and the ketoheptylperoxide, respectively.

It is possible to see that the intermediates typical of low temperature chain branching path are all formed and consumed before the pressure rise.

Ignition is commonly fixed, for combustion in internal combustion engines, at the point of zero pressure derivative: in the picture it is indicated through the black arrow. It can be noted that the mentioned species, due to their different stability, exhibit concentrations of different orders of magnitude.

This circumstance easily clarifies the reason why autoignition can be computationally critical: this feature and its impact on the mathematical solution of the model equation are addressed in the next paragraph.

---

[9] Dual stage ignition typically occurs when the heat release associated with the low-temperature chemistry causes a transition in the kinetics from the low- to the slower intermediate- temperature chemistry (Liu, 2004). Such kinetic dynamics is responsible for the appearing of cool flames during engines operated in PCCI mode, where the huge rate of premixing makes kinetic evolution more evident.
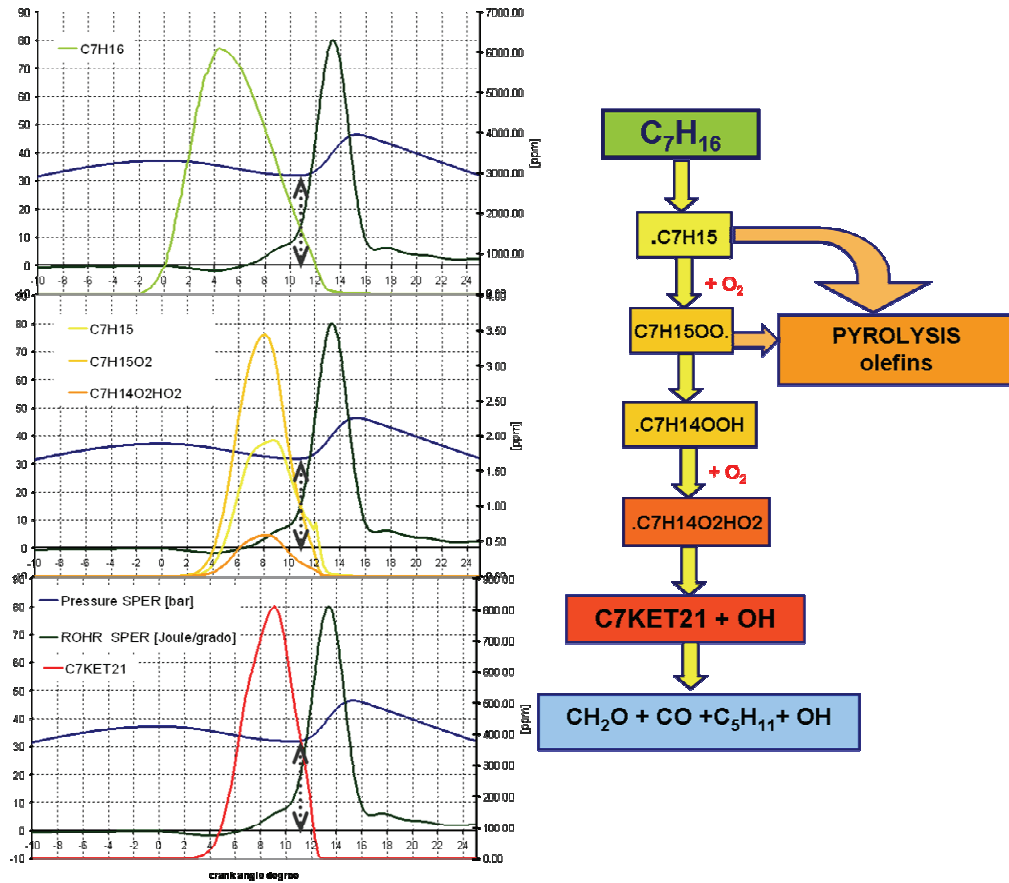
Figure 4.1 – Left: measured pressure cycle (blue), RoHR (green) and calculated vapour fuel (upper), heptyl radical and peroxides (middle), ketoheptilperoxide (lower). Right: general representation of competition between low temperature autoignition path and pyrolisis. The black arrows signal the ignition start.

4.2   Autoignition numerical tests: solver choice and stiffness analysis

The introduction of detailed kinetics in multidimensional diesel engine simulations not only requires the solution of a much higher number of equations, but the resulting mathematical system also exhibits some peculiar features.

As already discussed, detailed kinetics models include a high number of intermediate species whose concentrations can be very low, but dramatically affect the global reaction rates. Due to the extreme variability in the stability of the species considered, their characteristic times of reaction are very different too, thus the mathematical system is also very stiff.

Efficient and reliable integration of stiff equations requires proper implicit methods with suitable stability properties.

During the present work, two general-purpose stiff ODE solvers have been considered and their respective performances in the solution of the kinetic system have been assessed (Belardini, 2005): a switching criterion to select, during the calculation, the best solver has been set up (Belardini, 2006).

4.2.1 Test cases description

All the calculations results reported in the following refer to the diesel engine described in Chapter 2, with the piston bowl relative to a compression ratio value of 16.5, fuelled with commercial diesel fuel.

The experimental tests were performed at an engine speed equal to 1500 rpm, with an injected fuel quantity corresponding to a Mean Effective Pressure of 2 bars on the 4 cylinder engine: different values of Exhaust Gas Recirculation (EGR), rail pressure, and injection timing have been used. The operating test conditions are specified in Table 4.1 and relative in-cylinder pressure data are reported in Fig.4.2, together with the injector Energizing Current profiles.

Table 4.1 **Experimental operative conditions**

| Test case	Rail pressure [bar]	EGR %	SOI CAD BTDC	Injection duration CAD	Injected fuel [mg]
#1	500	40	12.7	7.3	8.0
#2	900	0	2.3	5.7	8.7
#3	500	0	2.1	7.3	8.5
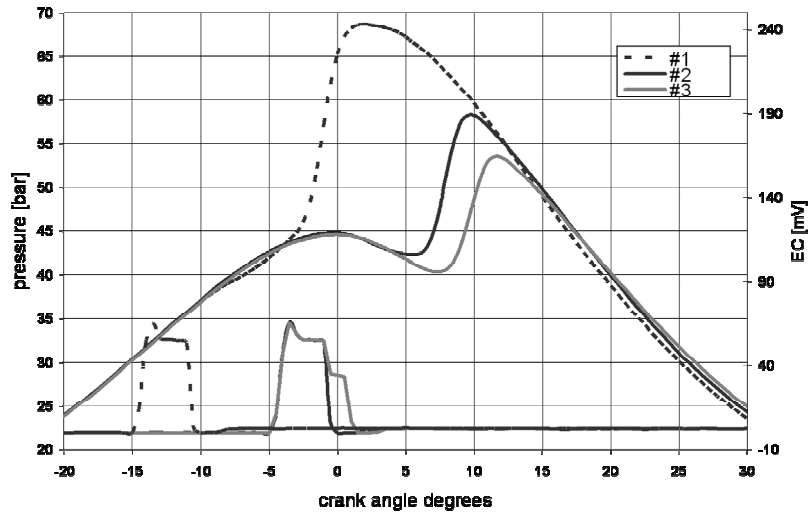
Figure 4.2 – Measured pressure and Energizing Current profiles

The kinetic mechanism used for the following tests is a modified version of the Chalmers model (Gustavsson, 2003) for n-heptane combustion. The mechanism has been extended to n-dodecane, more similar to a typical diesel fuel, linking its reactivity to the heptane's original autoignition scheme via production of heptyl radicals.

The starting reactions involving the species C_7H_{16} have been substituted by similar reactions for n-dodecane: it can undergo hydrogen abstraction through reaction with H, OH or HO_2 radicals (followed by β-scission) or direct pyrolisis. In both cases the products of such paths are heptyl radicals and species having five, three or two carbon atoms, already included in the original mechanism.

The reaction rate parameters for the elementary steps added to the scheme, when not reported in literature, have been estimated on the basis of similar steps for n-decane or n-esadecane.

In order to accept the modified mechanism, the reactivity of many intermediate species predicted by the two schemes have been compared: the concentration evolution of methane, ethylene, hydrogen peroxides and several other species are not affected by the mentioned modifications, thereby concluding that, at high temperature, the obtained set of reactions reproduces the original population of fragments.

The final reaction scheme is made up of 285 elementary steps, mostly reversible, and 62 species.

The computational mesh is a cylindrical sector of 51 degrees, as just one single jet of the 7 jets produced by the injector is considered (see Table 2.1).

4.2.2   *Stiffness of the equations system: VODE and SDIRK libraries*

The characteristic destruction time of a species provides an approximation of the absolute value of the real part of the eigenvalue correspondent to the respective component of the ODE system. The stiffness of the system is the ratio between the maximum and the minimum eigenvalue of the system, therefore the ratio of the maximum and the minimum characteristic destruction times, among all the considered species, can be used as an estimate of the stiffness.

Fig.4.3 displays the evolution of the ratio between maximum and minimum destruction time, among all the species, for test case #2, (the average value over all the computational cells is reported), together with the calculated pressure cycle.

The diagram indicates that stiffness values are higher during the low temperature combustion phase. In fact, in case #2 ignition occurs at about 7 CAD ATDC, while Fig.4.3 indicates that the highest stiffness values are attained earlier, within 5 CAD ATDC. As soon as the pressure rises, the stiffness is reduced and during the expansion phase a roughly constant value is established. It is noteworthy that even the lowest value still indicates a very high variability in the "numerical"[10] destruction times.

In conclusion, the highest stiffness values are attained during the ignition delay.
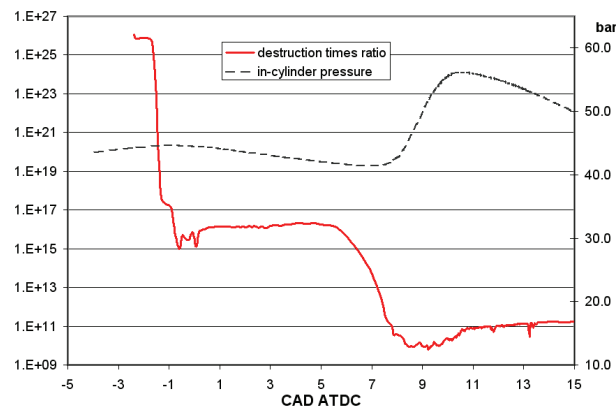

Figure 4.3 –Ratio of maximum to minimum – among all the species- characteristic destruction time and in-cylinder pressure (on the right axis) versus crank angle, for case #2.

Looking at the issue from a more physical point of view, the mixture composition has been calculated (for case #2) as represented in Fig.4.4, just prior to the ignition: it is

---

[10] The maximum destruction time corresponds to the less reactive species and, among all the species included in the reaction mechanism, nitrogen or carbon dioxide usually exhibit the highest value. On the contrary, the minimum value is relative to the species having the highest destruction rate, therefore usually corresponds to a very reactive intermediate or radical. It has to be said that a very small destruction time can also be calculated when the species concentration is very low, independently from its destruction rate. The ratio reported in Fig.4.3 is not meant to represent the "physical" variability in the reaction speeds, but gives an estimation of the numerical variability: in fact certain species, although practically absent in a certain cell, are still calculated and have very low destruction times because of their "numerically" non-zero (but dramatically low) concentration.

possible to note that, before the pressure rise, a significant percentage of the mixture is already made up of fragments of few carbon atoms. About 40% of the mixture, in that phase, is already made up of olefins and species with three carbon atoms. This suggests that, despite the negligible heat release associated to autoignition, the system composition has already changed significantly[11].
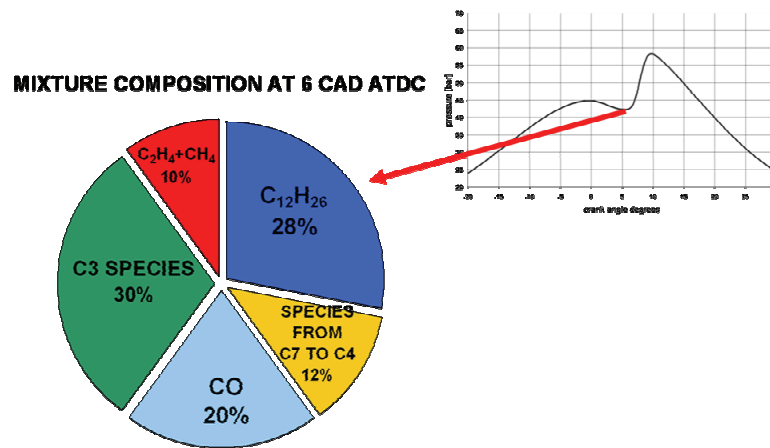

Figure 4.4 – Mixture composition calculated at 6 CAD ATDC for case #2

After the ignition delay, when the pressure rise starts, even though the heat release rate increases, and the combustion, as a whole, attains its maximum speed, the system dynamics becomes smoother.

The displayed stiffness values are referred to test case #2, but results are similar for the other cases too.

As a result, it is clear that the autoignition phase requires a proper mathematical treatment. The integration of stiff equations requires implicit methods with suitable stability properties and so high values of stiffness make the choice of the numerical solver very significant.

Two general-purpose ODE solvers have been tested: namely, the DVODE (Brown, 1989) and SDIRK4 (Hairer, 1996) packages. The VODE is based on linear multi-step formulas, while the second one is based on a one-step integration formula.

The package SDIRK4 is based on a 5-stages Singly Diagonally Implicit Runge-Kutta (SDIRK) method of order four, with variable step size control.

The main computational kernel in SDIRK4 solver is the solution of non-linear systems, performed by means of a simplified Newton method; at each time step, only one Jacobian evaluation and one LU factorization are required

---

[11] Of course the exact composition depends on the specific reaction mechanism adopted and the composition reported here is not meant to define the relative amounts of the various species at the end of the autoignition phase but is used as a general information on the progress of the global combustion process.

The VODE package is designed for both stiff and non-stiff systems. It uses variable coefficient Adams-Moulton methods and variable coefficient Backward Differentiation Formulas (BDF) in the non-stiff and stiff case, respectively. VODE implements BDF of orders q from one through five, with an automatic, adaptive technique for the selection of order and step size and provides several methods for the solution of the systems of algebraic equations.

Adaptivity properties of VODE, both in the formula order selection and in the Jacobian reusing, make this software very effective in the solution of stiff ODEs. However, in a parallel setting they motivate load imbalance. Indeed, one-step formulas allow fast increase in step size after a restart. For this reason, SDIRK4 revealed to be more effective in the high temperature combustion phase.

In Fig.4.5 the effect of the different solvers on the shape of the calculated pressure cycle, for case #2, is presented: SDIRK4 (red curve) is unable to follow the fast dynamics of the process in the low temperature chemistry, it predicts a longer ignition delay and, as a consequence, a lower peak of pressure. In comparison with VODE, SDIRK4 has the general tendency to smooth the pressure time derivative.
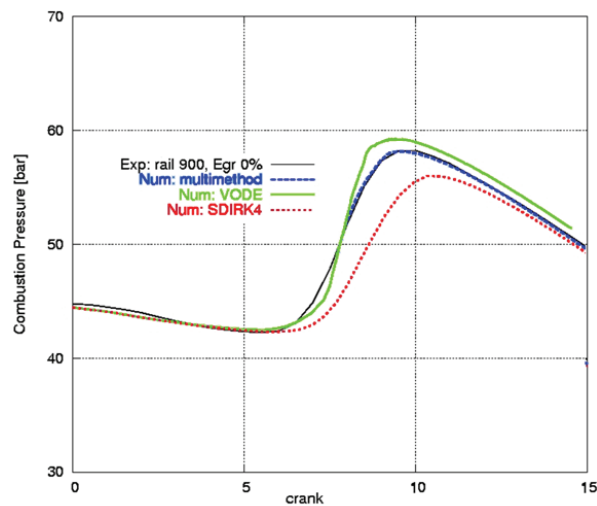

Figure 4.5 – Pressure cycles predicted using VODE, SDIRK or the combined method, compared with the measured pressure data for case #2

On the contrary, VODE predicts a shorter ignition delay time, but the subsequent pressure rise is slightly steeper. In practice, VODE seems better suited for the low temperature kinetics phase and generally more accurate than SDIRK. However, qualitatively, both solvers allow to obtain a reasonable agreement with the measured pressure data.

As regards the total computing times, Fig. 4.6 shows that, thanks to the parallelization, the total simulation time can pass from a maximum of 12 hours to about 50 minutes, when the mentioned reaction mechanism is used.
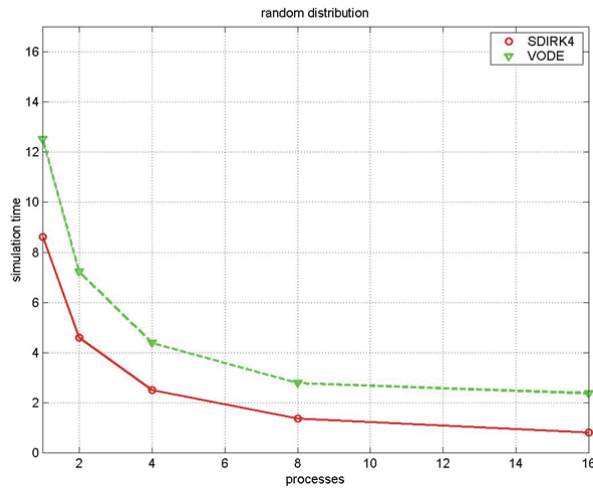
Figure 4.6 – Hours of simulation time employed to calculate from -5 CAD to 40 CAD ATDC for the tested solvers

Moreover SDIRK turned out to perform globally faster simulations with respect to VODE.

However, considering the variation in computational efficiency during the cycle, at the early stages of combustion VODE can be considered more efficient, while SDIRK4 is more efficient in the late combustion phase.

In fact in Fig.4.7 the number of function evaluations performed versus crank angle is displayed: typically this number is assumed as a measure of the computational complexity. During the autoignition, when the stiffness is at its highest values, VODE performs a smaller number of function evaluations, as its adaptivity properties make this software very effective in the solution of stiff ODEs, although in general more time consuming.

Therefore, as concerns computational times, the use of SDIRK4 allows instead to achieve a higher value of the global speed- up[12], when increasing the number of processors, as reported in Fig. 4.8. With this solver, the speed-up obtained with 16 processors over a full calculation reaches a value of nearly 11.

---

[12] In parallel computing, speedup refers to how much a parallel algorithm is faster than a corresponding sequential algorithm and is calculated as the ratio between the execution time of the sequential algorithm and the execution time of the parallel algorithm with a certain number of processors.
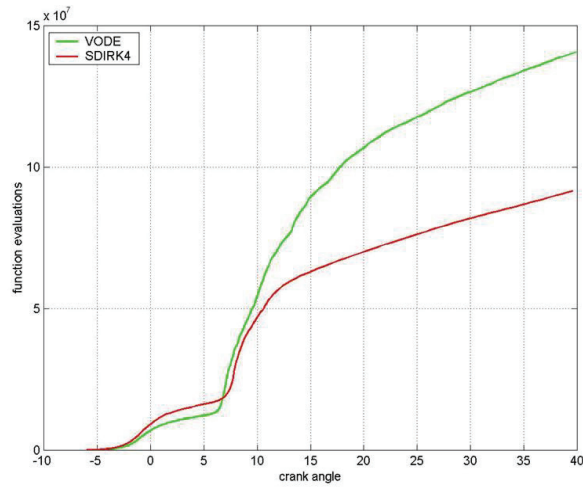
Figure 4.7 – Number of function evaluations performed by the two solvers
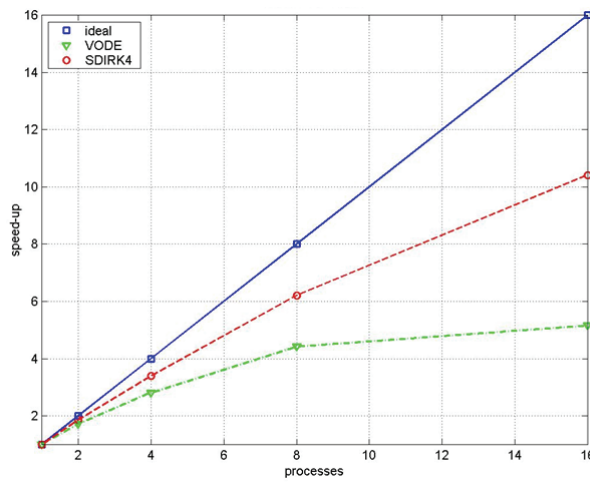

Figure 4.8 – Speed up obtained with the two solvers using the random partitioning of the computational domain

Finally, the absolute error in terms of mass conservation is represented in Fig. 4.9: although globally "slower", VODE has the highest accuracy in all the phases of the pressure cycle.
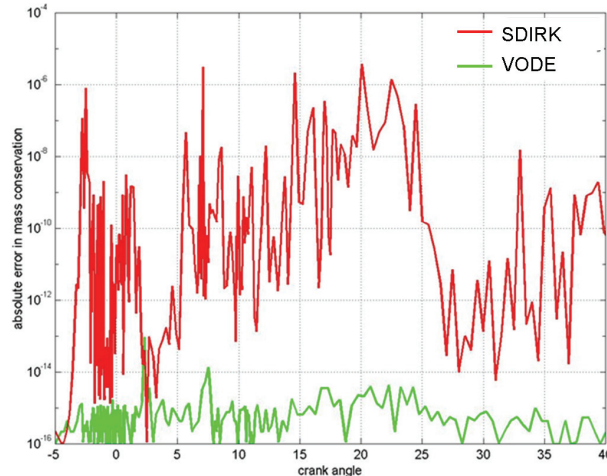
Figure 4.9 – Comparison in terms of absolute error in mass conservation

To sum up, SDIRK4 turned out to be more efficient than VODE over the total simulation, but VODE is more accurate in the whole calculation and also better suited to the critical autoignition phase. This suggested to use the one solver or the other according to the current stiffness and to the local conditions, in order to reduce the computing time and improve the accuracy of the solution, with respect to the use of a single solver.

4.2.3   *Switching criterion*

In order to distinguish between the autoignition phase at higher stiffness and the higher temperature phase, specific intermediate species have been used as markers.

The criterion to select the solver to be used at a certain time, in a fixed cell, is in fact based on the evaluation of a fixed species concentration. Two alternative species have been considered: the ketoheptylperoxide, responsible for the low temperature chain branching or the hydrogen peroxide, whose decomposition causes the massive OH radicals production. Their instantaneous values have been used for the solver selection.

More in detail, the calculation starts using VODE, then, cell by cell, as soon as the marker concentration attains its maximum value or, more precisely, as its derivative becomes negative, the code switches to the SDIRK solver. Therefore, as soon as in a cell low temperature autoignition kinetics is substituted by the higher temperature paths, the code can rely on a more efficient solver, while, when (and where) autoignition is still taking place, VODE better capabilities in the solution of stiff problems can be exploited.

Fig.4.10 displays the number of function evaluations performed combining the use of both the solvers. The multi-method predictions are more adequate than those obtained with a single solver in the ignition delay period as well as in the high temperature combustion phase.
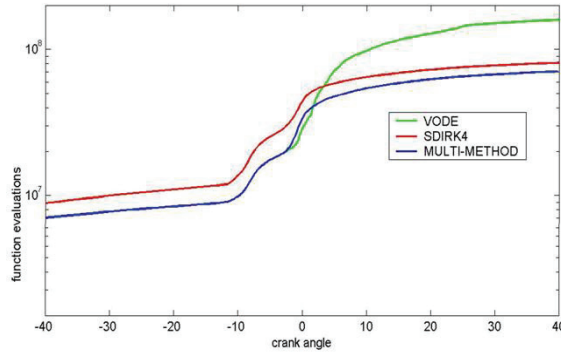
Figure 4.10 - Number of function evaluations performed by the different solvers

The combined method has been tested in the three test cases described in Table 4.1, having different conditions of injection and EGR. Figure 4.11 shows the computed pressure cycles (coloured lines), compared to the experimental curves (black solid lines): autoignition is properly depicted in all the cases.

In the lower part of the picture the time evolutions of the chain branching agent ketoheptylperoxide, (indicated as C_7KET_{21}) and hydrogen peroxide are also represented. In every condition the maximum H_2O_2 concentration is exactly phased at autoignition, while the peak of C_7KET_{21} appears always shifted in a slightly preceding phase. Low and high temperature kinetic mechanisms are clearly distinct and therefore it is possible to separate low and high temperature phases on the basis of the concentrations of these species.
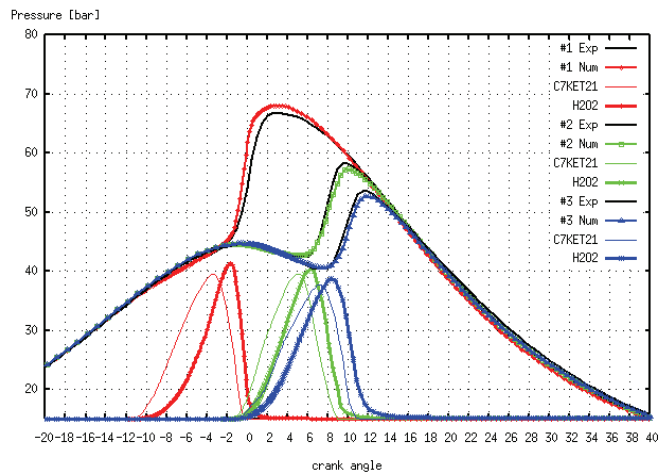

Figure 4.11 - Experimental and numerical comparisons of pressure cycles and non-dimensional concentrations of ketohydroperoxide and hydrogen peroxide (total amount in the domain)

4.3 Code validation through heptane combustion simulations

The parallelization and the work carried out on the solution methods for the chemistry solution have permitted to implement quite detailed reaction schemes, then a validation activity has been performed in order to verify the reliability of the modified version of the code.

4.3.1 Experiments with single-component fuel- motivations

In order to assure an easier comparison, experiments were performed in which heptane pure has been employed as fuel.

Diesel fuel is a complex blend of several hundreds of species, including paraffins, cycloparaffins and aromatics. Even though surrogates don't have to exactly resemble the real composition of the fuel, a certain matching of the chemistry surely permits a better agreement between models and real combustion behaviour: at the moment a proper surrogate for diesel fuel (mostly from a kinetic point of view) can be still considered a developing goal (Farrel, 2007).

In fact, kinetic mechanisms for aromatics and toluene - whose inclusion is recommended for diesel combustion simulation- are reported with discrepancies or validated in a very narrow range of conditions (Farrel, 2007). Therefore the choice to fuel a diesel engine with n-heptane was driven by the following considerations:

- Heptane mechanisms are more common in literature and thus it is possible to compare results using reaction schemes from different sources. Moreover many skeletal or reduced models are available, enabling a significant reduction in computational times.
- Reaction kinetics models should be employed without any tuning of the rate constants. Diesel fuel combustion is often simulated by means of mechanisms for heptane, since its cetane number is very similar to the diesel fuel one, but heptane mechanisms can still require some calibration of the rate parameters, when applied to real diesel ignition.
- Finally, from an experimental point of view, diesel fuel requires elevated temperatures before significant vaporization occurs, making it difficult to form a premixed homogeneous charge. On the contrary, being heptane much more volatile, in-cylinder premixed conditions can be easily obtained to realize PCCI-like conditions.

4.3.2 The choice of the reaction mechanism

Low temperature kinetics for autoignition description has been extensively studied (Westbrook, 2000) and some very detailed reaction mechanisms have been developed, even for long fuel molecules, as those making up diesel fuel. The subsequent mechanisms reductions have permitted to achieve a semi-detailed or also skeletal description of combustion (schemes made up of 30 or less species), especially suitable for multi-dimensional simulations of combustion in diesel engines.

On the other hand, as concerns high temperature reaction kinetics to model carbonaceous particulate matter formation, a very high number of species is necessary, but reduced schemes, capable to properly depict the process, are not widely used. Furthermore, the validation of an hypothetical reduced soot formation mechanism at engine conditions is quite difficult, thereby making impossible to eliminate species and paths from a detailed scheme in a correct manner.

The basic idea followed in the choice of the reaction mechanism has been to "spend" only a limited amount of the total computational effort on the autoignition scheme, thus relying on a mechanism (Liu, 2004) -made up of 44 species- that actually is not very detailed. Despite the parallelized code is capable of dealing with huger reaction schemes, in fact, it has been decided to "save" time for the subsequent implementation of the particulate formation kinetics, illustrated in Chapter 5.

In other words, which part of the reaction mechanism deserves the greatest "investment", in term of number of species and elementary steps, depends on the simulation purposes. Since one of the aims of the present activity concerns pollutants kinetics, the ignition part has a limited level of detail. However, generally speaking, more detailed mechanisms could be necessary if specific autoignition aspects are the main focus, like PCCI ignition, cool flames appearing in premixed conditions etc.

In the following paragraph the comparison between experimental data and numerical predictions is reported, in a wide range of engine operative conditions, while the extension of the reaction scheme for the particulate matter modelling is addressed in Chapter 5.

The adopted reaction scheme is a skeletal mechanisms developed in (Liu, 2004), reduced from a more detailed mechanism made up of 168 species and 1008 elementary steps for the ignition and combustion of n-heptane (Baulch, 1994).

This reduced mechanism consists of 44 species and 185 reactions : it has been chosen because it has been derived and validated in high-pressure conditions, not only in homogeneous conditions, but also in plug flow reactors and in a n-heptane counterflow diffusion flame (Liu, 2004).

It has to be pointed out that pollutants formation is not included in the model, therefore any influences of nitrogen oxides on the ignition delay are neglected. Still its use was not aimed at performing ignition delay studies, but it was meant to represent a test bed for the modified version of the code.

4.3.3   *Comparison between numerical predictions and measures at CR 16.5*

All the experimental data for the comparison with results from calculations have been collected operating the single cylinder diesel engine described in Chapter 2.

The tests have been realized at two values of the compression ratio-16.5 and 14.5 respectively. At each compression ratio value, one of the following parameters has been varied from time to time: total amount of fuel injected, injection timing, EGR rate, engine speed, air swirl ratio and pressure of the fuel inside the rail, in order to investigate the sensitivity of the code with respect to such variations.

The reaction scheme has been adopted without any tuning of the reaction rates and in all the conditions displayed here the only change among the cases lies in the initial and boundary conditions. In this respect, it is important to point out that neither the initial nor the boundary conditions have been adjusted to reach the agreement with the measured pressure cycles: it means that the variations in the conditions given as input to the code (like the amount of injected fuel, intake and exhaust temperature etc.) were always kept within the experimental uncertainty.

Tab.4.1 reports the conditions of four test cases: taking case #1 as reference, the subsequent ones have different start of injection time (SOEC[13]) and EGR rate.

Table 4.1 **Experimental operative conditions** – CR=16.5

Test case	Speed [rpm]	Rail pressure [bar]	EGR %	SOEC CAD BTDC	ET [µs]	IMEP [bar]
#1	1500	480	0	9	710	4.13
#2	1500	480	0	6.2	710	3.95
#3	1500	480	30	13	710	4.02
#4	1500	480	46.5	18	710	3.99

The experimental data set is here meant to identify interesting conditions for the numerical validation, therefore some cases do not differ in a single parameter. In fact the scope was not to investigate the effect of such parameters on the combustion features, but to select a range of representative operative points for comparison with computed pressure cycles.

With respect to case #1, in case #2 the injection timing is delayed, thus the ignition occurs nearly 10 CAD later: here the code sensitivity to different injection timing can be verified. Case #3 is representative of a non-zero EGR rate condition. In case #4 a further increase in the EGR rate is adopted, together with an earlier start of injection, thereby realizing LTC-like combustion conditions.

In Fig.4.12 the measured pressure cycles (averaged on 128 consecutive cycles) are compared with the calculated ones: the predicted ignition start accurately reproduces the measured one in all the cases and the curves slope are in good agreement with the experimental values too, however in case #2 the pressure peak is underestimated.

[13] Start of Energizing Current for the electroinjector.
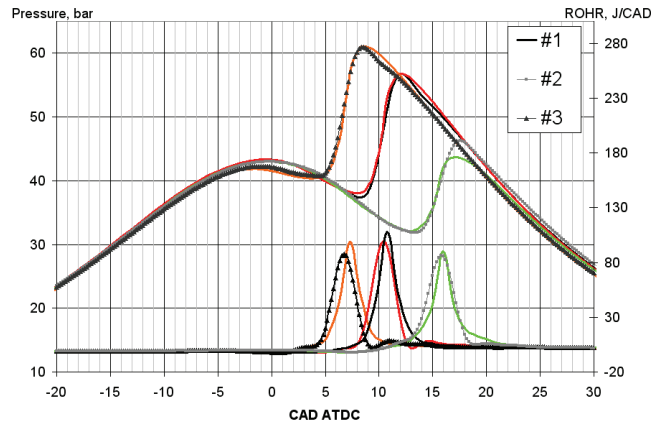
Figure 4.12 – Comparison between measured (black lines) and calculated (coloured lines) pressure cycles and ROHR varying injection timing and EGR rate

Generally speaking, it is not necessarily essential to try to reproduce a pressure profile perfectly superimposed on the measured data. Therefore, in order to verify which level of precision it is sensible to aim at, the cycle to cycle dispersion of this set of measurements has been estimated.
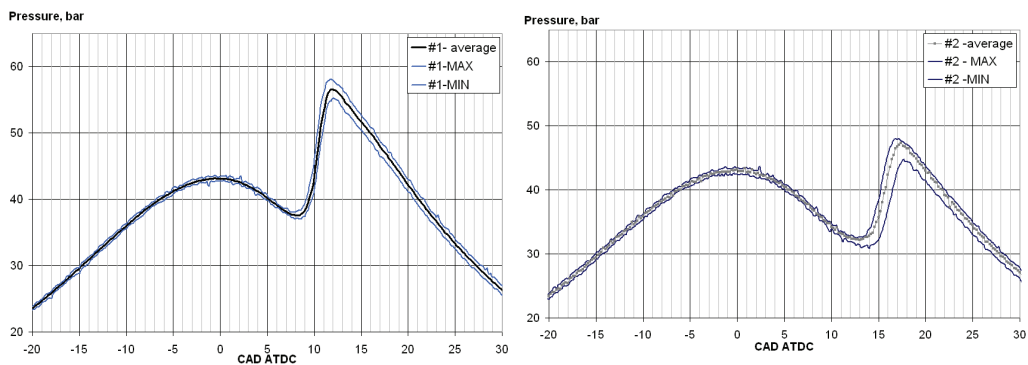

Figure 4.13 –Cycle to cycle dispersion: average measured pressure cycle (black) and respective minimum and maximum cycle

In Fig.4.13 the average cycle is reported together with the maximum and the minimum cycle among 128 consecutive cycles acquired for test cases #1 and #2.

It has to be noted that the cycle to cycle variability attains its maximum next to the pressure peak. Moreover, comparing the two cases, it is clear that later ignition (i.e. retarded with respect to the TDC) appears less stable and a considerable variation from cycle to cycle occurs, not only at the maximum pressure but also at the start of ignition.

These simple observations can be quantified calculating the relative standard deviation among all the acquired cycles at each value of the CAD. Therefore in Fig.4.14 the evolution of the relative standard deviation RSD[14] is displayed, according to the formula:

$$RSD = \frac{\sigma_p}{\bar{p}} = \frac{\sqrt{\dfrac{\sum_{i=1}^{n}(p_i - \bar{p})^2}{n}}}{\bar{p}} \qquad (1)$$

where n is the total number of cycles acquired.
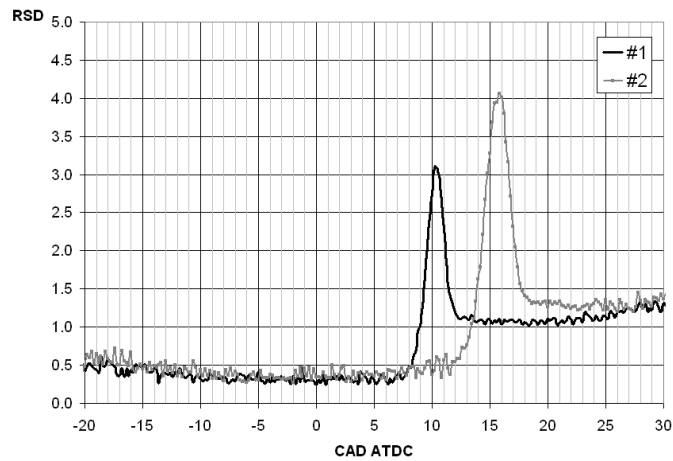
Figure 4.14 – Relative standard deviation versus crank angle for cases #1 and #2

From Fig.4.14 it is evident that the RSD starts to increase at the ignition and reaches its maximum at the maximum pressure.

As a consequence, it is reasonable to require that the computed pressure cycles fall in the band between the minimum and the maximum measured cycle, especially in the highest pressure phase. On the contrary, obviously, a more stringent comparison has to be expected during the compression stroke.

In Fig.4.15 the calculated pressure cycles are superimposed on the experimental data of Fig.4.13: it can be concluded that in case #1 the calculated values are well within the statistical variability of the data, while in case #2, despite the wider dispersion observed, the maximum pressure in the simulated cycle is definitely too low.

One of the possible reasons of such discrepancy is the inherent kinetic model behaviour when ignition takes place at lower pressures and temperatures, as it happens for ignition during the expansion phase.

---

[14] At each crank angle, RSD is the standard deviation normalized by the average value of the pressure.
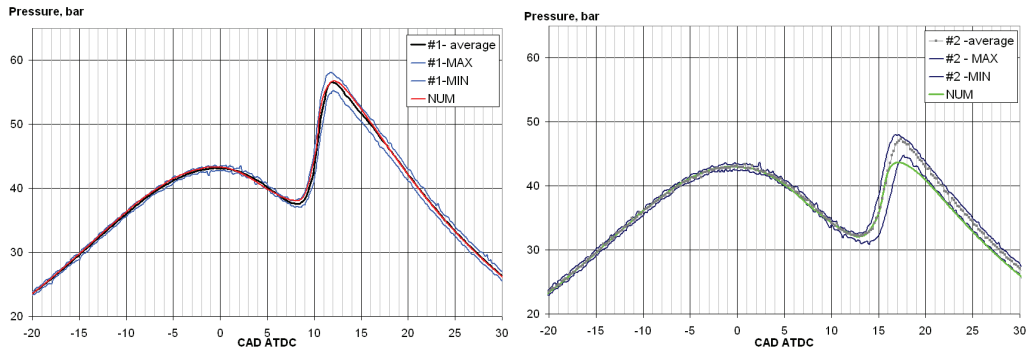
Figure 4.15 – Calculated pressure cycles and measured average, minimum and maximum cycles

Moving to the other test cases, in case #3 of Fig.4.12 an EGR rate equal to 30% is employed and the model is capable of properly depicting the pressure cycle: on the contrary, if an increase of the EGR to 50% and a simultaneous earlier injection is adopted, like in case #4, the model fails the prediction of the autoignition dynamics, as shown in Fig.4.16. As a matter of fact, the measured RoHR clearly indicates the presence of a cool flame prior to the main heat release, while the model gives rise to full ignition when the cool flame is instead expected.
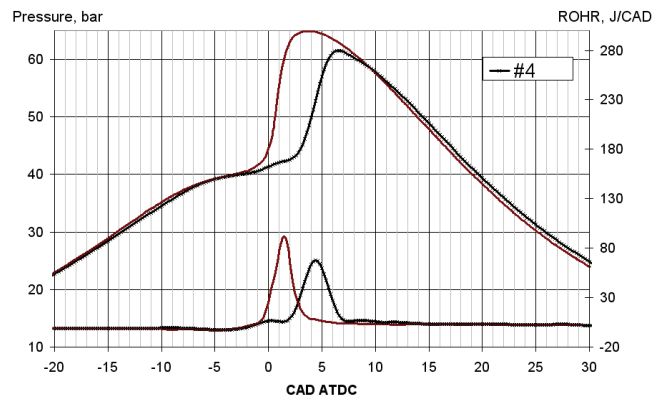

Figure 4.16- Experimental and computed pressure cycle and rate of heat release for case #4

In this condition, the spray dynamics is decoupled from the autoignition phenomenon, thus the droplets evaporation rate does not affect ignition delay, that is instead controlled by reaction kinetics and its interactions with the flow field. As a consequence, both the reaction mechanism and the way of modeling the effect of turbulence on the reactions rates play a more important role.

In this version of KIVA, as already mentioned, each computational cell is treated as a partially stirred reactor, thereby in practice ignition is kinetically controlled. An analogous

approach is adopted in (Genzale, 2008), where a similar "error" is detected (the predicted pressure rise also coincides with the cool flame heat release). The lack of accuracy for LTC simulations in (Genzale, 2008) is ascribed to the poor detail of the reaction mechanism used. However in the present simulations, it can be argued that, even though a more detailed reaction scheme could better depict multi-stage ignition, the poor performance of the simulation has to be also ascribed to an inaccurate representation of the local equivalence ratio distribution and to the oversimplified representation of the turbulent mixing effect on reactivity.

As a result, an improvement could possibly be reached increasing the mesh resolution and working on the modeling of the concentration and temperature fluctuations.

Then, still with respect to the case #1, the amount of fuel injected, at the same speed and EGR, has been varied for case #5, while in case #6 the engine speed has been increased to 2000 rpm, keeping constant EGR and injected quantity.

The respective operative conditions are reported in Tab.4.2.

Table 4.2 **Experimental operative conditions** – CR=16.5

Test case	Speed [rpm]	Rail pressure [bar]	EGR %	SOEC CAD BTDC	ET [µs]	IMEP [bar]
#5	1500	480	0	9	760	4.79
#6	2000	480	0	14.8	707	4.02

Fig.4.17 and 4.18 clearly show how the code adequately reacts to the variation of the mentioned operating parameters: in both the comparisons start of ignition and pressure derivative with respect to time are precisely reproduced.
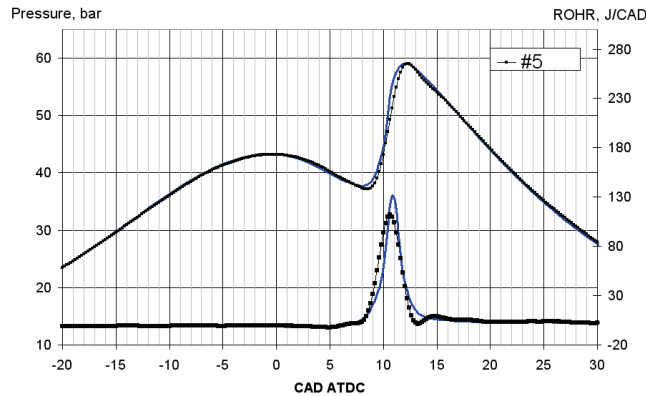

Figure 4.17 - Comparison between measured (black lines) and calculated (coloured lines) pressure cycles varying the amount of fuel injected
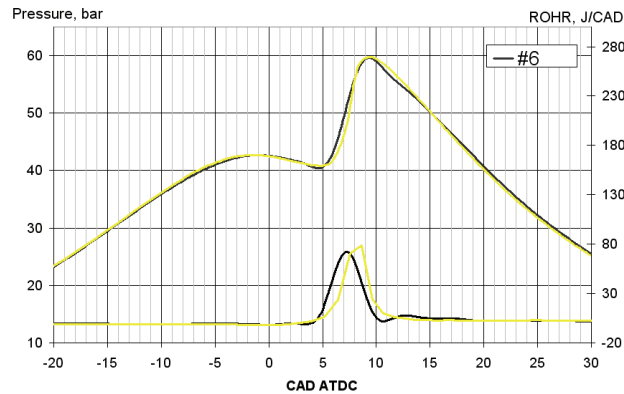
Figure 4.18 - Comparison between measured (black lines) and calculated (coloured lines) pressure cycles varying the engine speed

Once verified the comparison in terms of pressure, the exhaust gas composition measured in the mentioned cases is compared with the calculated one. In Fig.4.19 the carbon dioxide and the oxygen concentration calculated in these six test cases at 120 CAD ATDC are compared with the respective values measured at the exhaust: a good agreement with the experimental data is obtained in all the conditions, whereas the differences can generally be ascribed to the absence of the pollutants formation kinetics in the current tests.
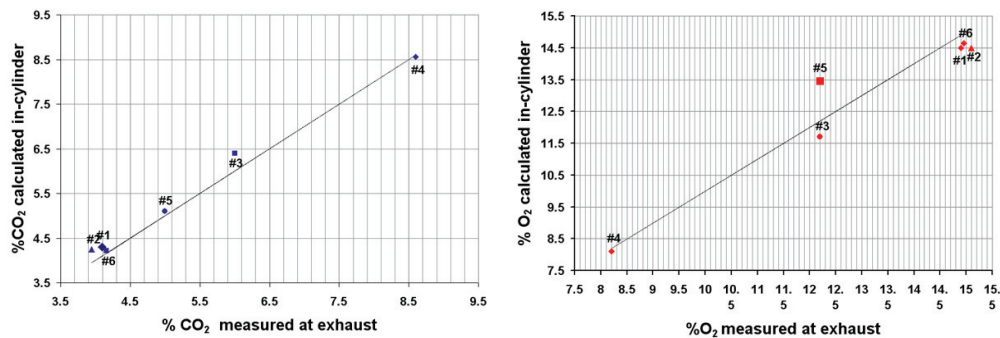

Figure 4.19 – Comparison between calculated and measured CO_2 and O_2 concentration respectively for all the test cases

In order to estimate the predicted amounts of unburned hydrocarbons, all the residual aliphatic and unsaturated hydrocarbons calculated at 120 CAD ATDC are summed and expressed as methane equivalents: the comparison with the values measured at the exhaust is displayed in Fig.4.20. In this case the deviation from the measured data is wider, nevertheless the normalized values of Fig.4.21 suggest that the model has the capability of following the reciprocal variations among the different operative conditions.
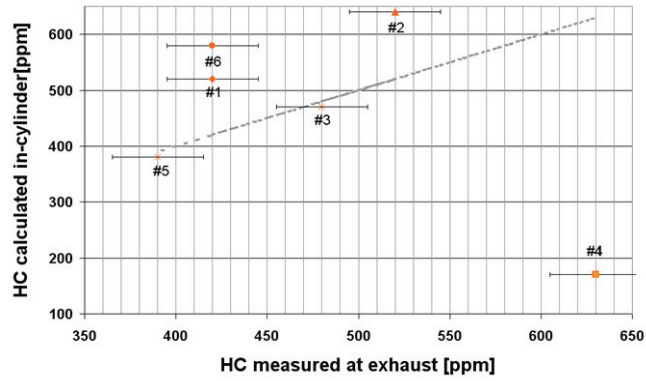
Figure 4.20 – Comparison between computed and measured unburned hydrocarbons for all the test cases – x error bars are referred to an experimental uncertainty of about 40 ppm
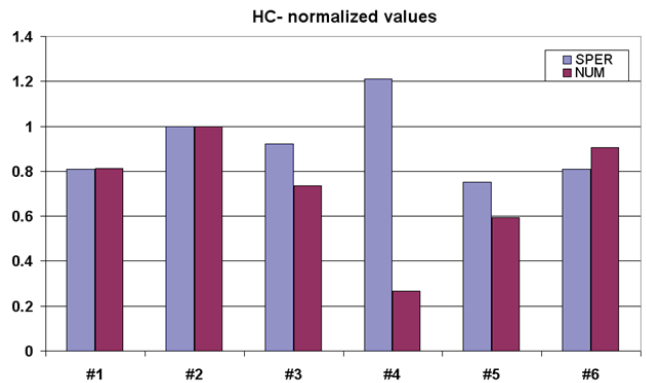

Figure 4.21 - Comparison between normalized values of computed and measured unburned hydrocarbons for all the test cases

The predicted value for case #4, corresponding to the LTC condition, is not acceptable, as the HC concentration is greatly underestimated: such circumstances clarifies that a failure in representing the autoignition dynamics also determines a subsequent error in the unburned hydrocarbon prediction.

It is possible to draw the conclusion that the modified version of the code, together with the mechanism by (Liu, 2004) can effectively capture the variations in the engine behaviour when different operative conditions are changed.

In order to avoid repetitions, the examination of the species spatial distributions and some additional combustion features are not reported here, as a full description of many species evolution is illustrated in Chapter 5.

4.3.4   Comparison between numerical predictions and measures at CR 14.5

In the following the simulations carried out for a lower engine compression ratio value are reported.

The current interest in the compression ratio effect on combustion features is due to its potentiality of affecting the combustion behaviour during LTC (see Par.1.2), as it was already put in evidence in previous studies (Cipolla, 2007).

The reduction of the engine compression ratio can be an efficient way to overcome the problem of extension of LTC application to NEDC engine operating area (Hamada, 2005), even if a deterioration of the fuel economy due to the loss of expansion ratio should be expected. At lower compression ratios correspond reduced in-cylinder temperatures and pressures at the end of the compression stroke, leading to an increase of the ignition delay time and a wider smokeless combustion range in terms of EGR and IMEP (Hamada, 2005).

Longer ignition delay time, in fact, can guarantee a good premixing level of the diluted air-EGR-fuel charge, giving the possibility to obtain premixed-low temperature condition in a larger working engine map. This in-cylinder charge conditions are directly connected to the well known advantages offered by LTC systems in terms of NOx and soot reduction.

In order to investigate the effect of the compression ratio reduction, the piston has been substituted (Beatrice, 2008), thus obtaining a compression ratio value equal to 14.5. In Fig.4.22 a sketch of the piston bowl profile in the two cases is displayed: the main difference lies in the height of the central peak, but the geometrical features of the two combustion chambers are kept similar, in order to obtain analogous flows patterns. In this way the effect of the compression ratio alone can be analysed.
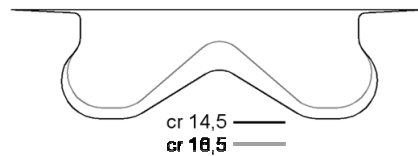

Figure 4.22 – Profiles of the piston bowl geometry at CR equal to 16.5 and 14.5

The mesh adopted for the reduced compression ratio value is represented in Fig.4.23, where the bigger combustion chamber volume for CR equal to 14.5 is clearly visible.
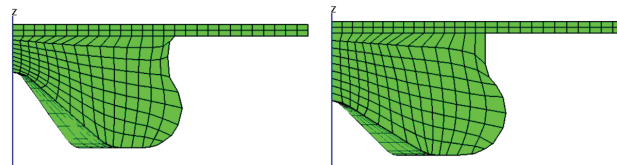

Figure 4.23 – Sections of the meshes adopted for the 16.5 (left) and the 14.5 (right) piston bowls, respectively.

In Tab 4.3 the main characteristics of the different operative points are listed and the comparison between experimental and calculated pressure cycles is shown in figures from 4.24 to 4.26.

Table 4.3 **Experimental operative conditions** – CR=14.5

Test case	Speed [rpm]	Rail pressure [bar]	EGR %	SOEC CAD BTDC	ET [μs]	IMEP [bar]
#7	1500	480	0	10	710	3.83
#8	1500	480	0	13	710	3.83
#9	1500	480	0	9	710	3.66
#10	1500	480	31	13	710	3.69
#11	1500	480	50	18	710	3.67
#12	2000	480	0	14.8	710	3.56

Fig.4.24 reports the comparison for cases #7, #8 and #9, that differ in the injection timing, while in Fig.4.26 the comparison for case #12 at a higher engine speed is displayed. All the mentioned cases are correspondent to conditions without EGR.
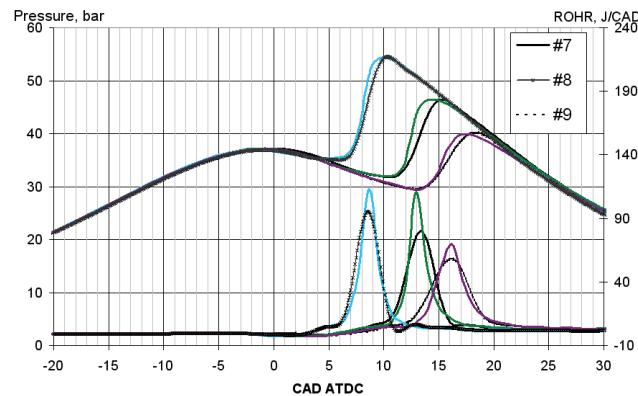

Figure 4.24 – Predicted (coloured) and measured (black) pressure cycles for test cases with different start of injection time

The comparison between measured and calculated pressure profiles indicates that the model has the tendency to slightly overestimate the pressure rise after ignition.

Moving to conditions at non-zero EGR rate, cases #10 and #11 are shown in Fig.4.25. With respect to case #10, having EGR rate equal to about 30%, in case #11 the EGR rate is increased up to 50%, simultaneously realizing an earlier injection. Case #11 can therefore be considered as representative of an LTC combustion condition: as a matter of fact, the correspondent pressure cycle displays the distinctive low temperature ignition before the main heat release.

Similarly to the results at CR equal to 16.5, the LTC-like condition of case #11 is not properly captured, as a full ignition occurs when the cool flame would instead take place.
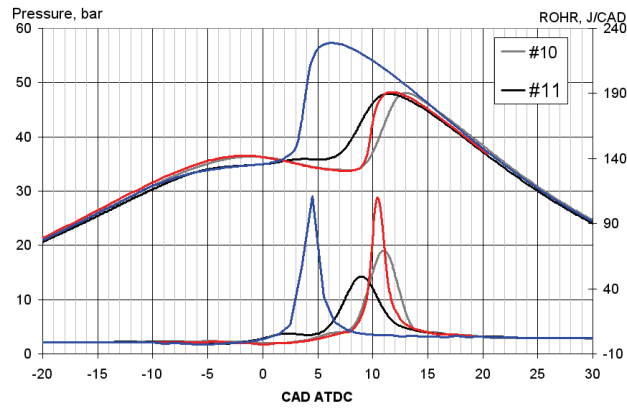
Figure 4.25 – Comparison between predicted (coloured) and measured (black) pressure cycle
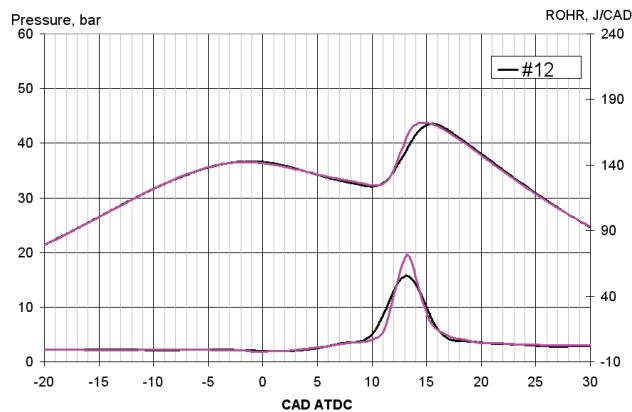

Figure 4.26 – Comparison between predicted (coloured) and measured (black) pressure cycle

In conclusion, the models implemented in the modified version of the code have proven to be capable of adequately representing the engine behaviour in many different engine operating conditions, properly reproducing a wide range of operative points, although in LTC-like conditions the comparisons are not very satisfying and several modifications need to be adopted.

The subsequent adoption of a more complex reaction scheme is addressed in the next chapter.

4.4   Summary and conclusions

The computational efficiency of the KIVA3V Release 2 code has been significantly improved with the use of parallel techniques for chemistry, jointly with the adaptative choice of the integration method.

In multidimensional simulations of combustion in diesel engines with detailed kinetics the mathematical system to be solved is very stiff: it turned out that the phase at highest stiffness is the autoignition. As a consequence, a proper mathematical treatment of the equations set is required.

The different characteristics of the autoignition and the high temperature phase during the combustion process have suggested to use different ODE solvers to improve the accuracy and the efficiency of the calculations. The cell by cell switching criterion is based on the in cylinder concentration of ketoheptylperoxide or hydrogen peroxide.

Once set up this selection criterion, some experiments have been carried out fuelling the single-cylinder engine with pure n-heptane, in order to perform a more appropriate comparison with simulations results. A wide range of operative parameters have been varied to test the code reliability with respect to different engine operative conditions. A reaction scheme for n-heptane ignition and combustion (Liu, 2004) has been used for the numerical simulations.

The combustion model seems to be very representative of the low temperature combustion process: in any of the chosen test cases the predicted ignition delay values are very close to experimental ones.

It is worth mentioning that the diesel simulation context is certainly inadequate to test the reaction mechanism capabilities, as the good agreement between predictions and measured pressure cycles has to be also ascribed to the spray model.

Still the full model as a whole, in the modified version of the code, has proven to be a reliable tool for diesel simulations and more detailed reaction schemes could be implemented as future developments of the activity.

In this respect, the simulation of alternative combustion modes (LTC/PCCI), where strong premixing determines a kinetic control of the phenomenon, are likely to require the implementation of more detailed reaction schemes, to depict the multi stage ignition dynamics typical of such combustion development, and more sophisticated models of turbulence-chemistry interaction.

For now, the current reaction scheme has been used for coupling with particulate matter formation modeling, as illustrated in the next chapter, yet the modularity of the mechanisms can of course allow the coupling of the soot model to different autoignition reaction schemes.

Bibliography

BAULCH, D.L., COBOS, R.A., COX, R.A., FRANK, P., HAYMAN, G., JUST, T, KERR, J.A., MURRELS, T., PILLING, M.J., TROE, J., WALKER, R.W., WARNATZ, J., Combust. Flame 98, 59-79, 1994.

BEATRICE, C., AVOLIO, G., DEL GIACOMO, N., GUIDO, C*., Compression ratio influence on the performance of an advanced single-cylinder diesel engine operating in Conventional and Low Temperature Combustion mode*, SAE Paper 2008-01-1678, 2008.

BELARDINI, P., BERTOLI, C., CORSARO, S., D'AMBRA, P., FRAIOLI, V., *Application of a multi-method ODE software component for simulations of ultra-low emissions diesel engines*, Fisita F2006P027, 10, 2006.

BELARDINI, P., BERTOLI, C., CORSARO, S., D'AMBRA, P*: The impact of different stiff ODE solvers in parallel simulation of Diesel combustion*. In LNCS Vol. 3726 "High Performance Computing and Communications", Springer Berlin, 2005.

BROWN P.N., BYRNE G.D., AND HINDMARSH A.C, *VODE: A Variable Coefficient ODE Solver*, SIAM J. Sci. Stat. Comput., 1989.

CIPOLLA G., VASSALLO A., CATANIA A. E., SPESSA E., STAN C., DRISCHMANN L., *Combined Application of CFD Modeling and Pressure-based Combustion Diagnostics for the Development of a Low Compression Ratio High-Performance Diesel Engine*, SAE PAPER 2007-24-0034, 2007.

H.J. CURRAN, P. GAFFURI, W.J. PITZ, C.K. WESTBROOK, Combust. Flame 114 (1–2), 149–177, 1998.

FARREL J.T., CERNANSKY N.P., DRYER F.L., LAW C.K., FRIEND D.G., HERGART C.A., MCDAVID R.M., PATEL A.K., MUELLER C.J., PITSCH H., *Development of an Experimental Database and Kinetic Models for Surrogate Diesel Fuels*, SAE 2007-01-0201, 2007.

GENZALE, C.L., REITZ, R., MUSCULUS, M., *Effects of Jet-Bowl and Jet-Jet Interactions on Late-Injection Low-Temperature Heavy-Duty Diesel Combustion*, THIESEL 2008.

GUSTAVSSON J., GOLOVITCHEV V.I., *Spray Combustion Simulation Based on Detailed Chemistry Approach for Diesel Fuel Surrogate Model*, SAE Paper 2003-0137, 2003.

HAIRER, E., WANNER, G., *Solving Ordinary Differential Equations II. Stiff and Differential-Algebraic Problems*, Second Edition, Springer Series in Comput. Mathematics, Vol.14, Springer-Verlag, 1996.

HAMADA K., NIIJIMA S., YOSHIDA KAZUNORI, YOSHIDA KOJI, SHOJI H., SHIMADA K., SHIBANO K., *The effects of the Compression Ratio, Equivalence ratio, and Intake Air Temperature on Ignition Timing in an HCCI Engine Using DME Fuel*, SAE PAPER 2005-32-0002, 2005.

KEE, F. M., RUPLEY, MILLER, J. A., *Chemkin-II: A Fortran chemical kinetics package for the analysis of gas-phase chemical kinetics*, SAND89-8009, Sandia National Laboratories, 1991.

LIU, S., HEWSON, J.C., CHEN, J.H., PITSCH, H., *Effects of strain rate on high-pressure nonpremixed n-heptane autoignition in counterflow*, Combust. Flame 137, 320-339, 2004.

RANZI, E., GAFFURI, P., FARAVELLI, T., AND DAGAUT, P, *A Wide Range Modeling Study of n-Heptane Oxidation*, Combust.Flame, 103, 1995.

TSANG W. *Progress in the development of combustion kinetics databases for liquid fuels*, Data Science Journal, 3, 2004.

WESTBROOK, C. K., *Chemical Kinetics of Hydrocarbon Ignition in Practical Combustion Systems*, Proc. of the Comb. Inst., 28, 2000.

ZHENG, J., MILLER, D.L., CERNANSKY, P., *A Global Reaction Model for the HCCI Combustion Process*. SAE 2004-01-2950, 2004.

Chapter five

Particles formation modeling

5.1 Introduction

Modelling the soot aerosol formation and dynamics during combustion in the diesel engine represents a challenging task.

Even neglecting that, as concerns the gas phase autoignition kinetics, the choice of a proper surrogate for complex fuels like diesel is still a developing goal, a lot of issues have to be addressed when an "aerosol phase" has to be modelled together with the diesel combustion system.

Some questions arising with soot simulation in CFD are:

o   Choice of the kinetic scheme for the gas phase.

First of all, since the soot formation process (see Par.1.1.3) involves a very high number of chemical intermediates acting as gaseous precursors of the solid phase, the inclusion of a very high number of species into the kinetic scheme is naturally required. Therefore, from a strictly computational point of view, a considerable effort is required in terms of time.

With respect to this point, it has to be added that mechanisms for soot precursors kinetics and those for autoignition kinetics have quite different "histories".

In fact, a lot of study and validation work has been carried out on autoignition kinetics, thus nowadays a wide choice of reduced schemes for fuels ignition, suitable for multidimensional simulations, is available in the literature. On the contrary, soot formation kinetics is still a contentious topic and computationally cheap models do not derive, as for gas kinetics, from activities like sensitivity analysis or reduction-validation, but are often defined as semi-empirical or phenomenological.

o   Solid phase model development.

The phenomenon itself is very complex, due, as an example, to the presence of nascent particles whose nature passes from huge gas molecules to a solid phase and a wide range of sizes is covered (giving rise to particles that can be either in a kinetic regime or in a continuum regime).

o   Coupling with turbulent flow in a CFD framework.

Finally, also the coupling of the aerosol dynamics with the flow calculations typical of 3D-CFD codes is a critical aspect to be taken into account. As an example, it is not straightforward to establish whether the typical

solutions for turbulence-chemistry interactions are adequate for solid particles formation too.

In the last years, several modeling approaches of various complexity and computational cost have been followed to incorporate soot modelling in 3D diesel calculations.

In order to solve, in general, the population balance of soot particles in flames, Frenklach et al. (Frenklach, 1990) proposed the method of moments, that permits to calculate the total particle number density, the mean particle diameter or the variance of the size distribution, but not its exact shape. On the other hand, the sectional model, originally proposed by (Pope, 1997), realizes a discretization of the particles size distribution function in a finite number of sections.

Mauss et al. (Priesching, 2005) solved the moments of the size distribution function for the discretized sections, combining this approach to a detailed kinetic model. This model has been applied to simulate soot formation in diesel spray combustion by means of commercial codes like STAR CD and FIRE.

In the work of (Hong, 2005) the basic framework of the soot modelling is the moment method, coupled to the Kitamura mechanism for soot surface growth and oxidation and implemented in KIVA3V: here also the importance of the particles transport is emphasized.

The computational modelling group of Cambridge performed the simulation of combustion in an HCCI Toyota engine fuelled with heptane (Mosbach, 2008), by means of a stochastic reactor model (inspired by PDF transport method) coupled with detailed kinetics. In this case soot formation has been described through a statistical site-counting approach: the particles are described by nine variables, including the number of different kind of aromatic sites (Celnik, 2007).

At Chalmers University (Gustavvsson, 2003) soot formation was modelled in KIVA directly linking its production to acenaphtylene and C_4H_2, generally postulating a graphitization rate: in this case only the total amount of soot could be predicted.

Finally, Reitz et al. adopted in KIVA3V a phenomenological soot model (Tao, 2006), made up of nine-steps and linked to the Shell ignition model.

In this work, an attempt to simulate the soot particles formation and the respective size distribution function has been carried out, taking advantage of the activities of parallelization and implementation of detailed kinetics previously illustrated.

The general modeling approach is described in the following paragraph, while in Par.5.3 the details of the adopted model are given.

In Par.5.4 some preliminary results are discussed, while Par.5.5 reports a first comparison with the measures of particle size distributions performed on the same engine used as reference for the simulations.

5.2   Particle formation modeling: the sectional approach

One of the simplest soot formation models implemented in multidimensional KIVA calculations, (Belardini, 1992), (Kong, 1995), was Hiroyasu model –(Hiroyasu, 1983), where the net rate of change in soot mass was calculated as the difference between the rates of soot formation and oxidation. The formation and the oxidation rates were expressed in an Arrhenius form, with empirical values of the activation energies and pre-exponential factors.

In a subsequent version of the KIVA code (KIVA3V - 1997), the Surovikin's model (Surovikin, 1976) for soot formation, together with the semi-empirical Nagle and Strickland-Constable's oxidation model (Nagle, 1962) was implemented.

Such model distinguished particles into radical nuclei and soot particles, but the process is oversimplified and no more adequate for the current modelling requirements.

As a matter of fact, in the current scenario of internal combustion engines development (see Par 1.1.1), simulations are required to give more details on particulate formation, especially if the importance of particles' size -in future emission limits and in toxicological studies- is taken into account.

Thanks to the implementation of detailed kinetics in the KIVA3V code, it has been possible to adopt an approach, for the particles formation modelling, that combines the aerosol equations to the elementary steps of the gas phase.

The method had been originally developed by Pope (Pope, 1997) and applied to soot formation modelling in premixed laminar flames of benzene by Richter (Richter, 2005).

Its main advantage is the possibility to couple the gas phase and the particles formation dynamics, solving the phenomena simultaneously. On the contrary, in older methods, like the method of moments (Mauss, 1994), the results from the gas-phase calculation were used as inputs for the aerosol dynamics modelling, thereby taking into account the soot effect on the precursors kinetics only at a limited extent.

The basic idea of the sectional approach is to subdivide the particles population into classes of fixed molecular weight or fixed particle dimension, called bins. More exactly, the continuous dimensional distribution function is discretized so that a certain bin "contains" all the particles whose molecular weight falls into a prescribed interval of values.

As a result, not only integral quantities like the total mass and number of particles can be calculated, but also the shape of the particles size distribution function.

Furthermore, the coagulation between particles, the reaction with molecules from the gas phase and the mass depletion via oxidation at the particle surface are formally represented as further reactions of the kinetic mechanism. In practice the sectional equations are converted into elementary steps, in order to solve at the same time both the gas and the solid phase.

The bins include all the species having a molecular weight beyond a certain threshold value v_0 and bin boundary are usually spaced linearly with $\ln(v)$.

In the original work of Pope, collision frequencies for reactions between particles and gas molecules were calculated from the gas kinetic theory, therefore the aerosol was assumed to be in free molecule regime. In this limit the mean free path of molecules is

much larger than the particle diameter, as a consequence, the gas phase see the particle just as another molecule[15].

5.3   The adopted model

In the present work, the low temperature kinetics for heptane autoignition from (Liu, 2004), (used for the autoignition simulations in the previous chapter) has been linked to the model for gas precursors. Reactions are added to account for the formation of benzene, including acetylene reactivity and the formation of PAHs up to pyrene (D'Anna, 2006).
Finally the sectional equations from (D'Anna et al., 2008) are included, to account for particle formation.

The gas-phase precursors model and the sectional model used in this work have been validated against measures in rich premixed flames (D'Anna, 2008) and coflowing diffusion flames of ethylene (D'Anna, 2006). The model has also been tested comparing species concentrations in nonpremixed laminar flames of methane, ethylene and butene (D'Anna et al., 2008).

The full set implemented in the modified version of KIVA is made up of 82 gas species – to describe autoignition and gaseous precursors kinetics- plus 50 species accounting for the sectional model, therefore the complete reaction scheme comprises 132 species and 2206 reaction steps.

With respect to the code version used for the simulations in Chapter4, some modifications were necessary to implement the sectional model: the Chemkin Interpreter has been modified to accommodate species made up of large numbers of carbon atoms, while the ChemKin Library incorporated in KIVA has been updated to the version 4.3, in order to accept fractional stoichiometric coefficients.

As regards the reaction mechanism, the formation and growth of aromatic compounds links the main oxidation chemistry and particulate formation. During oxidation, the fuel generates small radicals which react to form the first aromatic ring.

The formation of phenyl radical and benzene is considered to occur through the addition of n-C_4H_3 and n-C_4H_5 to C_2H_2, leading to phenyl and benzene + H, respectively, and the self-combination of propargyl radicals. The formation of naphthalene, the first compound in the PAH series, is modelled through two routes: the first is the sequential addition of C_2H_2 to phenyl radical (HACA mechanism); the second is the combination of resonantly stabilized radicals. This process is also used here to model the formation of multiring structures such as phenanthrene and pyrene (the largest compound modeled explicitly). By-products of the HACA process are ethynyl-substituted PAH and five-membered aromatics such as acenaphthylene.

Two different reaction sequences of resonantly stabilized radicals are included for the formation of naphthalene: the combination of two cyclopentadienyl radicals and the combination of benzyl and propargyl radicals.

The mechanism consists in the sequential addition both of acetylene and aromatic molecules to aromatic radicals.

[15] Strictly speaking, such assumption is rigorous, at ambient air, only for particles having diameters smaller than 10nm, as in this case Knudsen number is much smaller than unity.

Acetylene addition is the extension of the HACA mechanism to larger compounds with the assumption that, due to the high number of sites where acetylene can be attached, each acetylene addition sequence forms a closed aromatic ring and hence leads to the formation of fully condensed aromatic structures.

Aromatic molecule addition to aromatic radicals leads to the formation of aromatic-aliphatic linked, biphenyl-like, compounds. This reaction sequence is favoured by the presence of a non negligible concentration of five-member ring PAHs in the PAH inventory.

These compounds grow rapidly forming resonantly stabilized radical intermediates. Acetylene and the aromatic addition sequences begin with the H-loss of an aromatic compound, to produce the corresponding PAH radical either through decomposition reactions of aromatics or H-abstraction by H and OH radicals. Aromatic radicals can react with other aromatic radicals or with H atoms ending the growth sequence. Iteration of these pathways leads to the formation of a large number of high-molecular-mass compounds and of its structural isomers.

Starting from pyrene, classes of compounds, each covering a mass range, have been utilized. Classes are characterized by their average molecular mass and by the number of carbon and hydrogen atoms. Reactions are treated in the same way as for gas-phase chemistry.

The aromatic growth and oxidation mechanism is schematized as follows:

(Rx1) $Ai \rightarrow Ri+H$
(Rx2) $Ai+H \rightarrow Ri+H_2$
(Rx3) $Ai+OH \rightarrow Ri+H_2O$
(Rx4) $Ri+H_2 \rightarrow Ai+H$
(Rx5) $Ri+H_2O \rightarrow Ai+OH$
(Rx6) $Ri+C_2H_2 \rightarrow Ai+H$
(Rx7) $Ri+Aj \rightarrow Ai+j+H$
(Rx8) $Ri+Rj \rightarrow Ai+j$
(Rx9) $Ri+H \rightarrow Ai$
(Rx10) $Ai+OH \rightarrow Ak+HCO$
(Rx11) $Ri+O_2 \rightarrow Ak+2CO$
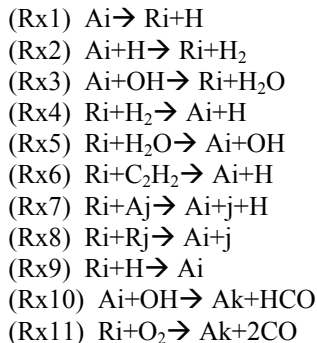
Here, Ai is an aromatic compound having a molecular mass corresponding to the ith class of compounds and Ri is its radical.

The first lumped species (Ai and Ri with i=1) have 24 C-atoms and are formed by the self-combination of gas-phase aromatic radicals and reactions between gas-phase aromatic radicals and gas phase aromatic molecules.

The sectional size dependence in reactions Rx1 and Rx6 are obtained by interpolating the kinetic data of the MIT kinetic scheme (Richter, 2005). For all other reactions size dependence is obtained from gas-kinetic theory with an exponent of 2/3 for a gaseous species colliding with a particle (surface area to volume ratio) and with 1/6 for a particle to particle collision based on the average size of the two particles.

Rate constants for the aromatic growth mechanism are evaluated on the basis of structural similarities with the reaction rates of PAHs.

The rate of hydrogen loss via the unimolecular reaction (Rx1) is evaluated using as reference the rate of benzene decomposition.

Initiation reactions (Rx2 and Rx3) are reversible, and the forward reaction rates are assumed to be equal to H atom abstraction from naphthalene molecules. The reaction rate is scaled by the variation in collision efficiencies to take into account the increase of reactivity.

Equilibrium of the initiation reactions (Rx4 and Rx5) is strongly affected by the number of C atoms in the molecule. Radical compounds composed of a large number of C atoms are stable enough to survive in their radical form, because of the delocalization of the unpaired electron resulting in a lower rate of the reverse reactions.

At present, reverse reaction rates (Rx4 and Rx5) for the lumped species belonging to the first three classes of compounds (300–1200 Da) are here evaluated from equilibrium constant of coronene. For larger molecular masses, thermodynamic properties are not known; in these cases, reactions Rx4 and Rx5 are considered irreversible.

The rate constant for acetylene addition to aromatic radicals (Rx6) is based on the reaction rate of naphthyl + acetylene scaled by increasing collision efficiencies.

On the basis of structural similarity, the rate constant for phenyl + benzene is used as the reference for the corresponding aromatic radical + aromatic molecule reaction (Rx7) which is scaled for variation in collision efficiencies. Termination reactions of aromatic radicals with other aromatic radicals (Rx8) or with H atoms (Rx9) ending the growth sequence have rate constants evaluated from the collision efficiencies of the reacting species.

Hydroxyl radical OH was identified to be the dominant oxidizing species of soot in flames. The activation energy for Rx10 is estimated from similar reactions for benzene and PAH's, and the collision frequency accounts for the size of the oxidized particles from Neoh et al. data. Oxidation by O_2 molecules (Rx11) uses the rate constant of naphthyl + O_2 accounting for the increase of the collision efficiency of large species.

The aromatics growth process can occur also by formation of molecular clusters after the collision of molecular compounds.

$Ai+Aj \rightarrow Ai+j$ (Rx12)

Colliding molecular particles coalesce completely yielding new spherical structures, whereas larger particles may agglomerate into chainlike structures. At present, the model does not account for the formation of chainlike structure, and each collision is considered coalescent.

The interaction energy in this case is due to van der Waals forces. Small molecular mass aromatics may exhibit low interaction energy to form a stable three-dimensional structure at flame temperatures. As the molecular mass of the aromatic compounds increases, the van der Waals interaction energy between high molecular mass aromatic molecules increases and coagulation efficiency becomes more effective.

In Tab.5.1 the main features of each class are reported, together with the equivalent diameter corresponding to every section.

Table 5.1 **Classes defining the particles population**

BIN	# C atoms	# H atoms	H/C	Mass (amu)	Dp, nm	Density, g/cm³
1	24	12	0,500	3,0000E+02	0,94	1.20
2	48	24	0,500	6,0000E+02	1,12	1.41
3	96	48	0,500	1,2000E+03	1,38	1.52
4	193	84	0,435	2,4000E+03	1,71	1.60
5	388	144	0,371	4,8000E+03	2,14	1.64
6	778	264	0,339	9,6000E+03	2,67	1.67
7	1560	480	0,308	1,9200E+04	3,35	1.70
8	3124	912	0,292	3,8400E+04	4,21	1.71
9	6256	1728	0,276	7,6800E+04	5,29	1.72
10	12528	3264	0,261	1,5360E+05	6,63	1.75
11	25088	6144	0,245	3,0720E+05	8,31	1.77
12	50240	11520	0,229	6,1440E+05	10,45	1.78
13	100608	21504	0,214	1,2288E+06	13,13	1.79
14	201472	39936	0,198	2,4576E+06	16,47	1.82
15	403456	73728	0,183	4,9152E+06	20,73	1.82
16	807936	135168	0,167	9,8304E+06	26,01	1.84
17	1617920	245760	0,152	1,9661E+07	32,69	1.86
18	3239936	442368	0,137	3,9322E+07	41,14	1.86
19	6483968	835584	0,129	7,8643E+07	51,61	1.88
20	12972032	1622016	0,125	1,5729E+08	65,00	1.88
21	25944100	2464690	0,095	3,1379E+08	81,57	1.90
22	51888250	4773718	0,092	6,2743E+08	102,67	1.91
23	103776600	9028564	0,087	1,2543E+09	129,30	1.91
24	207557000	17019674	0,082	2,5077E+09	162,63	1.91
25	415150000	33212000	0,080	5,0150E+09	204,70	1.92

BINs 1 to 3 ideally correspond to the largest precursors, while the three subsequent classes can respresent nascent soot particles.

5.4   Results and discussion

The VODE library has been used for the kinetics solution and the switching to the SDIRK library (described in Par.4.2) has not be adopted for the following simulations, in order to exclude, in these preliminary tests, any possible sources of uncertainties deriving from the usage of different solvers.

The operative condition adopted[16] for the first simulation tests corresponds to the experimental test in Table 5.2, with the piston bowl corresponding to a compression ratio value of 16.5. The engine is fuelled with pure heptane.

Table 5.2 **Experimental operative conditions** – CR=16.5

Speed [rpm]	Rail pressure [bar]	EGR %	SOEC CAD BTDC	ET [μs]	IMEP [bar]
1500	480	0	9	710	4.13

In Fig 5.1 the measured pressure cycle and the respective rate of heat release are reported: in-cylinder pressure starts to rise at about 8 CAD ATDC and the pressure peak is located at 12 CAD ATDC, when the heat release rate returns to zero.
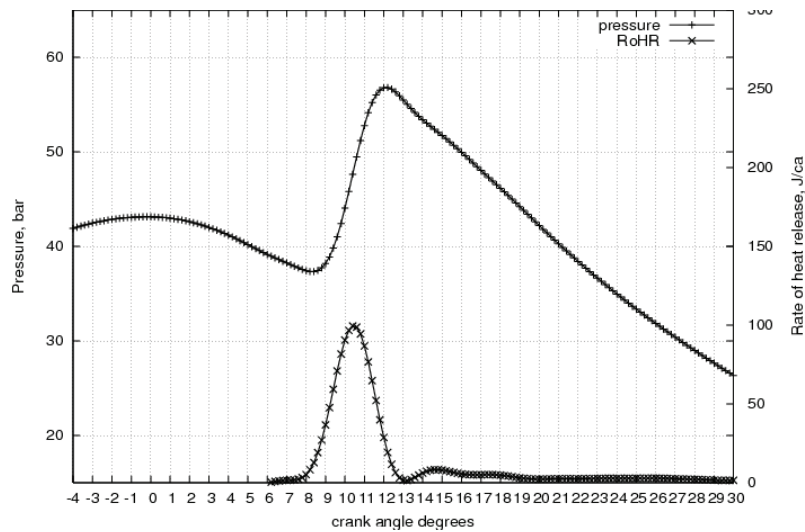
Figure 5.1 – Measured in-cylinder pressure profile and rate of heat release for case "jv15x2001"

This case has been computed with and without the particle formation model, thereby making possible a preliminary evaluation of the effect of the different reaction sets implemented on the predicted pressure cycle.

---

[16] It has to be said that this operative condition is not a very sooting one, but it has been chosen for these first numerical tests because, as first implementation, it allows not to take into account the effect of particles recirculation.

Simulations have been performed using three reaction schemes: the original 44-specie mechanism for autoignition (Liu,2004), the scheme obtained adding, to the previous one, only the gas phase precursors kinetics and the full set of reactions, including the sectional model for the particles formation.

As noticeable from Fig.5.2, in all the cases the comparison with the measured pressure cycle is satisfactory and both the ignition delay and the high pressure phase are properly captured. The main differences concern the pressure rise, as the PAH inclusion without the particles tends to enhance the combustion speed.

Once the soot formation model is added, the pressure time-derivative becomes less steep and the only difference with the 44-species mechanisms is in the lower pressure peak.
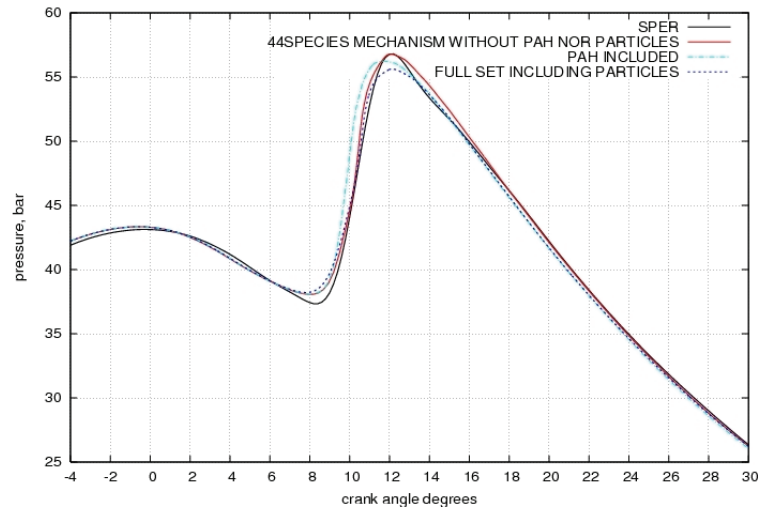
Figure 5.2 – Effect of the reaction mechanism on the predicted pressure cycle: 44 species scheme by (Liu, 2004) – red line, addition of PAH and acetylene kinetics – green dashed line, full set including sectional model – blue dotted line. Measured values- black line.

In Fig.5.3 the sum of some stable reaction intermediates is reported versus crank angle, calculated by the original autoignition scheme and by the full reactions set, respectively: the addition of the particles formation scheme keeps the low temperature gas-phase dynamics practically unchanged, preserving a similar composition of the gas mixture during the combustion phase. Although this is a rather obvious result, it is however a necessary verification for the subsequent analysis.
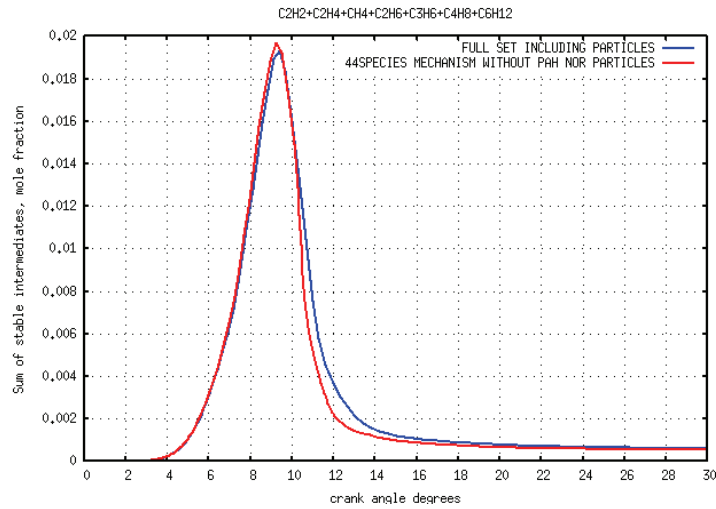
Figure 5.3 – Sum of stable intermediates (acetylene, ethylene, methane, ethane, propilene, butane and esene) calculated with the autoignition reaction mechanism (red line) and with the full reaction set including the particle sectional model – (blue line)

Finally, looking at CO_2 and CO concentrations in Fig.5.4, it is also possible to verify that the inclusion of the sectional model does not affect significantly the final values of these combustion products, even though a slightly higher concentration of carbon monoxide is calculated between 14 and 64 CAD ATDC, produced during particles oxidation.
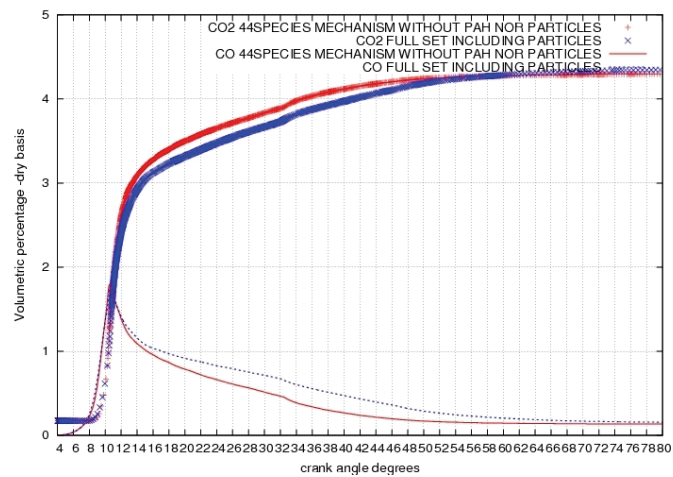
Figure 5.4 – CO_2 and CO concentrations predicted by the 44 species reaction scheme (Liu, 2004) – red lines- and by the full reaction set including sectional model – blue lines.

In conclusion, the kinetic mechanism modification and the addition of the sectional equations do not alter significantly the general predictions in terms of combustion timing and pressure evolution.

A qualitative overview on the predicted general combustion development is now given.

It is possible to see from Fig.5.5 that the liquid jet is directed downwards: the average spray direction forms an angle of roughly 60° with the vertical cylinder axis. It follows that, in general, at CAD values near TDC, the combustion process will evolve "moving" towards the bowl walls.
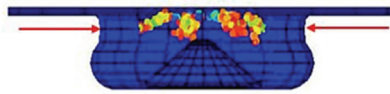
Figure 5.5 – General view of the combustion chamber at top dead centre with magnified fuel droplets.

Differently from the domain depicted in Fig.5.5, however, for the subsequent calculations the computational mesh is a 51° sector of the full cylinder that contains only one of the seven jets sprayed by the 7-holes injector.
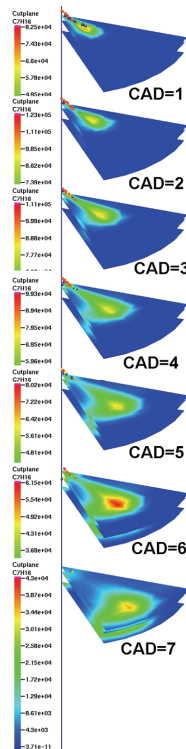
Figure 5.6 – Vapour fuel spatial distribution from 1 to 7 CAD ATDC – the fuel spray droplets are magnified and displayed as coloured circles. The scale of fuel vapour concentration is expressed in ppm.

In Fig.5.6 the vaporized fuel distribution in the computational domain is depicted, in a plane that cuts the bowl at a fixed height. The fuel is spread around the liquid jet and the vapour cloud is also deformed by the air motion, as the air is swirled (clockwise in the current view) thanks to the intake ducts shape (see Par.2.3).
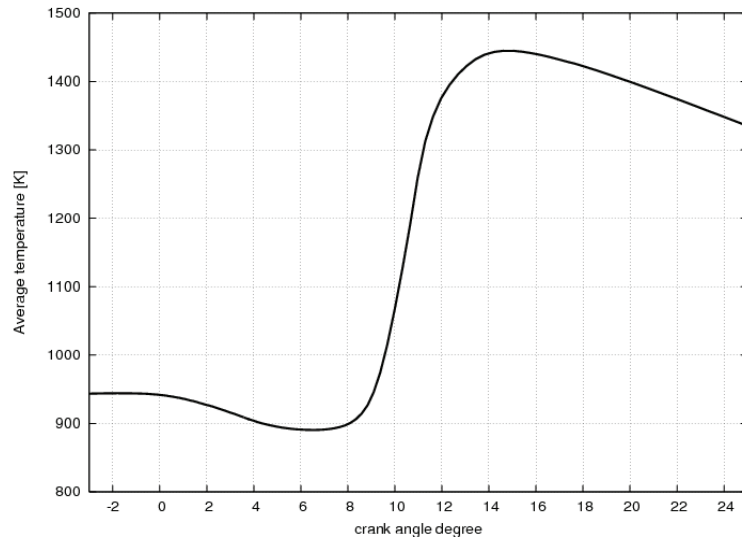

*Figure 5.7* – Calculated in-cylinder average temperature
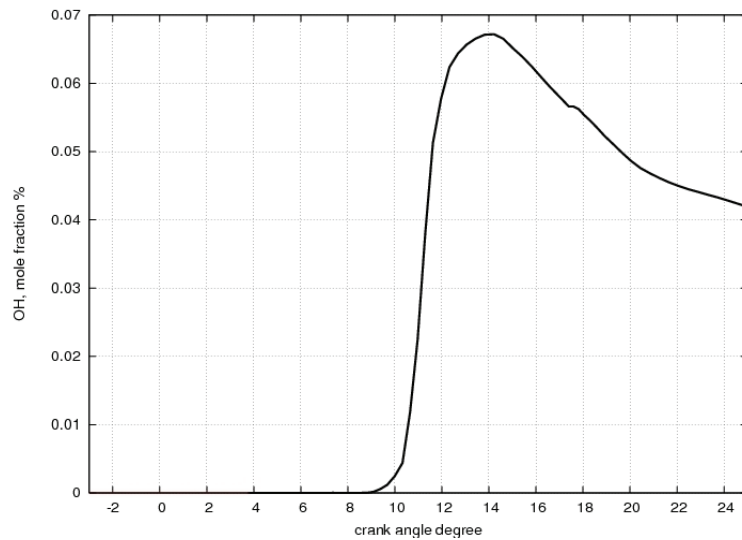
Figure 5.8 – Temporal evolution of total in-cylinder content of hydroxyl radical (OH) - mole fraction

Looking at the average temperature and hydroxyl radical concentration profiles, in Fig.5.7 and Fig.5.8 respectively, it is possible to establish that ignition occurs at 9 CAD ATDC, as the instant of maximum OH radicals release, from hydrogen peroxide decomposition.

In Fig.5.9 the evolution of the temperature distribution is represented, in comparison with the spatial distributions of oxygen, carbon monoxide and carbon dioxide, hydroxyl radical and ethylene. Carbon dioxide is located where the highest temperature values are attained, while carbon monoxide is concentrated inside the ring of maximum dioxide concentration.
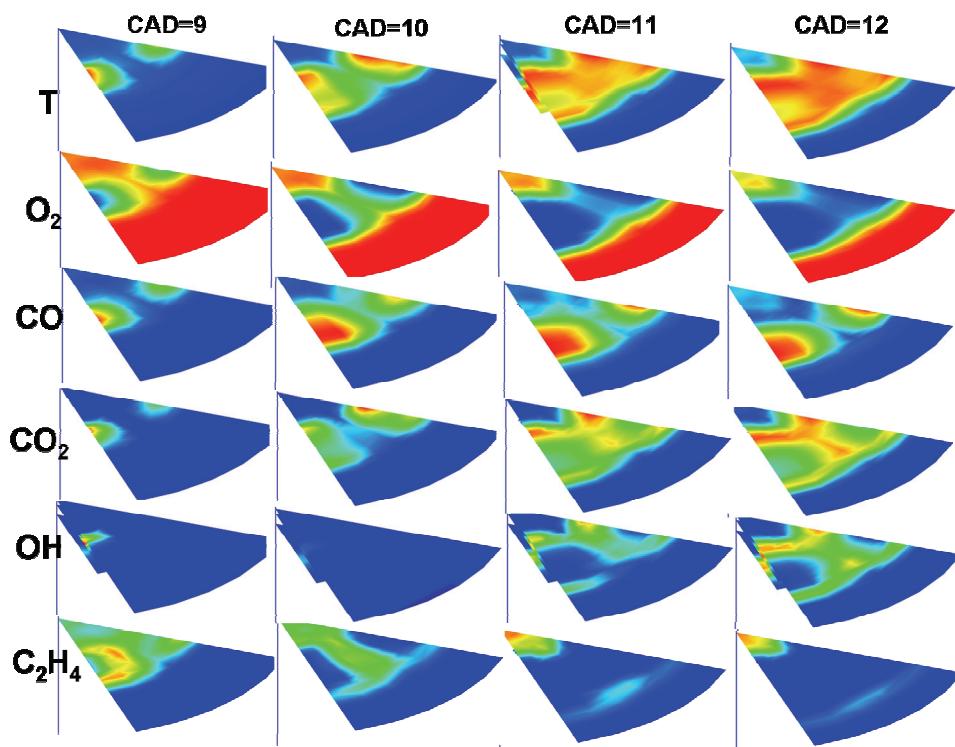
Figure 5.9 – Comparison of the spatial variation of temperature, oxygen concentration, carbon monoxide and carbon dioxide (volumetric ppm) from 9 to 12 CAD ATDC

OH radicals are located in the hottest cells, while ethylene, whose role is crucial during the autoignition, is mostly concentrated in the areas at intermediate temperatures and low oxygen concentration.

In Fig.5.10 some gaseous combustion products, calculated at the exhaust valve opening, are compared with the respective quantities measured at the exhaust tail pipe.

It is important to verify that oxygen and carbon dioxide in the exhaust gas are in perfect agreement with computed values, in order to be sure that the total carbon mass content, introduced through the fuel injection, has been properly set.

In the present test case such agreement is obtained, while carbon monoxide is highly overestimated.
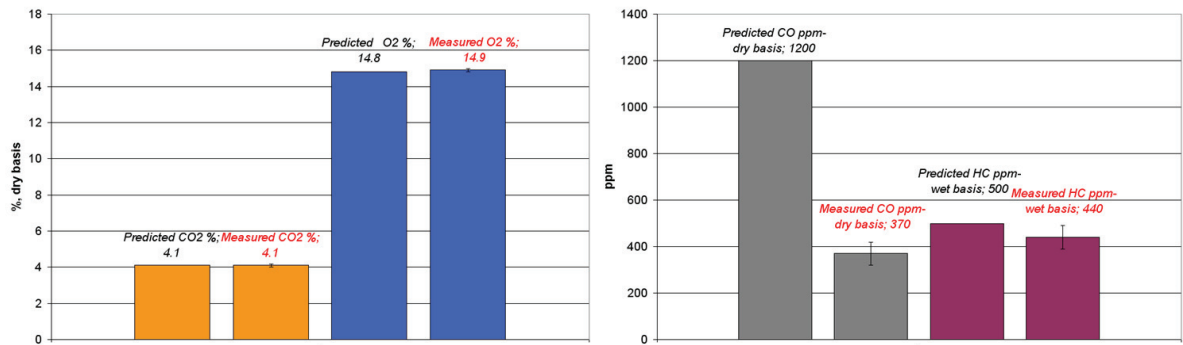

Figure 5.10 – Comparison between concentration measured at the exhaust and in-cylinder values computed at the end of the expansion phase, for oxygen, carbon dioxide, carbon monoxide and unburned hydrocarbons.

Unburned hydrocarbons are expressed as total carbon content in terms of ppm of methane equivalent and are calculated summing all the residual quantities of aliphatic hydrocarbons, olefins and alkynes included in the reaction mechanism.

Taking into account also the experimental uncertainty in the HC measure, the predicted quantity is in reasonable agreement with the measured data.

In Figs 5.11 to 5.14 the concentration profiles of acetylene and some PAH are reported.
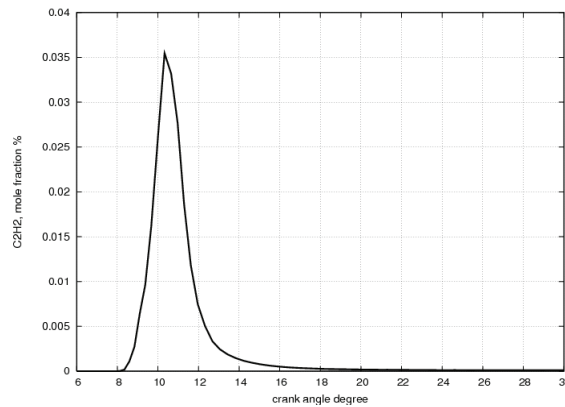
*Figure 5.11* – Acetylene (C2H2) in-cylinder total concentration -mole fraction, percentage.
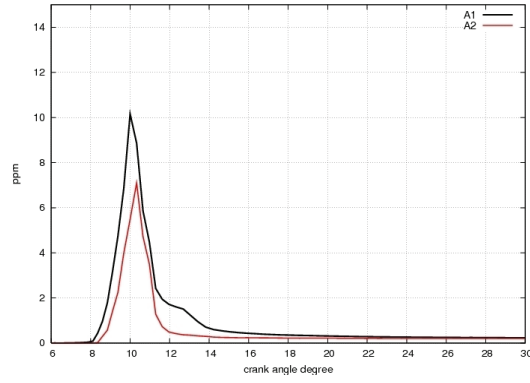
*Figure 5.12* – Benzene (A1) and naphthalene (A2) in-cylinder total concentration - ppm
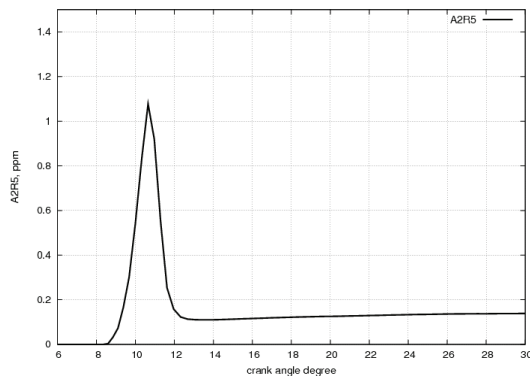
*Figure 5.13* – Acenaphthylene (A2R5) in-cylinder total concentration - ppm
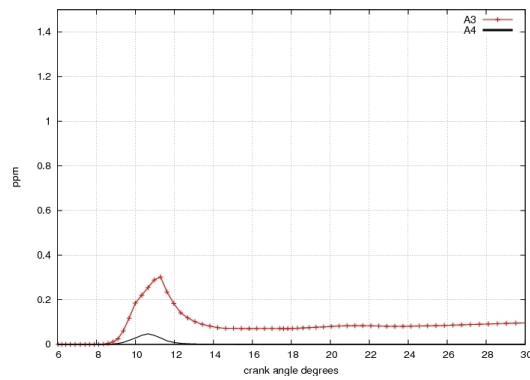
Figure 5.14 – Phenantrene (A3) and pyrene (A4) in-cylinder total concentration - ppm

In Fig.5.15 the temporal evolution of the mass concentration of the particles classes is represented: particles are grouped according to their different formation-destruction dynamics. The upper left part of the figure includes largest PAH and nascent particles, with an equivalent diameter varying from 1 to 3nm: in the present simulation, such structures appear as soon as ignition starts, showing, as expected, a decreasing formation rate as the diameter increases.
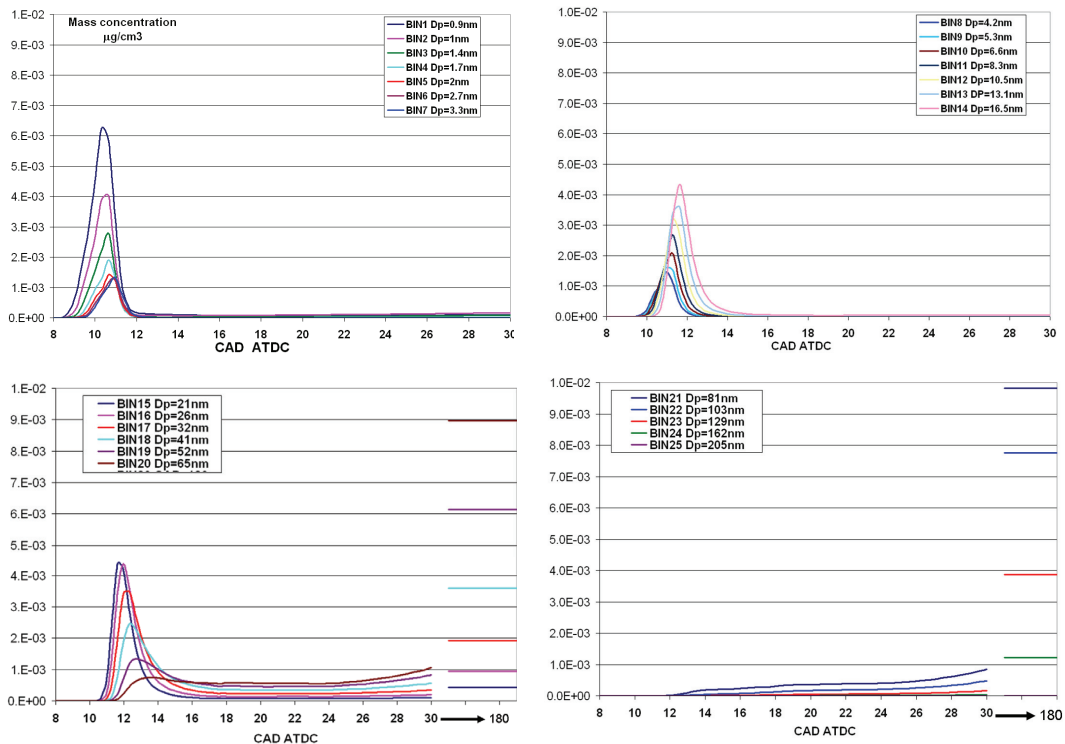

Figure 5.15 – Mass concentration of the classes of particles against crank angle degree: the classes are grouped according to their different formation dynamics

Particles whose size ranges from 4 to 16 nm (upper right picture) form around 10 CAD ATDC and exhibit a formation dynamics different from the previous group: here larger particles are produced at a rate that increases as the diameter grows, one of the causes being the higher temperatures present at this stage of the combustion.

Between 10 and 12 CAD ATDC (lower left picture), when the maximum temperature and pressure values are attained, particles having diameters ranging from 20 to 65nm are formed: now the formation rate starts decreasing again with the particle dimension, while a non-zero value is reached after the oxidation phase. In fact such particles not only attain a nearly constant mass concentration between 18 and 25 CAD, but they also start further accumulating from 25 degrees on. The same picture also reports the asymptotic values reached at 180 degrees ATDC.

Finally, particles with diameters ranging from 80 to 200nm (lower right picture) exhibit a continuous increase in their mass concentration: the final concentration value is attained at about 120 CAD. Contrary to the previous group of particles, the asymptotic values are scaled inversely to the particle size, since final values of mass concentration, for particles larger than 80 nm, are reduced according to the increase in the diameter.

It has to be pointed out that the concentration of the last class (bin25) is always negligible, thus assuring an accurate prediction in terms of dimensional spacing in the model discretization[17].

In Fig.5.16 the temporal evolution of temperature spatial distribution is compared with correspondent distributions of three classes of particles.

---

[17] Radicals correspondent to these largest particles are progressively more stable as the diameter increases, thus a quantitative comparison for the last sections– here not available- should also consider the radical bins concentration.
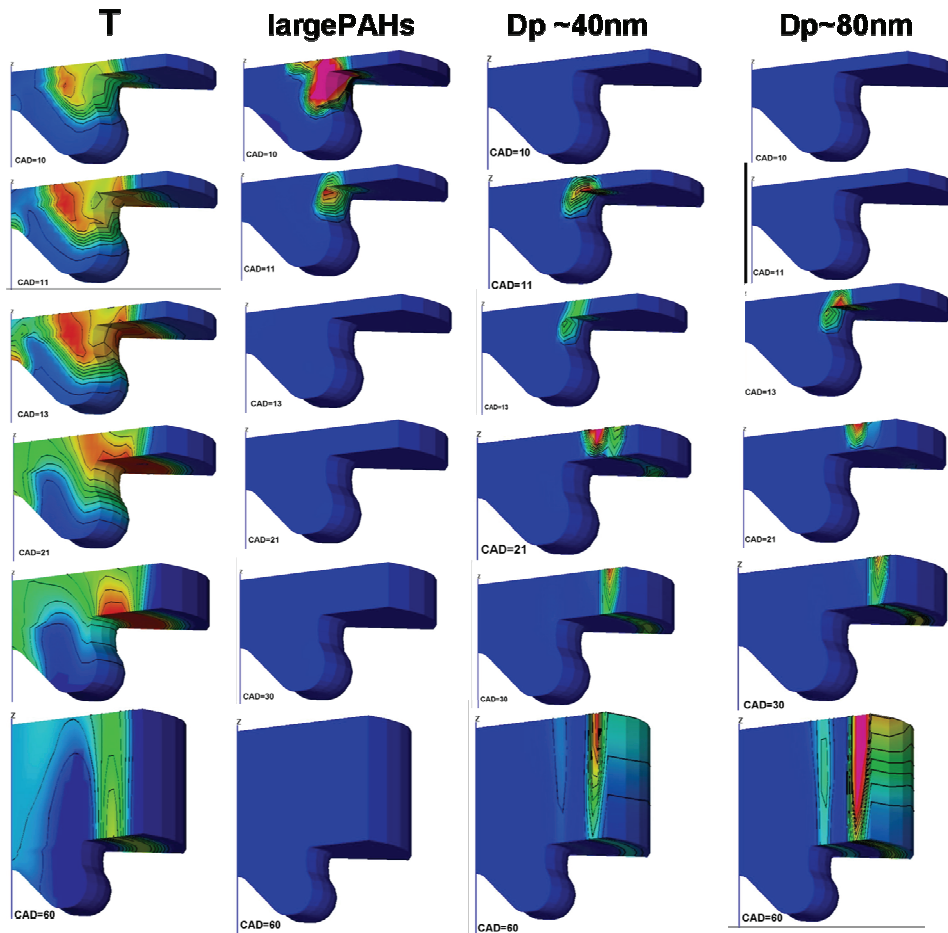
Figure 5.16- Evolution of temperature, soot precursors and of two classes of particles at six values of the crank angle: 10-11-13-21-30-60 CAD ATDC. Temperature- first column- varies between 800K (blue) and 2770K (red).

Looking, at first, at the temperature column, it can be noted that, between 10 and 13 CAD ATDC, the central hottest area is broadened: as the piston is pushed down, the zone of maximum temperatures moves towards the squish zone (or over the piston flat area) and at 60 CAD ATDC a hot ring survives in the whole volume, whereas the piston bowl and the cylinder walls are the coldest areas.

The temperature maps and the localization of the hottest cells look quite similar to those predicted in (Gustavvsson, 2003) for a Volvo NED5 DI diesel engine.

In the second column the concentration of the first section –BIN1- is displayed: according to the model predictions, nascent soot particles are formed next to the wall, downstream the highest temperature core (frames referred to 13 to 60 CAD appear

completely blue because the representation is in a fixed scale for all the degrees – 0-5 ppm).

At about 11-12 CAD larger particles appear –third column- and at 21 CAD the maximum concentration is attained in a ring corresponding to intermediate temperatures.

The stripe of particles with equivalent diameter of 40nm gradually moves towards the cylinder wall, as visible from the picture at 60 CAD.

Moving to the fourth column, it is possible to notice that particles of 80nm still accumulate in a band, slightly more external then the 40nm's one, corresponding to lower temperatures. This band too, during the expansion from 30 to 60 CAD ATDC, gets closer to the cylinder wall.

In Fig.5.17 a top view of the spatial distribution of the BIN21concentration gives a better idea of such localization with respect to the temperature map.
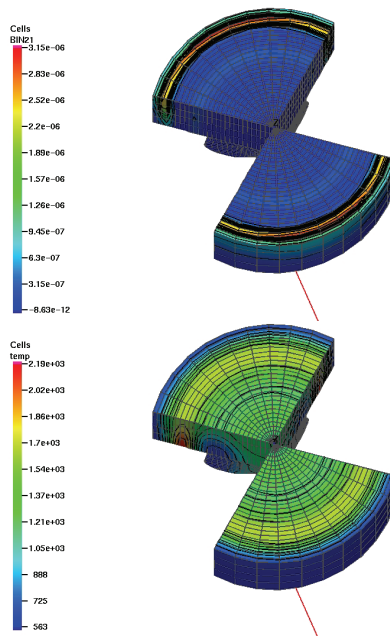

Figure 5.17 – Upper: spatial distribution of the concentration of section BIN21- corresponding to a mean diameter of 80nm- values are displayed in ppm. Lower: spatial distribution of temperatures – expressed in K- at the same CAD value.

In Fig.5.18 the mass concentration of the particles forming at the very early stages of combustion and during the high temperature phase is displayed: within 11 CAD ATDC the nascent particles, having radii between 1 and 3 nm, represent the total mass. As soon as the maximum pressure is attained, at 12 CAD, particles with sizes between 3 and 200nm completely account for the total mass concentration.
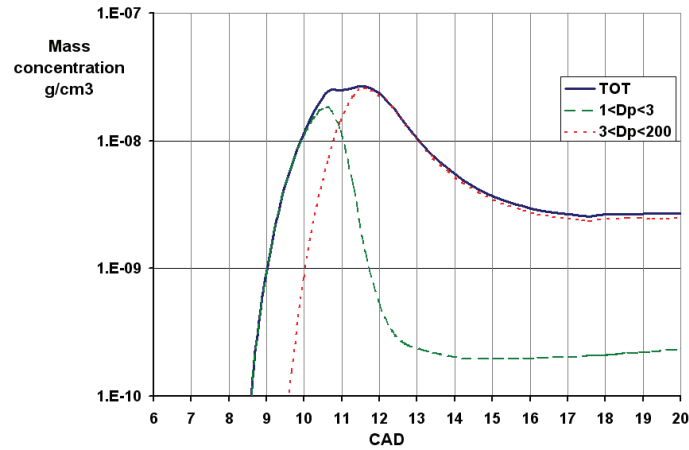
Figure 5.18 - Predicted mass concentration due to particles with sizes in the range 1-3 nm, 3-200 nm and total mass during the main heat release phase.

In the subsequent expansion phase, the smallest particles contribution to the total mass concentration is absolutely negligible, as illustrated in Fig. 5.19.
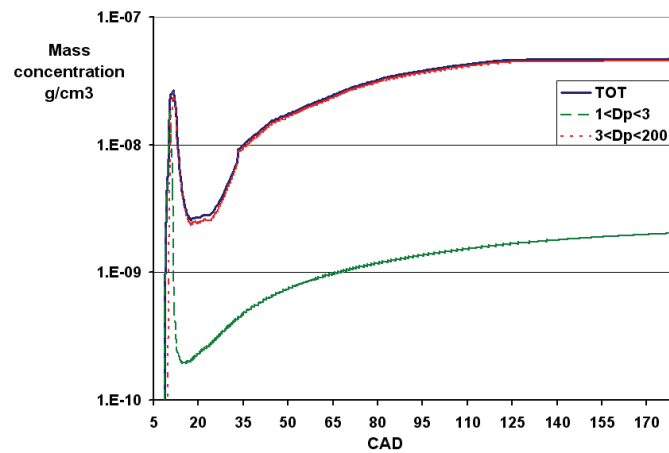

Figure 5.19 - Predicted mass concentration due to particles with sizes in the range 1-3 nm, 3-200 nm and total mass during the expansion phase.

Carbonaceous particles are produced during combustion and simultaneously oxidized between 5 and 20 CAD ATDC: an increase in the mass concentration can be ascribed to superficial growth of the particles due to the addition of species from the gas phase or to particle inception. However further analysis should be carried out to establish whether the marked increase up to an asymptotic value beyond the maximum concentration reached

during combustion -reported in Fig.5.19- is acceptable: it is likely that the model has overestimated the total amount of mass produced. This conclusion is confirmed and further discussed in par.5.5, where a comparison with measured data is presented.

Moving to the number concentration, the nascent molecular particles account for the total value during the whole cycle, as Fig.5.20 indicates. According to the model prediction, after 20 CAD ATDC, the total number of particles does not decrease and the number of particles with a size larger than 3 nm keeps increasing during the whole expansion phase. It is rather difficult to evaluate whether the smallest nascent particles presence until the exhaust valve opening is an acceptable prediction and further activity is necessary to develop an opinion with respect to this point.
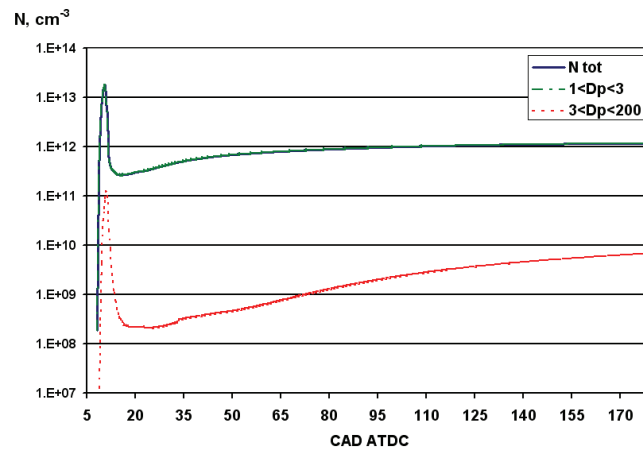

Figure 5.20 - Number concentration of particles in the 1-3nm size range and 3-200nm.

More in detail, the temporal evolution of the predicted size distribution function is reported in Fig.5.21 from 8 to 30 CAD ATDC.

In the earlier stages of the engine combustion (8-10 CAD ATDC), the number weighted particle distribution is mono-modal and the number density of nanoparticles less than 3nm in diameter starts to increase steeply. With the progress of the engine combustion the number weighted particle size distributions change from monomodal into bi-modal: after 12 CAD, the first mode corresponds to particles smaller than 3nm and the second mode corresponds to a peak between 30 and 60 nm.

This general behaviour is in agreement with the simulations and the measures performed in (Mosbach, 2008) on a single cylinder HCCI engine.

It has to be noted that, in this time interval, the first mode of the number size distribution, after the steep reduction from 1.0E+13 to 1.0E+12, keeps slowly increasing, suggesting that precursors from the gas phase keep holding the nucleation process up. As already mentioned, the first mode increase continues up to the exhaust valve opening, as also shown in Fig.5.23 and Fig.5.24.

The second mode, at 30 CAD, is rather large, indicating that particles with equivalent diameters in the range from 5 to 80 nm are present in comparable numbers.
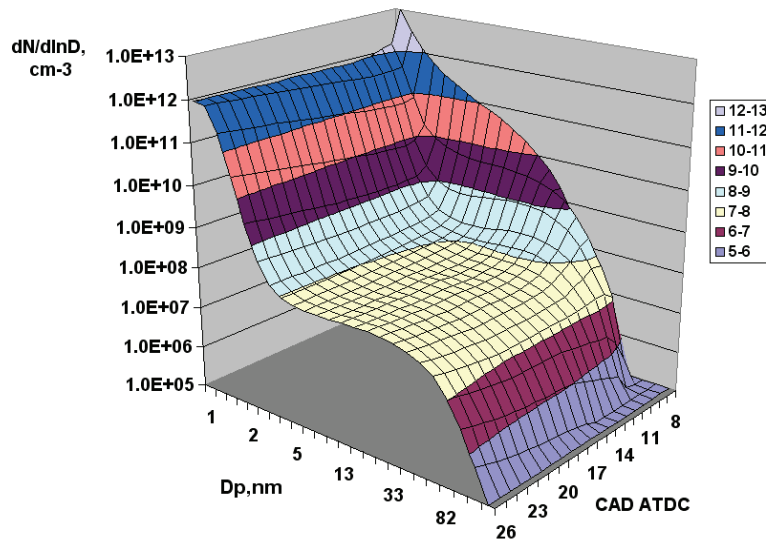
Figure 5.21- Predicted temporal evolution of the aggregate size distribution function between 8 and 30 CAD ATDC
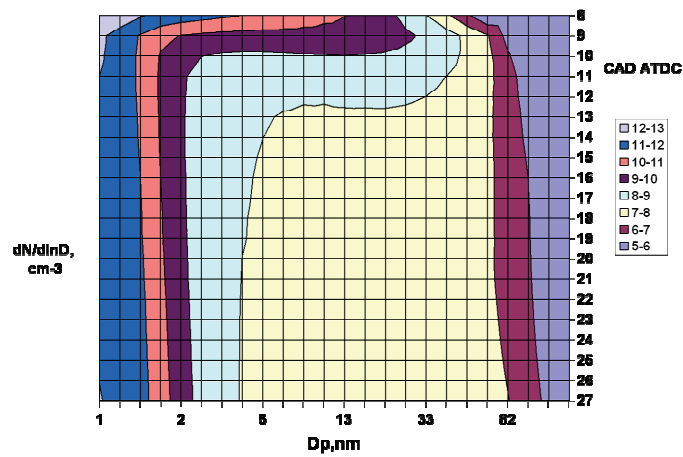

Figure 5.22- Values of Fig. projected on the base plane

After 30 CAD, the first mode gets gradually larger, indicating a marked growth of the smallest particles towards higher diameters, whereas bigger particles, with a diameter more than 10 nm, grow in number and get somewhat larger too.
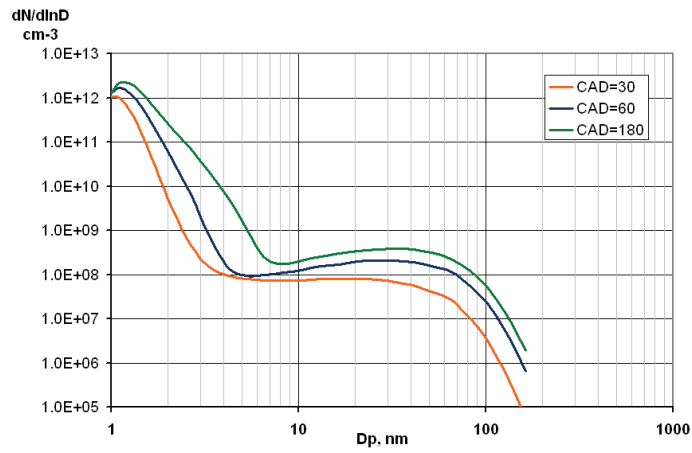
Figure 5.23 – Size distribution function predicted at three values of the crank angle, 30, 60 and 180 degrees after the top dead centre.

For sake of completeness, the temporal evolution of the number size distribution from 30 to 180 CAD ATDC is reported in Fig.5.24.
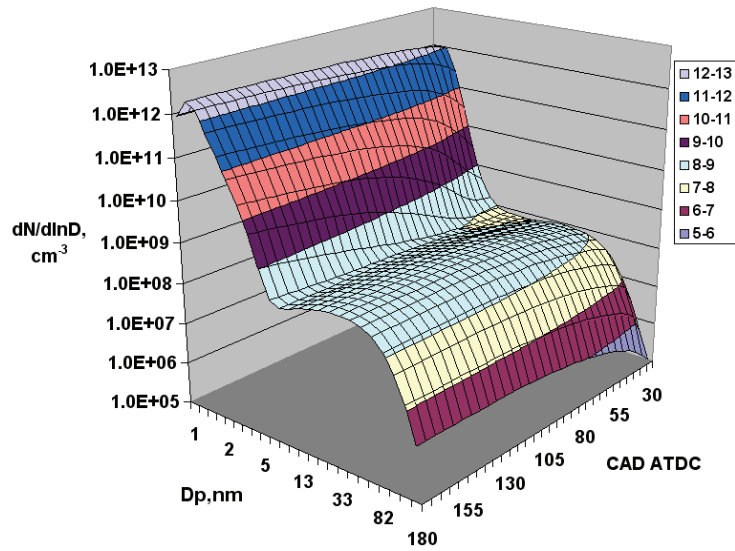

Figure 5.24- Predicted temporal evolution of the aggregate size distribution function between 30 and 180 CAD ATDC

The already mentioned enlargement in the first mode is clearly visible from the projection of Fig.25 and also the continuous increase in the value corresponding to the maximum.
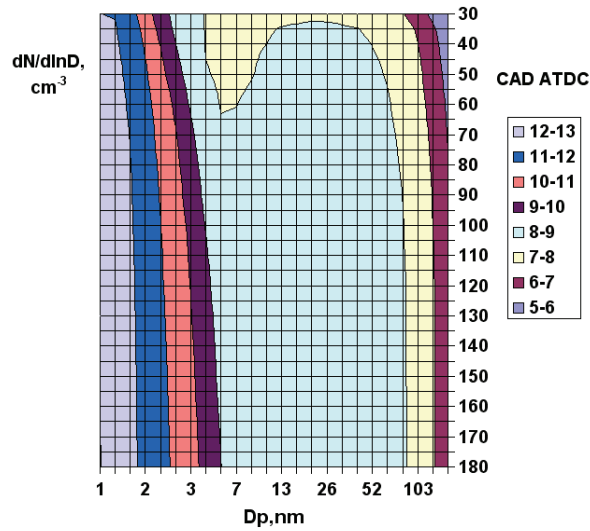
*Figure 5.25*- Values of Fig.23 projected on the base plane

As regards the particles mass, several distribution functions are reported in Fig.5.26, where the relative contribution of the two modes to the total mass concentration is visible: here of course the peak of the second mode is more distinct and accounts for the total mass emitted.
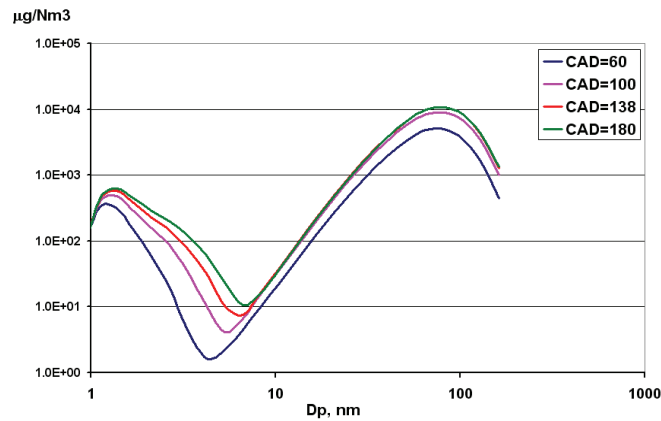

Figure 5.26 – Mass distribution function at various crank angle values

Then the simulation of a different engine operating condition has been carried out, in order to verify the sensitivity of the predictions to some parameters.

The operating test point differs from the previous one in the adoption of a non zero value of the EGR and its main characteristics are listed in Tab.5.3

Table 5.3 **Experimental operative conditions** – CR=16.5

Speed [rpm]	Rail pressure [bar]	EGR %	SOEC CAD BTDC	ET [μs]	IMEP [bar]
1500	480	38	13	710	4.22

In Fig.5.27 the comparison between measured and calculated pressure cycle is reported.
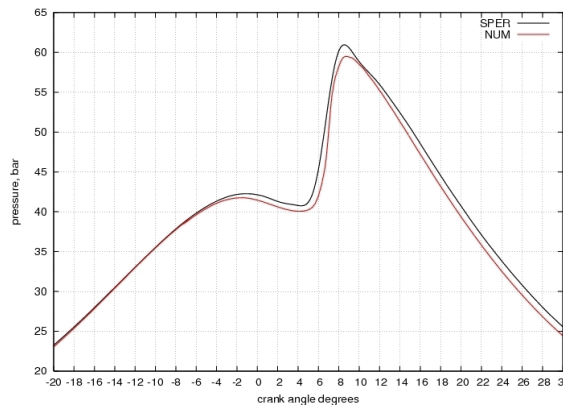
Figure 5.27 – Comparison between measured and computed pressure cycle for case in Tab 5.3.

As displayed in Fig.5.28, the number weighted particle size distribution functions calculated at 30 and 150 CAD ATDC, still exhibits a bi-modal shape.
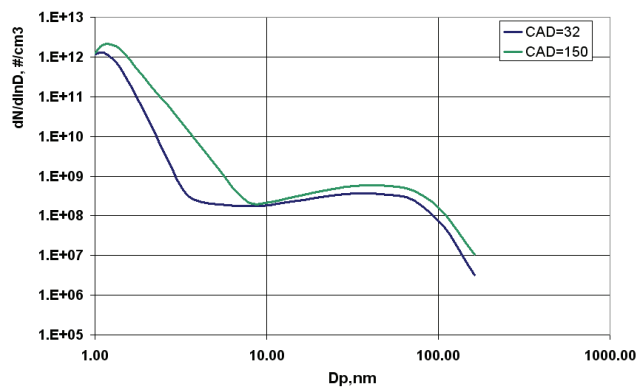
Figure 5.28 – Size distribution function calculated at two values of the crank angle, 32 and 150 degrees after the top dead centre.

The first mode "enlargement" towards higher particle sizes takes place similarly to the case without EGR.

The results for these two cases, in terms of particles size distribution function, look very similar and therefore it is necessary to refer to the measured distribution functions in order to draw a conclusion on the model sensitivity.

The comparison with some experimental data, collected at the exhaust, is reported and discussed in the next paragraph.

A comment

It has to be pointed out that, in engine simulations, the pollutants formation kinetics often takes place also during the expansion phase, when the mesh gets coarser to reproduce the piston motion. KIVA3V moves the computational domain increasing (or decreasing during the compression) the cell size up to a fixed limit. Then, when such limit is reached, an additional layer of cells is added to the mesh (or removed), in order to keep the cell size within a maximum dimension, as shown in Fig.5.29.
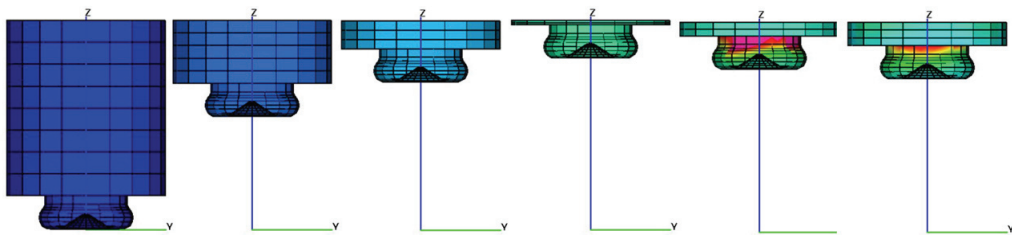
Figure 5.29 – Addition and removal of layers in the mesh motion

In this framework, mesh motion and mesh resolution during the expansion phase deserves a special care, especially when pollutants kinetics is still taking place: in fact, both the nitrogen oxides and the particulate calculation can be influenced by the addition or removal of layers.

Furthermore, with respect to the ignition, where the reactions essentially occur inside the piston bowl, the particles dynamics also involve many cells in the cylinder, thereby requiring a proper mesh resolution in this part of the domain too.

That is why a mesh that can be accepted when simulating only autoignition is not necessarily suitable for pollutants formation modelling too.

Looking at Fig.5.17, it can be seen that the mesh used in the present tests has a cylindrical symmetry also next to the axis, thus cells next to the centre of the domain have a high curvature. This cell skewness could be responsible for bad calculation performance, so the mesh geometry has to be corrected adopting a cartesian geometry around the vertical axis.

To sum up, some future activity should also include mesh sensitivity tests and the mentioned correction of the cells shape.

5.5   DMA experiments at the exhaust

In the following are reported some measures (De Filippo, 2008) of the particulate size distribution function at the exhaust of the same engine used as reference for the simulations. Such data are collected at Istituto Motori –CNR on the diesel single-cylinder engine described in Chapter 2 (see Tab 2.), with a compression ratio value equal to 16.5.

It is not possible to directly correlate the predicted particle size distributions with the experimental data, as the aerosol features, both in terms of mass and of size distribution, keep changing along the exhaust pipe, while the simulations only resemble in-cylinder events, up to the exhaust valve opening. However the comparison can still be helpful to develop a preliminary evaluation of the simulation results.

Size distributions are recorded with a TapCon EMS DMA 3/150[18] -Differential Mobility Analyzer.

This instrument performs a measure of the electrical mobility diameter the aerosol and has also been used to measure on-line the size distributions of inception particles in atmospheric pressure premixed ethylene flames (Sgro, 2007). It consists of an Am[241] bipolar ionizer, a cylindrical classifier and a Faraday Cup Electrometer.

In the present sampling layout, the exhaust gas is sampled 1m downstream the engine-out, just after the damping volume reported in the sketch of Fig.2.9, using one ejector pump diluter (Dekati Ltd.). This stage provides a dilution factor of ~ 3.5, calibrated measuring carbon dioxide concentrations in the exhaust and after the sampler. The diluted flow is transported to the analysis system through a 2m long copper tube (OD=6mm). The measured temperature at the sampling point is ~ 190°C.

Tests are taken with the DMA operated with a sheath flow of 50 L/min and an aerosol flow of 5 L/min with an applied voltage of 0-1250 V and 0-12500V, which respectively covers the 0.6-28 nm and 2-100nm size regions. The data are not corrected for diffusion losses during transport and within the analysis system. The applied dilution is taken into account and the data are reported as particle concentration in engine exhaust.

The engine operating conditions, reported for sake of completeness in Table 5.4, are exactly the same conditions adopted for the simulations described in the previous paragraph. Moreover, the engine is fuelled with pure n-heptane.

Table 5.4 **Experimental operative conditions** – CR=16.5

CASE	Speed [rpm]	BMEP [bar]	Rail pressure [bar]	EGR %	SWIRL	SOEC main CAD BTDC	ET - main [µs]
1	1500	2	480	0	5%	9	710
2	1500	2	480	38	5%	13	710

The electrical mobility diameter measured by the DMA has been corrected to the real diameter subtracting a value of 0.5[19].

---

[18] The DMA employs a cylindrically symmetric electric field applied to the electrostatic classifier (EC) to separate the charged aerosol particles. The size distribution is calculated while varying the applied voltage or the electric field in the classifier, in terms of mobility diameter.

Further details on this class of instruments for the measurement of number size distributions of aerosols and for the generation of monodisperse particles can be found at http://www.emsvie.at.

Fig.5.30 shows the collected data in the two conditions, while in Fig.5.31 and 5.32 the measured number size distribution functions are compared to the predicted ones for case 1 and 2 respectively.
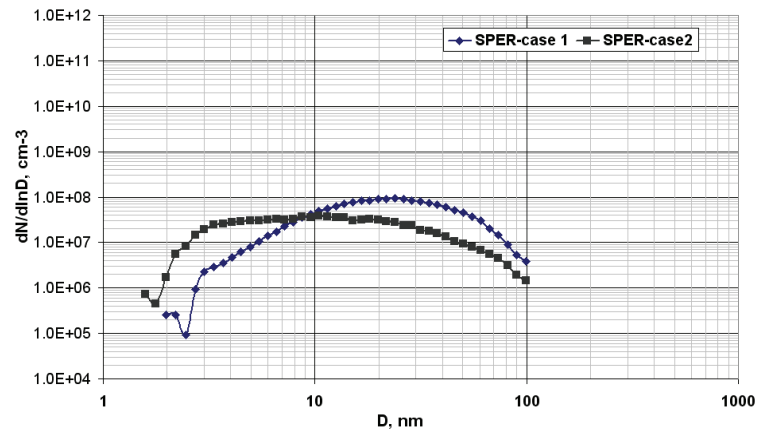

Figure 5.30 – Number weighted particle size distribution measured by DMA in the two operative conditions

The measured functions are substantially mono-modal and, in case 2, a slight shift towards smaller sizes is observable.

---

[19] To correlate the mobility diameter with the actual diameter (geometric diameter of known spherical particles), it is necessary to consider an effective diameter of the gas in which the aerosol is immersed for the measurement.

The real diameter is obtained by subtracting from the mobility diameter this gas effective diameter.

For air at standard conditions, Fernandez de la Mora et al. (2003) experimentally measured a value of do~0.53 nm, not far from Tammet's estimated 0.6 nm (Tammet, 1995) and in good agreement with a more general relationship derived by Li & Wang (2003) who considered the potential energy of interactions between particles and gas molecules in terms of the reduced collision integral.
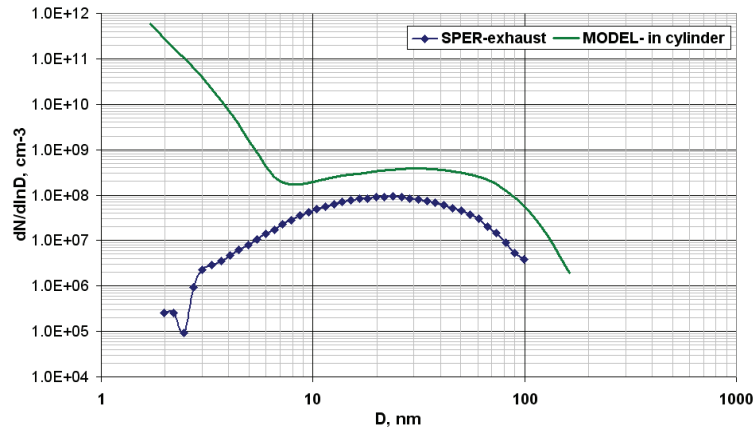
Figure 5.31 – Number weighted particle size distribution measured by DMA compared with the simulation results at 180 CAD ATDC

The comparison with the simulation results of Fig.5.31, for the second mode of the size distribution function, indicates an in-cylinder maximum value of 3E+08 against a value of 1.0E+08 measured at the exhaust.

With respect to the order of magnitude of this size range, the model predictions and the measure give therefore a good qualitative agreement.

On the contrary, the predicted number concentration corresponding to the first mode has not an experimental correspondence in the reported measure.
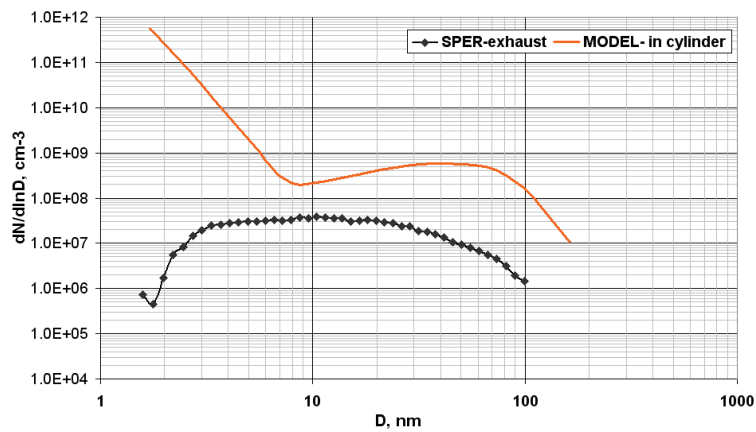
*Figure 5.32* – Number weighted particle size distribution measured by DMA compared with the simulation results at 180 CAD ATDC

Similar considerations apply for case 2, but it is useful to notice that the scarce experimental sensitivity to the operating parameters (EGR) corresponds to an analogous behaviour on the modelling side. In other terms, it seems that n-heptane, at low loads, (with the adopted experimental device) does not present a significant variability of the particulate population produced, when varying EGR. It follows that the computed profiles could possibly look very similar just because of an intrinsic similarity of the production process.

In this respect it has to be said that, although only the test cases correspondent to the simulations have been reported, the analysis of the full set of measures can give some additional insights (De Filippo, 2008). In fact a bi-modal shape of the distribution function turned out to be detected, in analogous operative conditions, with diesel fuel combustion. It has also been observed that the distribution function shape varies according to the dilution ratio: whether the absence of the first mode is attributable to the measurements conditions or is a modelling mistake, remains, at the moment, uncertain.

The only way to draw a reliable opinion on such results is to widen the set of experiments and of simulation test cases and hopefully include other measurements techniques.

In other works (Mancaruso, 2008) a considerable difference (about two orders of magnitude) was found in the particulate number concentration measured in-cylinder (by optical techniques) and at the exhaust (by ELPI-Electrical Low Pressure Impactor). It is not possible to relate quantitatively these results with the present comparison, due to the differences in the engine configuration, in the exhaust layout, the sampling points and the measurements techniques. However it is possible to conclude that comparisons like that of Fig.5.31 and 5.32 are meant to give a first idea on the model performance and the agreement in the second mode appears quite satisfying.

The total mass concentration obtained by integration of the experimental data in Fig.5.31, in the reported size range, calculated assuming an average particle density of 1.8 g/cm^3, is about 6 mg/m^3.

The total particulate mass predicted in the calculations corresponds to about 40mg/m^3: even though the comparison between these two values is not straightforward (one of the reasons being, as an example, the interaction between unburned hydrocarbons and particles along the exhaust tail pipe), it is possible to conclude that the model is overestimating the total particulate mass.

On the other hand, since the dimensional range of the DMA is limited within a maximum value of the mobility diameter of 100nm, bigger clusters undergoing further agglomeration during the exhaust could not be seen by the instrument. So it is also possible that the effective amount total emitted mass (excluding the effect of condensed hydrocarbons) lies in between.

However, taking into account how different are the "histories" of these two numbers, having obtained the same order of magnitude suggests that the adopted model has good potentialities.

Two comparisons are not sufficient to make up a judgment on the model performance and reliability, all the same the activities in current progress start from the mentioned scenario and require to carry out an extensive experimental campaign for a more rigorous validation.

5.6   Summary and conclusions

A model to represent soot particles formation in multidimensional CFD calculations has been implemented in the modified version (see Chapter 3 and 4) of the KIVA3V code.

Such model follows the sectional approach (Richter, 2005): the particle size distribution function is discretized into 25 classes and linked to a detailed kinetics model to represent autoignition and gaseous precursors of soot.

Simulations have been carried out for two test conditions in which the engine was fuelled with heptane and from the analysis of the first numerical results it is possible to conclude that the model predicts the general combustion features (pressure cycle, gas-phase products, ignition timing etc.) in a quantitatively satisfying manner and a reasonable aerosol evolution.

The particle size distribution functions have been compared to measured data from a DMA, referred to gas sampled at the exhaust. The model and the experiments provided similar values of the size distribution function for particle sizes between 10 and 100nm, while calculations also predict a nucleation mode that is not experimentally detected.

In order to build a sensible opinion on these preliminary results, further numerical tests are definitely necessary, as the model sensitivity to different operative conditions needs to be investigated. A reliable validation campaign will not only require to apply the model to many different engine conditions, but also to carry out a supporting experimental activity; as an example, a proper comparison could be achieved directly sampling in-cylinder gas.

It would be interesting to explore the response to the variation of EGR and see how the recirculation of particles can affect the predictions.

In this respect, one of the priorities in future work should be the reduction of the computational time, performing, for this kinetic model, a mathematical study analogous to that carried out for autoignition kinetics (Chapter 3-4). In addition, how these results are affected by the mesh quality has to be determined, as explained in Par.5.4.

Finally, the interaction between chemistry and turbulence described in Par.3.5 is oversimplified to adequately represent the effect of the flow characteristics on the solid phase reactivity, therefore also this aspect surely deserves some work.

However the feasibility of a sectional model implementation in engine simulation has been assessed and the preliminary results reported in this chapter can be considered a satisfying starting point.

Bibliography

BELARDINI, P., BERTOLI, C., CIAJOLO, A., D'ANNA, A. AND DEL GIACOMO, N., *Three - dimensional calculations of DI diesel engine combustion and comparison with in cylinder sampling valve data.* SAE paper 922225, 1992.

CELNIK, M.S., RAJ, A., PATTERSON, R.I.A., WEST, R.H., KRAFT, M., *A statistical approach to develop a detailed soot growth model using PAH characteristics*, Tech. Rep.53, c4ePreprint-Series, Cambridge 2007.

D'ANNA, A., KENT, J.H., *Modeling of particulate carbon and species formation in coflowing diffusion flames of ethylene*, Combust. Flame 144, 249-260, 2006.

D'ANNA, A., KENT, J.H., *A model of particulate and species formation applied to laminar, nonpremixed flames for three aliphatic-hydrocarbon fuels*, Combust. Flame 152, 573-587, 2008.

D'ANNA, A., *Detailed kinetic modeling of Particulate Formation in Rich Premixed Flames of Ethylene*, Energy Fuels 22, 1610-1619, 2008.

DE FILIPPO, A., Characterization of carbonaceous nanoparticle size distributions (1-10nm) emitted from laboratory flames, diesel engines and gas appliances, PhD Thesis, 2008.

FERNANDEZ DE LA MORA, J.J., DE JUAN, L.L., LIEDTKE, K., SCHMIDT-OTT, A., *Mass and size determination of nanometer particles by means of mobility analysis and focused impaction*, Journal of Aerosol Science 34 (2003) 79-98.

FRENCKLACH, M., WANG, H., *Detailed modeling of Soot Particle Nucleation and Growth*, Proc. Comb. Inst. 23, 1559-1566, 1990.

GUSTAVVSSON, J., GOLOVITCHEV, V.I., *Spray Combustion Simulation Based on Detailed Chemistry Approach for Diesel Fuel Surrogate Model*, SAE Paper 2003-01-37, 2003.

HIROYASU, H., KADOTA, T. AND ARAI, M., *Development and use of a spray combustion modeling to predict diesel engine efficiency and pollutant emissions (Part 1: Combustion modeling)*, Bulletin of the JSME, 26: 569-575, 1983.

HONG, S., WOOLDRIDGE, M.S., IM, H.G., ASSANIS, D.N., PITSCH, H., *Development and application of a comprehensive soot model for 3D CFD reacting flow studies in a diesel engine*, Combust. Flame 143, 11-26, 2005.

KONG, S.-C., HAN, Z.Y., AND REITZ, R.D*., The development and application of a diesel ignition and combustion model for multidimensional engine simulation,* SAE paper 950278, 1995.

LI, Z., WANG, H., *Drag force, diffusion coefficient, and electric mobility of small particles. I. Theory applicable to the free-molecule regime,* Physical Review E 68 (2003) 061206, 1-9.

LIU, S., HEWSON, J.C., CHEN, J.H., PITSCH, H., *Effects of strain rate on high-pressure nonpremixed n-heptane autoignition in counterflow*, Combust. Flame 137, 320-339, 2004.

MANCARUSO, E., DI IORIO, S., VAGLIECO, B.M., *Particle Size Distribution in DI Diesel Engine Operating with Conventional and Advanced Strategies*, Conf. on Thermo- and Fluid Dynamic Processes in Diesel Engines Thiesel, 2008.

MAUSS, F., TRILKEN, B., BREITBACH, H., PETERS, N., *Soot formation in Partially Premixed Diffusion Flames at Atmospheric Pressure*, in Mechanisms and Models of Soot Formation – Lecture Notes in Physics, Springer-Verlag New York, chap. 21, 1994.

MOSBACH, S., CELNIK, M.S., RAJ, A., KRAFT M, H.R. ZHANG, KUBO S., KIM K.-O., *Towards a detailed soot model for internal combustion engines*, poster 32nd International Symposium on Comb., Montreal, 2008.

NAGLE, J., STRICKLAND-CONSTABLE, R.F., *Oxidation of carbon between* 1000-2000°C, Proceedings of the 5th Carbon conference, 1, 265-325, 1962.

POPE, C.J., HOWARD, J.B., *Simultaneous Particle and Molecule Modeling (SPAMM): An Approach for Combining Sectional Aerosol Equations and Elementary Gas-Phase Reactions*, Aerosol Sci. Technol. 27, 73-94, 1997.

PRIESCHING, P., TATSCHL, R., MAUSS, F., SARIC, F., NETZELL, K., BAUER, W., SCHMID, M., LEIPERTZ, A., MEROLA, S.S., VAGLIECO, B.M., *Soot Particle Size Distribution- a Joint Work for Kinetic Modeling and Experimental Investigations*, SAE Paper 2005-24-053, 2005.

RICHTER, HOWARD, J.B., *Formation of polycyclic aromatic hydrocarbons and their growth to soot- a review of chemical reaction pathways*, Prog. Energy and Comb. Science 26, 565-608, 2000.

RICHTER, H., GRANATA, S., GREEN, W.H., HOWARD, J.B., *Detailed modelling of PAH and soot formation in a laminar premixed benzene/oxygen/argon low-pressure flame*,. Inst, 30, 1397-1405, 2005.

SGRO, L.A., DE FILIPPO, A., LANZUOLO, G., D'ALESSIO, A., *Characterization of nanoparticles of organic carbon (NOC) produced in rich premixed flames by differential mobility analysis*, Proc. of the Comb 31, 631-638, 2007.

SUROVIKIN, V.F., *Analytical description of the processes of nucleus-formation and growth of particles of carbon black in the thermal decomposition of aromatic hydrocarbons in the gas phase*, Solid Fuel Chemistry, 10, 92-101,1976.

TAMMET, H., *Size and mobility of nanometer particles, clusters and ions,* Journal of Aerosol Science 26 (1995) 459-475.

TAO, F., FOSTER, D.E., REITZ, R.D., *Soot Structure in a Conventional Non-Premixed Diesel Flame*, SAE Paper 2006-01-0196, 2006.

Chapter six

Conclusions

6.1   Summary of results

A parallel version of KIVA3V has been used to implement detailed reaction schemes for diesel combustion simulations: how autoignition kinetics affects the mathematical stiffness of the equations set has been studied.

The different characteristics of the autoignition and the high temperature phase during the combustion process have suggested to use different ODE solvers to improve the accuracy and the efficiency of the calculations: VODE and SDIRK4.

SDIRK4 turned out to be more efficient than VODE over the total simulation, while VODE is more efficient and accurate in the critical autoignition phase. This suggested to use the one or the other according to the current stiffness and to the local conditions, in order to reduce the computing time and improve the accuracy of the solution, with respect to the use of a single solver. The cell by cell switching criterion is based on the in cylinder concentration of ketoheptylperoxide or hydrogen peroxide.

Once set up this selection criterion, some experiments have been carried out fuelling the single-cylinder engine with pure n-heptane, in order to perform a more appropriate comparison with simulations results. A wide range of operative parameters have been varied to test the code reliability to different engine operative conditions. The combustion model seems to be very representative of the low temperature combustion process: in any of the chosen test cases the predicted ignition delay values are very close to experimental ones.

A model to represent soot particles formation in multidimensional CFD calculations has been implemented in the modified version of the KIVA3V code.

Such model is based on the sectional approach: the particle size distribution function is discretized into 25 classes and linked to a detailed kinetics model to represent autoignition and gaseous precursors of soot.

Simulations have been carried out for two test conditions in which the engine was fuelled with heptane and from the analysis of the first numerical results it is possible to conclude that the model predicts the general combustion features (pressure cycle, gas-phase products, ignition timing etc.) in a quantitatively satisfying manner and a reasonable aerosol evolution.

The particle number size distribution function has been compared to measured data from a DMA, referred to gas sampled at the exhaust. The model and the experiments provided similar values of the size distribution function for particle sizes between 10 and

100nm, while calculations also predict a nucleation mode that is not experimentally detected.

However the feasibility of a sectional model implementation in engine simulation has been assessed and the preliminary results reported in this chapter can be considered a satisfying starting point.

6.2   Recommendations for future work

An operative plan for future work can be organized in long and short term objectives respectively.

As a matter of fact, some inherent weak points of the exploited modelling approach, need a considerable time to be overcome, also including the time for code developing.

In this respect, it would be crucial to address the chemistry-turbulence interaction issue, especially if LTC combustion conditions have to be simulated: however a fast tentative, without code modifications, to reproduce multi-stage ignition could be the straightforward adoption of more detailed reaction mechanisms. On the contrary, the implementation of a more complex flow-kinetics interaction would certainly require a longer time, yet a transported PDF method could represent an investment for the quality of future simulations.

In addition, some proper experimental activity has to be planned to perform an extensive validation activity to evaluate the predictions of the particles formation model. As the engine is a unique combustion device, it is not obvious to transport mechanisms validated elsewhere.

Finally, another option to be taken into account could be to transfer the achieved insights and solutions to a different numerical code, that could hopefully simplify some tasks, like an easier generation of finer meshes or alternative solutions to the turbulence-chemistry interaction issue.

In the short term, the nitrogen oxides kinetics has to be added to the reaction schemes, both to predict emissions and to take into account the effects of the NOx on the fuel ignition delay.

As concerns the particles formation modelling, further analysis on the soot model behaviour in different engine conditions should be carried out: the sensitivity of the numerical results to important parameters like EGR, swirl ratio (that influences the level of fuel-air mixing) has to be investigated. It would also be worth performing further simulations and experiments at higher engine speed and load, in order to make up a wider scenario.

It would be interesting to investigate the effect of particles recirculation with high EGR rates.

Moreover, further grid sensitivity tests should be performed when mechanisms including gaseous pollutants and particles formation are included and a different cells geometry is definitely desirable.

It is rather difficult to estimate the time necessary to reach the goal of predicting particles size distribution functions for engines operating in alternative modes: models are always imperfect, yet also a non perfect model can provide us with very useful insights on the modelled phenomena, suggesting possible answers or indicating new questions.